

N 70-27181

COVER SHEET FOR TECHNICAL MEMORANDUM

TITLE-Lunar Trajectory Geometry

TM-69-2011-3

DATE- December 23, 1969

FILING CASE NO(S)- 310

AUTHOR(S)-K. M. Carlson

FILING SUBJECT(S)- Lunar Trajectories
(ASSIGNED BY AUTHOR(S)- Trajectory Analysis
Celestial Mechanics

ABSTRACT

The principal features of earth-moon trajectories are analyzed using a geometric approach and "patched conic" trajectories. The influence of significant parameters is shown in a step by step manner until a comprehensive picture of earth-moon trajectories is created. In addition, a series of plots of the aimpoint on the moon's sphere of influence for various Keplerian elements of the trajectories is included.

These plots, together with the analysis presented, provide the basis for a thorough understanding of the geometry of lunar trajectories. The techniques developed are used to illustrate some of the significant features of lunar landing missions and free return circumlunar trajectories.

CASE FILE
COPY

NASA FILE COPY
Return to
NASA HQ LIBRARY (878-10)
WASHINGTON, DC 20546 STOP 85
HQ LIBRARY (878-10)

BA-145A (8-68)

SEE REVERSE SIDE FOR DISTRIBUTION LIST

DISTRIBUTIONCOMPLETE MEMORANDUM TO

CORRESPONDENCE FILES:

OFFICIAL FILE COPY

plus one white copy for each
additional case referenced

TECHNICAL LIBRARY (4)

NASA Headquarters

T. A. Keegan/MA-2

MSC

H. D. Beck/FM5
R. L. Berry/FM5
M. D. Cassetti/FM7
K. J. Cox/EG23
J. C. McPherson/FM4
R. O. Nobles/FM7
J. D. Yencharis/FM5

MSFC

V. L. Buckelew/STE-AERO-MFG
D. C. Chandler/R-AERO-G
A. W. Deaton/R-AERO-G

Bellcomm, Inc.

G. M. Anderson
D. R. Anselmo
I. Y. Bar-Itzhack
R. A. Bass
H. B. Bosch
A. P. Boysen, Jr.
J. O. Cappellari, Jr.
D. A. Corey
D. A. DeGraaf
F. El-Baz
D. G. Estberg
A. J. Ferrari
J. T. Findlay

COMPLETE MEMORANDUM TO (CONT.)Bellcomm, Inc.

W. B. Gevarter
D. R. Hagner
W. G. Heffron
H. A. Helm
N. W. Hinners
T. B. Hoekstra
B. T. Howard
D. B. James
F. LaPiana
M. Liwshitz
H. S. London
D. Macchia
J. L. Marshall, Jr.
K. E. Martersteck
J. Z. Menard
L. D. Nelson
J. M. Nervik
B. G. Niedfeldt
J. J. O'Connor
G. T. Orrok
P. E. Reynolds
J. A. Schelke
J. J. Schoch
R. V. Sperry
W. B. Thompson
J. W. Timko
A. A. Vander Veen
R. L. Wagner
Members of Department 2011
Department 1024 File

COVER SHEET ONLY TO

I. M. Ross
M. P. Wilson

SUBJECT: Lunar Trajectory Geometry
Case 310

DATE: December 23, 1969

FROM: K. M. Carlson

TM-69-2011-3

TECHNICAL MEMORANDUM

INTRODUCTION

The behavior of trajectories to the moon is extremely complex. The analyst attempting to investigate some phase of the lunar trajectory problem may find himself with unexpected and confusing results. However, the basic geometry of lunar trajectories can be understood using simplified and easily visualized geometric models. In this study, "patched conic" analysis is used and functional relationships between the "aimpoint", or patch point, on the moon's sphere of influence and selected trajectory parameters are explored. The analysis culminates in a series of plots of the loci of the required aimpoints on the moon's sphere of influence for constant values of the Keplerian elements of earth-moon trajectories.

Although the analysis techniques developed here are not suitable for precise targeting of specific missions, they do provide a basic understanding of the fundamental geometric features of lunar trajectories. The insight gained in this manner can be very useful in the development of algorithms for specific mission targeting. In order to demonstrate the utility of this study, the general features of targeting a lunar landing mission and a free return circumlunar trajectory are discussed.

BASIC GEOMETRY

Coordinate System

A coordinate system which provides the greatest ease of visualization is needed for this study. The moon's orbit plane (MOP) has been chosen as the reference plane for the coordinate system since it contains the earth, the moon and the moon's velocity vector. The lines from the moon to the earth in selenocentric space, and from the earth to the moon in geocentric space, have been chosen as the reference directions, as the moon's velocity vector is always nearly perpendicular to these lines (see Figure 1). Throughout the study, latitude and longitude on the moon's sphere of influence (MSI) are referenced to this selenocentric coordinate system rather than to the usual selenographic system. Likewise, all orbital

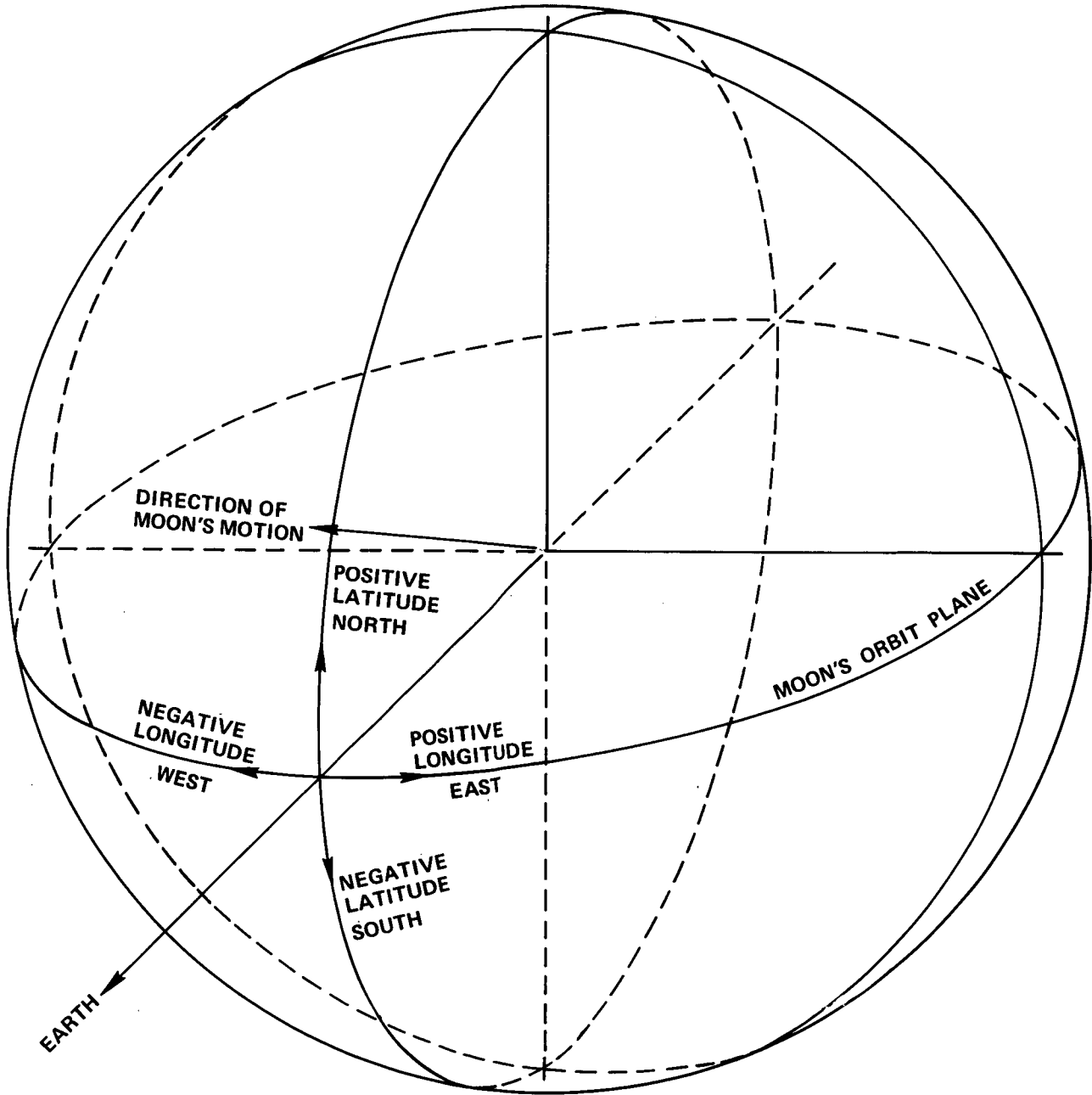


FIGURE 1 - THE SELENOCENTRIC COORDINATE SYSTEM

inclinations are referenced to the coordinate systems defined here. As a point of perspective, note that geocentric inclinations of as much as 57.2° are possible in this system with a due east launch from Cape Kennedy.* Note also that these coordinate systems sidestep the problems associated with the declination of the moon.

The Effect of Changing Geocentric Energy and Lunar Position on the MSI Aimpoint

Changing geocentric energy changes the geocentric velocity at any given distance according to:

$$V = [2(E + \mu/r)]^{1/2} \quad (1)$$

where μ is the gravitational constant of the attracting body and r , E , and V are the radius, energy and velocity of interest. Thus, changing the energy really amounts to changing the velocity all along the trajectory, including at the MSI.

To visualize the effect of energy changes on the MSI entry aimpoint, consider trajectories with rectilinear selenocentric and geocentric portions, that is, trajectories which ascend from the earth vertically and descend to the moon vertically. Such trajectories will be referred to as pure rectilinear trajectories. Radii of perigee and periselene are zero and inclination is meaningless. The trajectory must lie in the MOP, since the moon's velocity vector lies in this plane. If the geocentric portion of the trajectory were to be outside the MOP, the vehicle would have a velocity component at the MSI normal to the MOP and directed away from the MOP. When the moon's orbital velocity is subtracted from the vehicle's geocentric velocity to obtain the vehicle's selenocentric velocity, the normal component of vehicle velocity is transposed intact, and the resulting selenocentric velocity vector could not point at the moon's center, as is required for rectilinear trajectories. Figure 2 shows the geometry for two geocentric energies. As the velocity at MSI entry decreases, the aimpoint required to produce the rectilinear selenocentric portion is forced westward.

*The moon's orbit is inclined to the ecliptic by 5.15° and the earth's axis is inclined by 23.45°. As Cape Kennedy has a latitude of 28.6°, the total possible inclination is 57.2° for a due east launch.

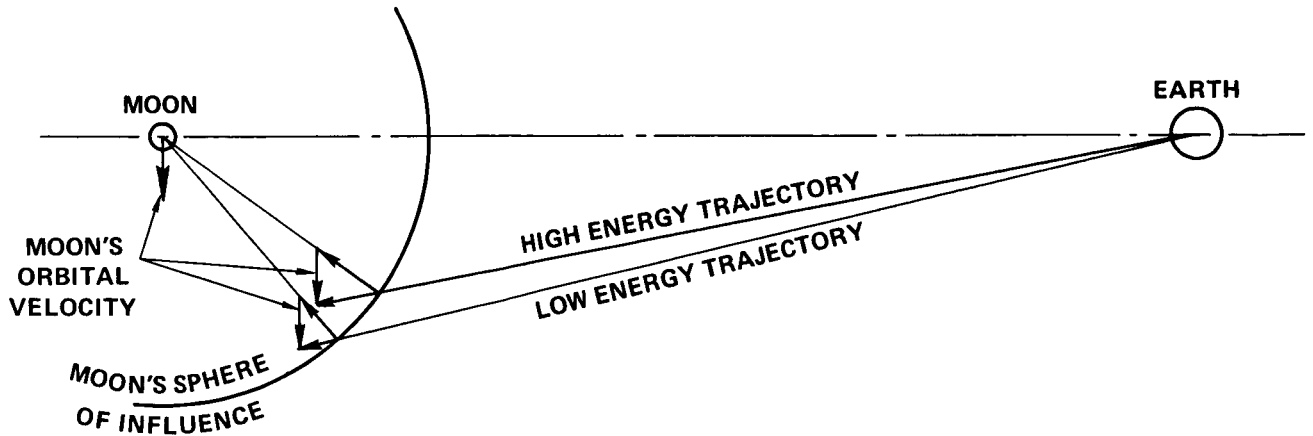


FIGURE 2 - HIGH & LOW ENERGY PURE RECTILINEAR EARTH-MOON TRAJECTORIES

Figure 3 shows the variation of MSI aimpoint longitude for a wide range of energies and confirms the predicted behavior. As the energy increases toward infinity, the aimpoint longitude will asymptotically approach zero. That is, at infinite energy the trajectory will simply follow the earth-moon line. On the other hand, if the aimpoint longitude moves westward, the energy will decrease, asymptotically approaching a minimum. The minimum possible energy is that which allows the vehicle to just reach the MSI with zero velocity.

Figure 3 also shows that the longitude of the pure rectilinear trajectory aimpoint varies during the lunar month due to the slight ellipticity of the moon's orbit. For high energy trajectories, the effect is small since the vehicle's velocity vector (magnitude and direction) at MSI entry changes very little as the earth-MSI distance changes. At energies near the minimum, however, the vehicle's velocity vector at MSI entry changes substantially with changing earth-MSI distance, and the required change in the MSI aimpoint is correspondingly larger.

The difference in Figure 3 between the two curves for the moon at mid-distance results from the radial component

of the moon's velocity. The crossover point on the curves for the moon at apogee and perigee occurs at a vehicle energy equal to the moon's orbital energy.

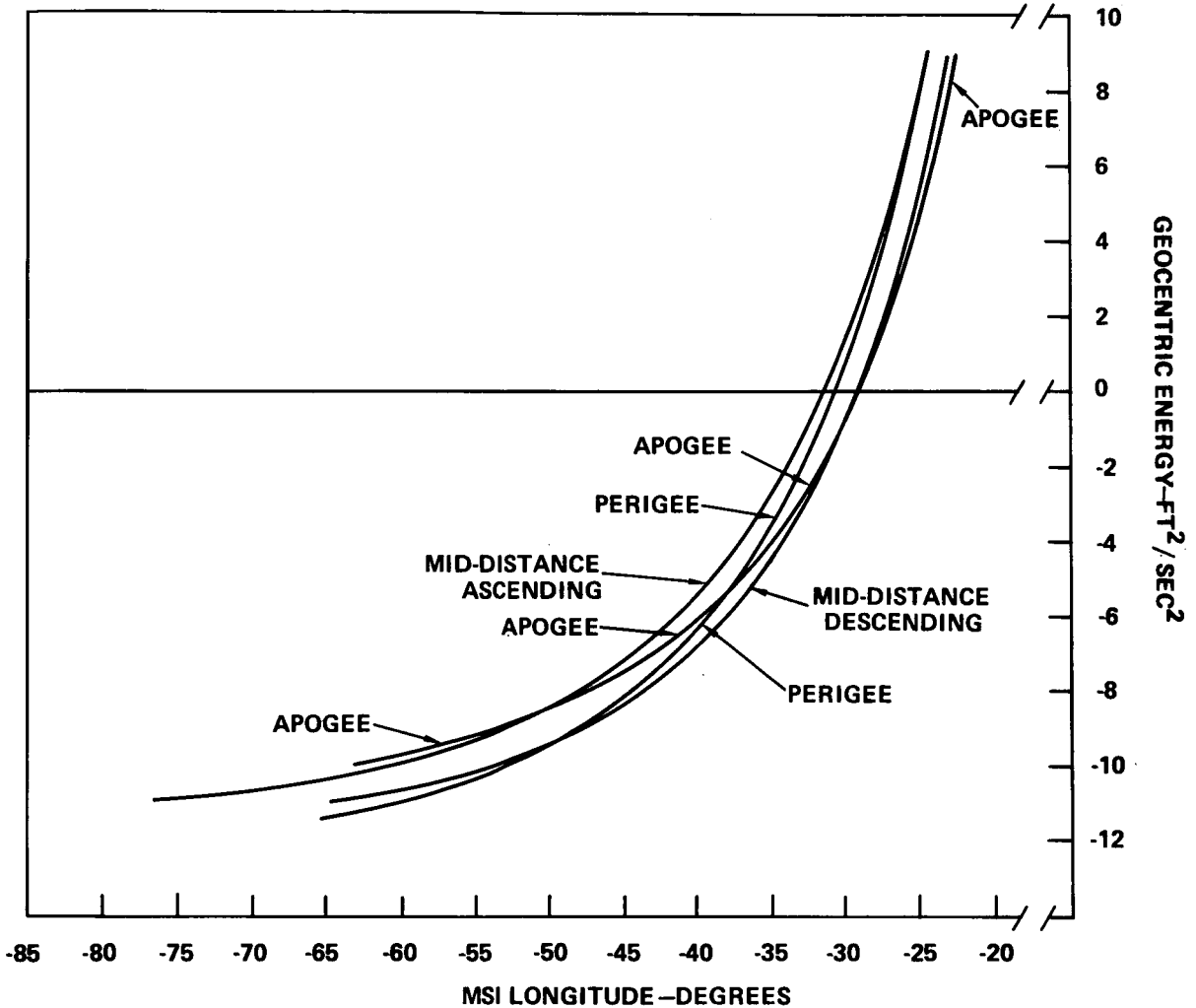


FIGURE 3 - MSI ENTRY LONGITUDE VS. GEOCENTRIC ENERGY FOR PURE RECTILINEAR TRAJECTORIES AND FOUR LUNAR POSITIONS

The motion of the pure rectilinear aimpoint is quite important. Subsequent development will show that the aimpoint locus for all lunar trajectories of a fixed geocentric energy is symmetrical about the pure rectilinear trajectory aimpoint for that energy. Therefore, the general aimpoint locus moves with the pure rectilinear aimpoint.

The Influence of Perigee Radius on the MSI Aimpoint

A non-zero perigee radius causes the geocentric portion of the trajectory path to be a conic section curve; consequently, the velocity vector is no longer aligned with the radius vector. This will cause the MSI entry conditions to be altered as shown in Figure 4. For the moment, the selenocentric portion of the trajectory is considered to be rectilinear and the geocentric inclination is kept at zero, that is, the geocentric trajectory lies in the MOP. In Figure 4, trajectories of equal energy but different perigee radii are shown. As the perigee altitude is increased, the angle of incidence of the trajectory with respect to the MSI deviates farther and farther from the pure rectilinear trajectory incidence angle. As a consequence, the aimpoint moves farther and farther away from the pure rectilinear aimpoint, eastward for posigrade trajectories and westward for retrograde trajectories.

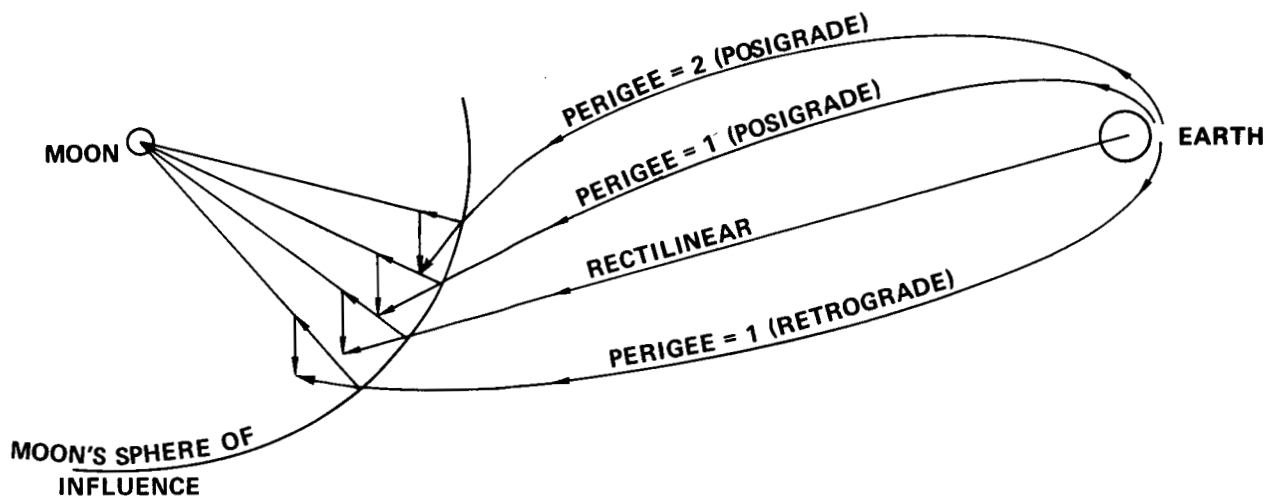


FIGURE 4 - THE EFFECT OF CHANGING PERIGEE RADIUS FOR TRAJECTORIES WITH RECTILINEAR SELENOCENTRIC PORTIONS

It can be shown that the movement of the aimpoint away from the pure rectilinear aimpoint is not symmetrical. That is, a given perigee radius will not produce identical eastward and westward aimpoint displacements. This results from the curved surface presented by the MSI and from the changing vehicle velocity and flight path angle caused by the changing aimpoint-earth distance. Nonetheless, over most of the range of geocentric energies of interest, the movement

of the aimpoint away from the pure rectilinear aimpoint is roughly symmetrical. This is shown in Table I for a series of cases. Only for the relatively extreme case of a 90 hour trip to a moon at perigee does the aimpoint motion become seriously asymmetrical. (These results can also be seen on Figure 8, which includes the effect of geocentric inclination, discussed in the next section).

TABLE I

Effect on Aimpoint Longitude of a 100 N.M.
Perigee Altitude for Trajectories Lying in the MOP

LUNAR POSITION	ENERGY (FT ² /SEC ²)	TRIP TIME	λ_{PR}^*	$\Delta\lambda_{RST}^{**}$	
				POSIGRADE GEOCENTRIC	RETROGRADE GEOCENTRIC
Apogee	-2.80×10^6	60 HRS	-33.5°	5.7°	-4.5°
Apogee	-9.17×10^6	90 HRS	-55.0°	6.0°	-5.5°
Perigee	-7.73×10^6	60 HRS	-43.5°	6.0°	-6.2°
Perigee	-11.47×10^6	90 HRS	-65.4°	1.4°	-6.9°

The Influence of Geocentric Inclination on the MSI Aimpoint

Again, consider trajectories with a rectilinear selenocentric portion, but now no longer restricted to be in the MOP. The geometry of such inclined trajectories is shown in Figure 5. The primary effect of inclining the geocentric trajectory to the MOP is the appearance of a velocity component normal to the MOP at MSI entry. As a consequence, the

* λ_{PR} = pure rectilinear aimpoint longitude.

** $\Delta\lambda_{RST}$ = shift in aimpoint longitude from λ_{PR} for a trajectory with a non-zero radius of perigee but a rectilinear selenocentric trajectory.

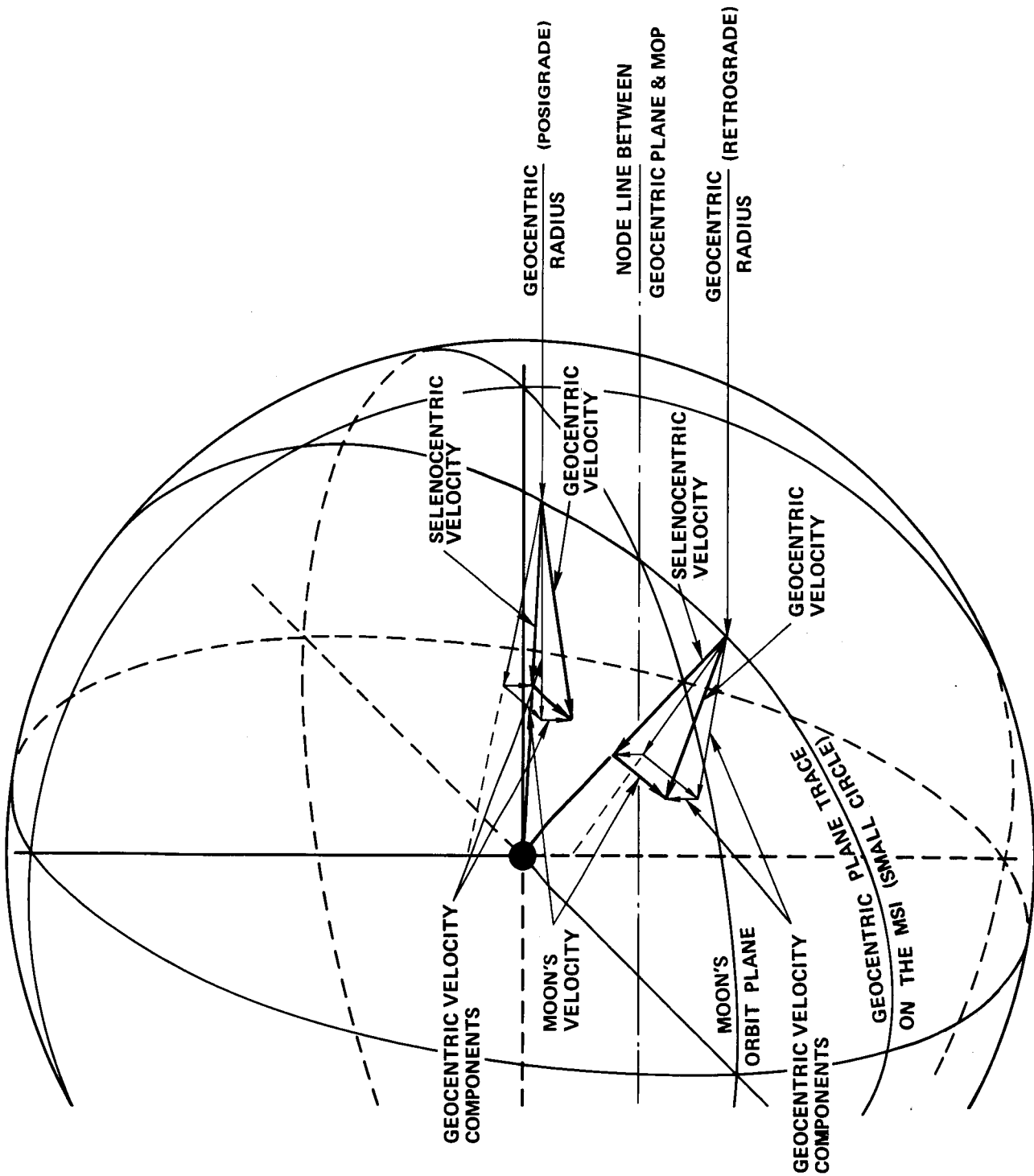


FIGURE 5 - MSI ENTRY GEOMETRY FOR AN EARTH-MOON TRAJECTORY WITH A NON-ZERO
 GEOCENTRIC INCLINATION AND PERIGEE RADIUS AND A RECTILINEAR
 SELENOCENTRIC TRAJECTORY

MSI aimpoint must move away from the MOP. The magnitude of the normal component increases as the geocentric trajectory plane becomes more and more nearly normal to the MOP. Thus the MSI aimpoint latitude should reach a maximum at an inclination near 90° .

The change in MSI aimpoint longitude with changing inclination can be seen by noting in Figure 5 that the moon's velocity vector modifies only the component of geocentric velocity which is parallel to the MOP. The component normal to the MOP is transposed intact. As the geocentric inclination increases, the incidence angle of the geocentric velocity component parallel to the MOP approaches the incidence angle for pure rectilinear trajectories. Consequently, the aimpoint longitude moves toward the pure rectilinear aimpoint as the geocentric trajectory plane becomes more nearly normal to the MOP. Thus, the resulting locus of aimpoints for rectilinear selenocentric trajectories (RST) for varying geocentric inclinations will form a closed curve, as shown in Figure 6. The curve is approximately elliptical. The points lie above the MOP if the geocentric trajectory lies above the MOP during the translunar phase and vice versa. Note that there are two solutions for any given inclination. These two solutions have ascending nodes which are approximately 180° apart. The aimpoint for a pure rectilinear trajectory lies almost exactly at the center of the RST aimpoint ellipse. Figure 7 shows the effect of different radii of perigee on the RST aimpoint ellipse, while Figure 8 shows the effect of different translunar energies and lunar positions.

Requirements for a Non-Zero Radius of Periselene

A non-zero periselene radius will occur anytime the selenocentric velocity vector is not pointed directly at the moon's center. In the previous analysis, it was shown that selecting a geocentric energy and a radius of perigee defined an aimpoint locus which produced rectilinear selenocentric trajectories (RST). Hitting any other aimpoint will misalign the velocity vector and a hyperbolic selenocentric trajectory will result. Figure 9 shows the effect of simply changing the geocentric ellipse orientation (argument of perigee) for a trajectory lying in the MOP. Whether the resulting hyperbola is posigrade or retrograde depends on whether the aimpoint is east or west of the RST aimpoint. The altitude of periselene can be shown to be primarily a function of the selenocentric angular distance between the actual aimpoint and the aimpoint for an RST. With a bit of manipulation, the hyperbolic orbit equations yield the following relationship for the radius of periselene:

(continued on Page 13)

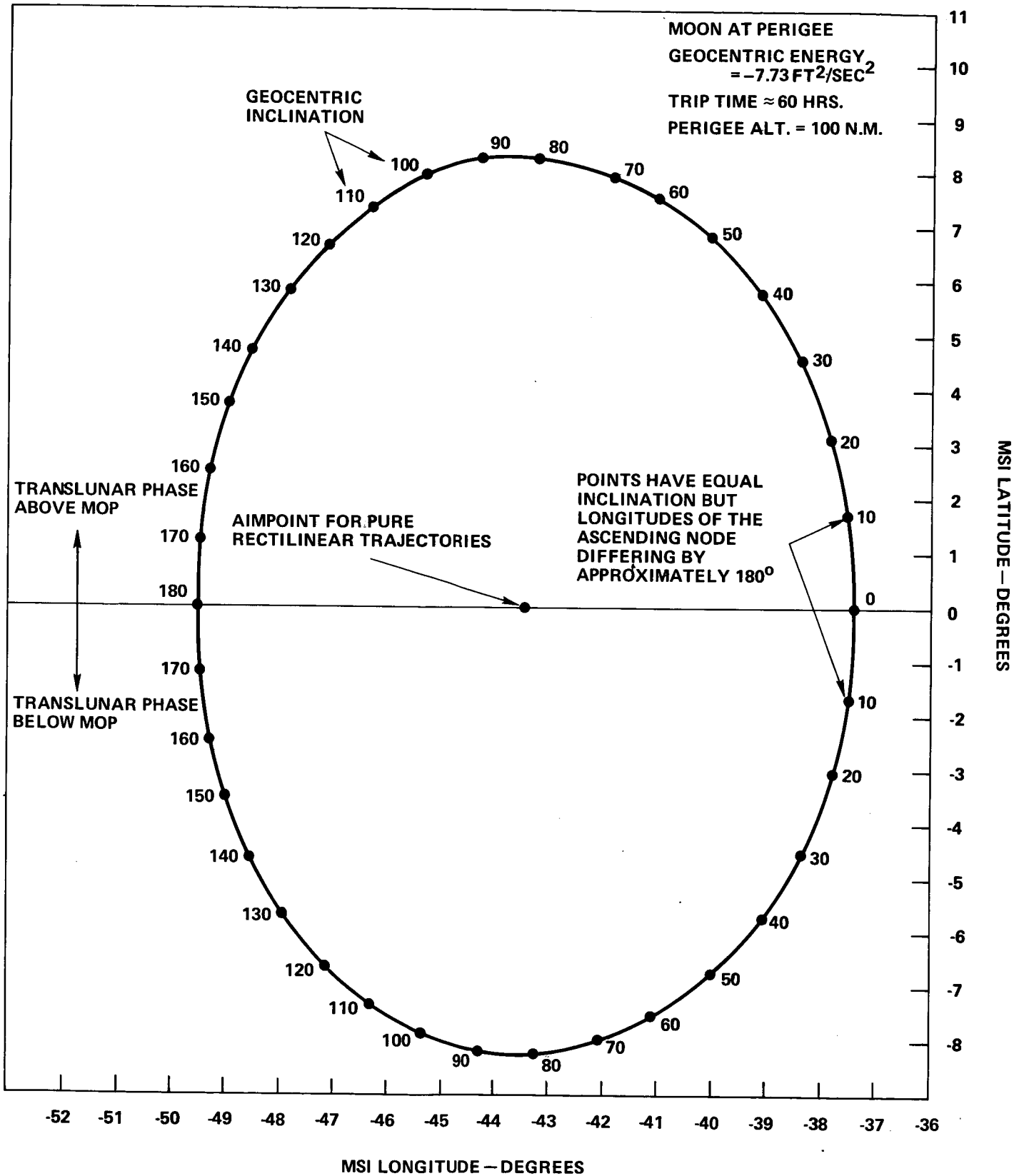


FIGURE 6 - MSI AIMPOINT LOCUS FOR RECTILINEAR SELENOCENTRIC TRAJECTORIES AND VARIOUS GEOCENTRIC INCLINATIONS

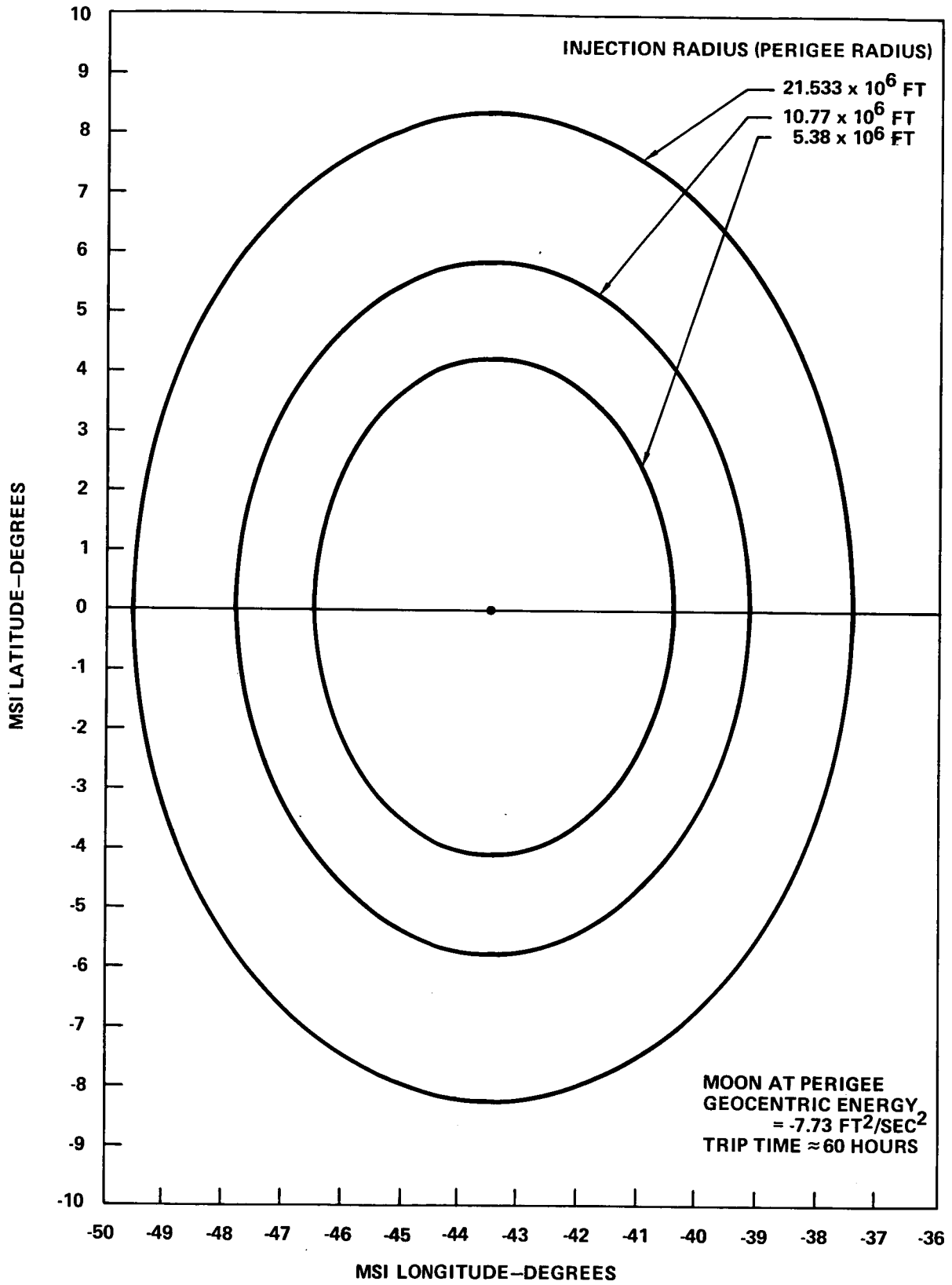


FIGURE 7 - MSI AIMPOINT LOCI FOR RECTILINEAR SELENOCENTRIC TRAJECTORIES WITH DIFFERENT INJECTION RADII

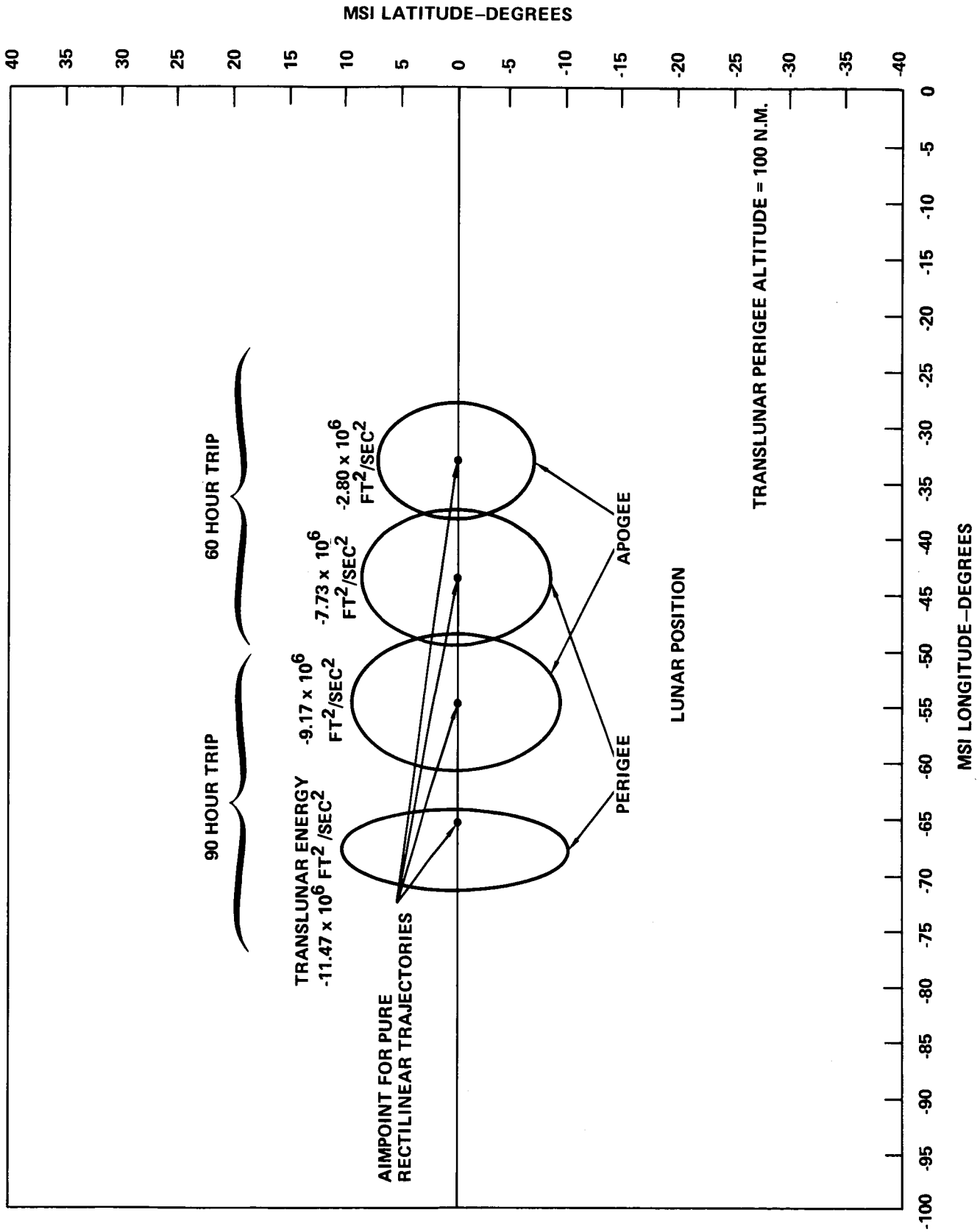


FIGURE 8 - MSI AIMPOINT LOCI FOR RECTILINEAR SELENOCENTRIC TRAJECTORIES FOR VARIOUS
GEOCENTRIC ENERGIES AND LUNAR POSITIONS

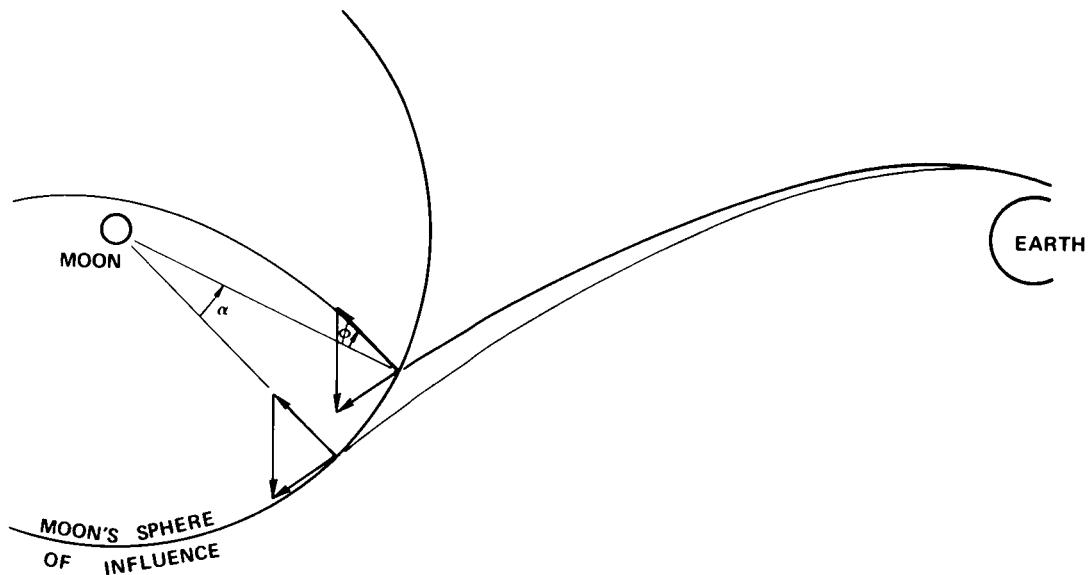


FIGURE 9 - THE EFFECT OF OFFSETTING THE AIMPOINT FROM THE RST AIMPOINT
CONSTANT RADIUS OF PERIGEE AND GEOCENTRIC ENERGY

$$r_p = \left[\left(\frac{\mu}{2c} \right)^2 + r \left(\frac{\mu}{c} + r \right) \sin^2 \phi \right]^{1/2} - \frac{\mu}{2c} \quad (2)$$

where

ϕ = the angle between the selenocentric radius vector and velocity vector

$c = \frac{1}{2} v^2 - \frac{\mu}{r}$, the hyperbolic orbital energy.

Now, for no change in the geocentric inclination or energy and small displacements of the aimpoint, the geocentric flight path angle and velocity at the MSI will not change significantly. Therefore, the selenocentric velocity will be approximately equal in magnitude and parallel to its direction at the aimpoint for a RST. As a result, the moon-centered flight path angle, ϕ , will be nearly equal to the angle between the RST aimpoint and the actual aimpoint. Equation 2 can now be written

$$r_p = (A^2 + B \sin^2 \alpha)^{1/2} - A \quad (3)$$

where A and B are taken as constant and α is the angular displacement of the aimpoint from the RST aimpoint. While the argument so far presented is easiest to visualize for trajectories in the MOP, it is valid for all trajectories.

It is a simple geometric problem to show that the selenocentric trajectory plane must pass through both the actual aimpoint and the RST aimpoint for the same geocentric inclination and energy. The hyperbolic velocity vector is approximately parallel to the rectilinear velocity vector. If they were exactly parallel, they would define a plane which contains the moon's center, the RST aimpoint, the actual aimpoint, and consequently, the radius vector to the hyperbolic aimpoint. The hyperbolic orbit plane is defined by the orbit radius and velocity vectors and is, therefore, coincident with the first plane, defined by the two parallel vectors. Therefore, the orbit plane contains the RST aimpoint. The two velocity vectors are, however, only approximately parallel and the orbit plane will only approximately pass through the RST aimpoint. As the geocentric energy approaches its lower limit, the velocity vectors become less and less parallel, so the approximation becomes less and less accurate.

Thus, the aimpoint loci for trajectories with a given geocentric energy, eccentricity, inclination, and radius of periselene should be a circular curve separated from the RST aimpoint by the angle α of Equation 3. The resulting selenocentric orbit planes are defined by the RST aimpoint and the actual aimpoints. Results from a typical case are shown in Figure 10. The actual curve is elliptical rather than circular and the plane traces do not quite contain the RST aimpoint. The deviation from the prediction is caused by the non-parallel nature of the RST and hyperbolic velocity

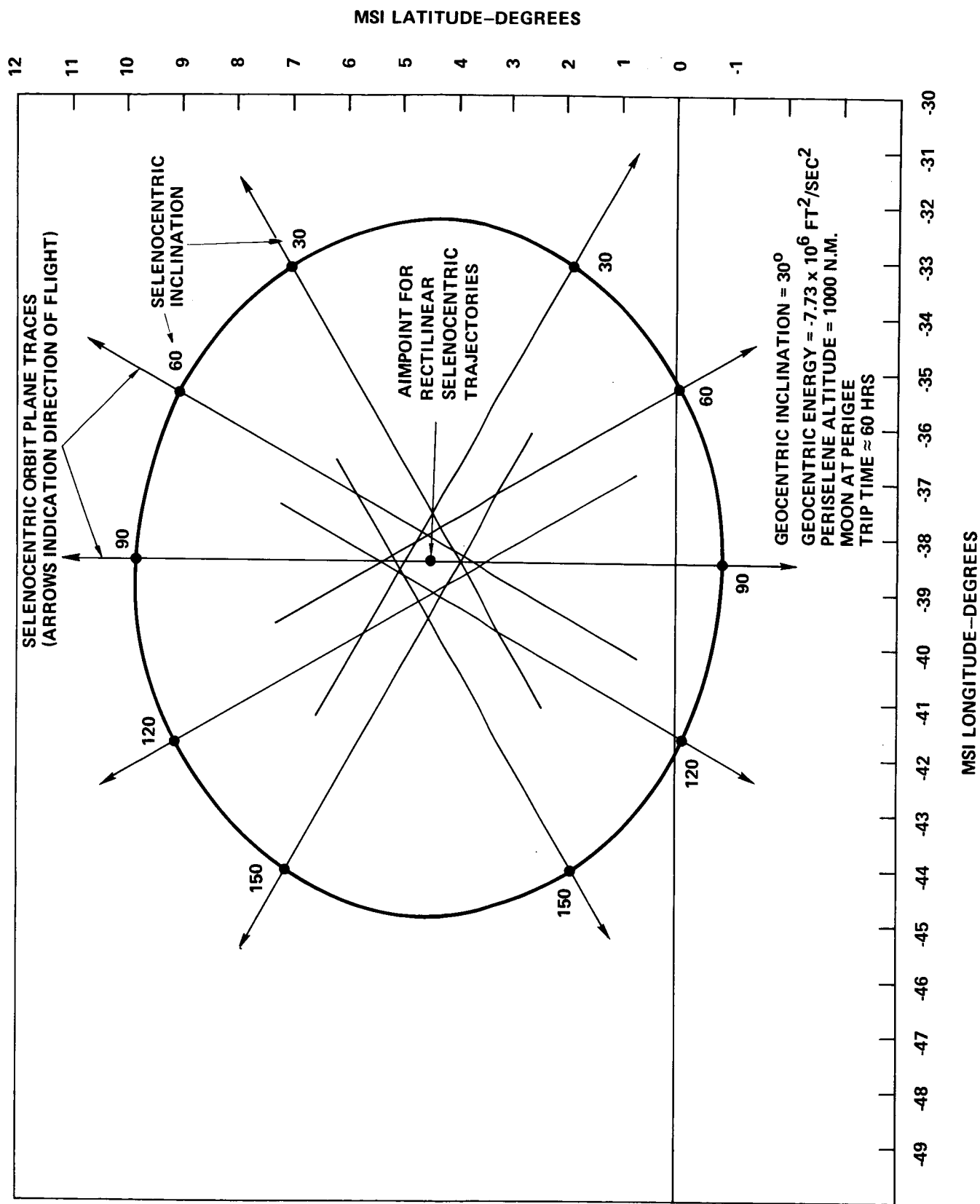


FIGURE 10 - MSI AIMPOINTS AND RESULTING ORBIT PLANE TRACES AND FLIGHT DIRECTIONS

vectors. Aimpoint loci for different radii of periselene will be a set of concentric curves as shown in Figure 11. The loci for constant selenocentric inclination are seen to be straight lines radiating from the RST aimpoint. Note on Figure 10 and 11 that there are two solutions for a given inclination, the ascending node of these solutions differing by approximately 180° .

MSI Aimpoint Maps

In order to complete the picture of the aimpoint that has been built up, Figure 10 has been made into an overlay (Figure 12b) and combined with Figure 6, redrawn as Figure 12a. In addition, a plot of constant selenocentric inclination contours has been added (Figure 12c). Viewing the overlay, the symmetry of the aimpoint region for a fixed trajectory energy is emphasized. In Figure 12a, the aimpoint for pure rectilinear trajectories lies at the approximate center of the locus of aimpoints for a non-zero radius of perigee and a rectilinear selenocentric trajectory, as initially shown in Figure 6. Each point on the RST aimpoint locus, representing a trajectory with a particular geocentric inclination, lies at the center of the locus of aimpoints for trajectories with the same geocentric inclination and a non-zero radius of periselene, as shown in Figure 12b (initially shown in Figure 10). Each point on this second locus represents a particular selenocentric inclination. Figure 12c is a joining of aimpoints for constant values of selenocentric inclination and here again, elliptical curves result. There are two loci on Figure 12c for a given inclination, the ascending nodes of the two loci differing by approximately 180° . The plots in Figure 12 have been expanded in Figures 25 to 54 to include selenocentric longitude of the ascending node, geocentric longitude of the ascending node and argument of perigee and to cover a series of energies and lunar positions. The plots are all for a perigee altitude of 100 N.M. and a periselene altitude of 60 N.M. The radius of the MSI was taken as 1.8×10^8 feet (consistent with BCMASP). Energies have been chosen to roughly correspond to 60 and 90 hour trips to the moon when it is at perigee and apogee and 90 hour trips to the moon halfway between perigee and apogee on both the ascending and descending legs. It should be emphasized again that the MSI latitude and longitude and the inclinations plotted in these figures are referenced to the MOP.

A note on the reading of these graphs is in order. Since for a given energy, there are generally two possible trajectories through an MSI aimpoint and sometimes four, it was necessary to split the graphs into two sets to prevent them from being completely unreadable. Thus, for every

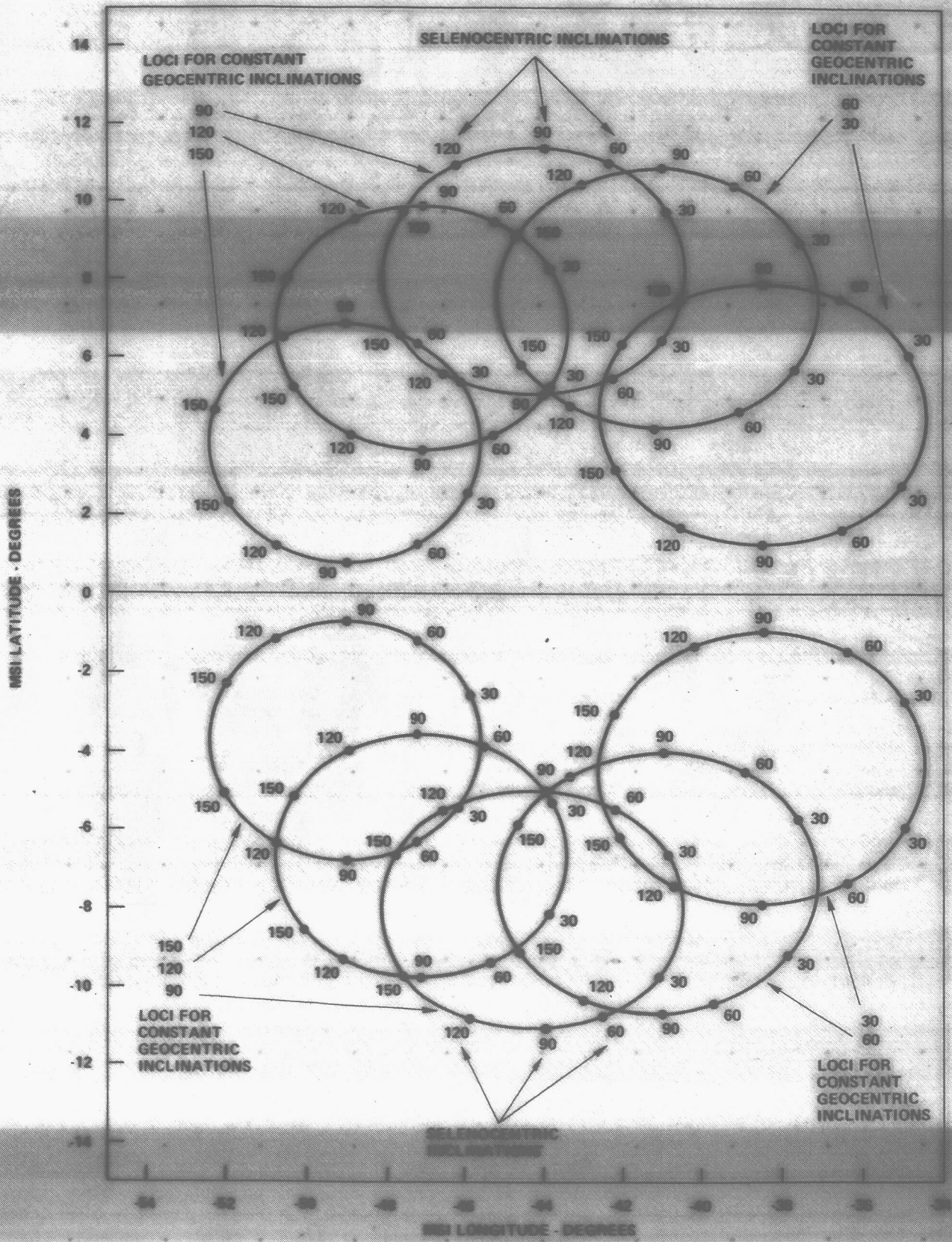


FIGURE 12b

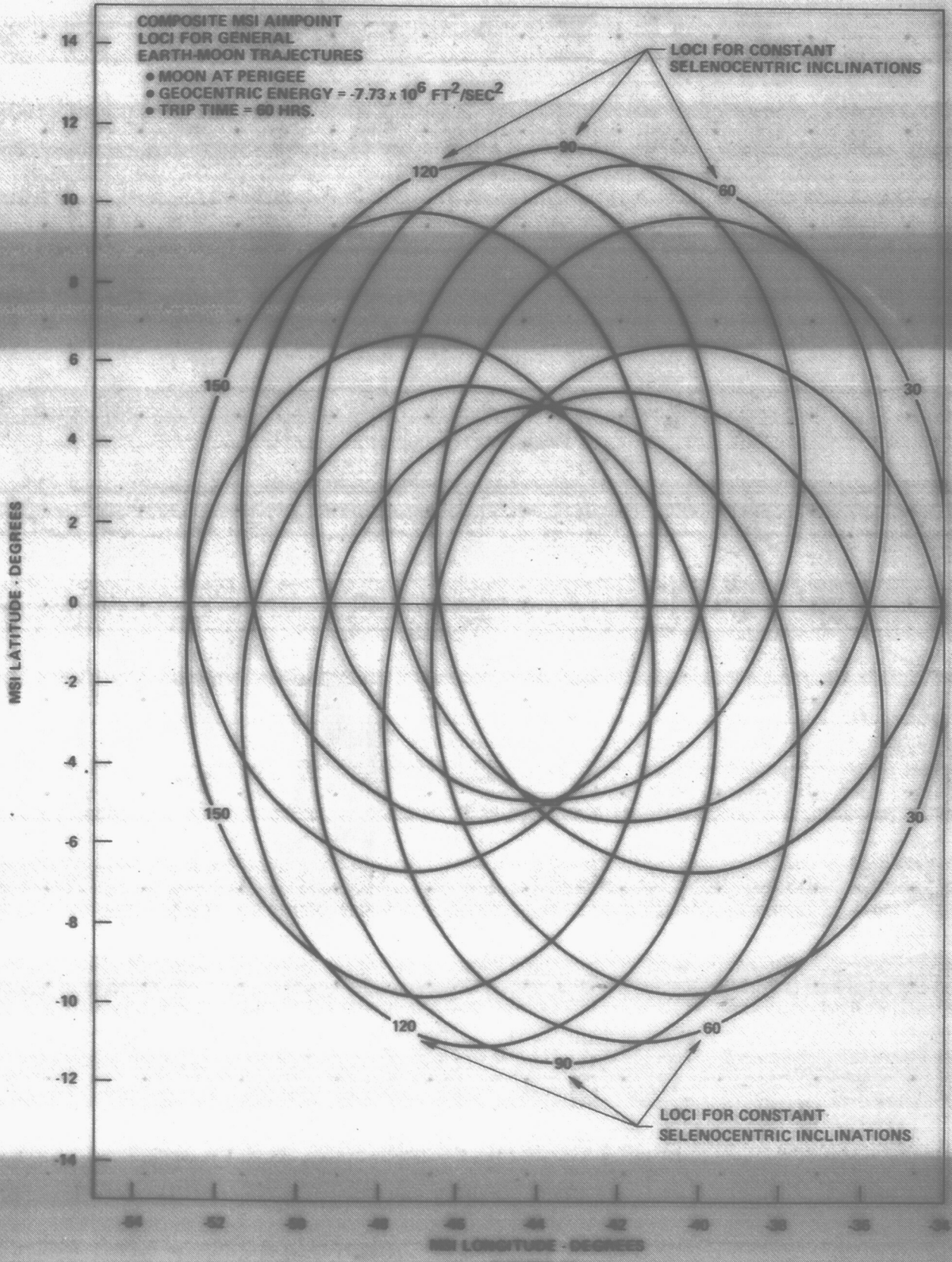
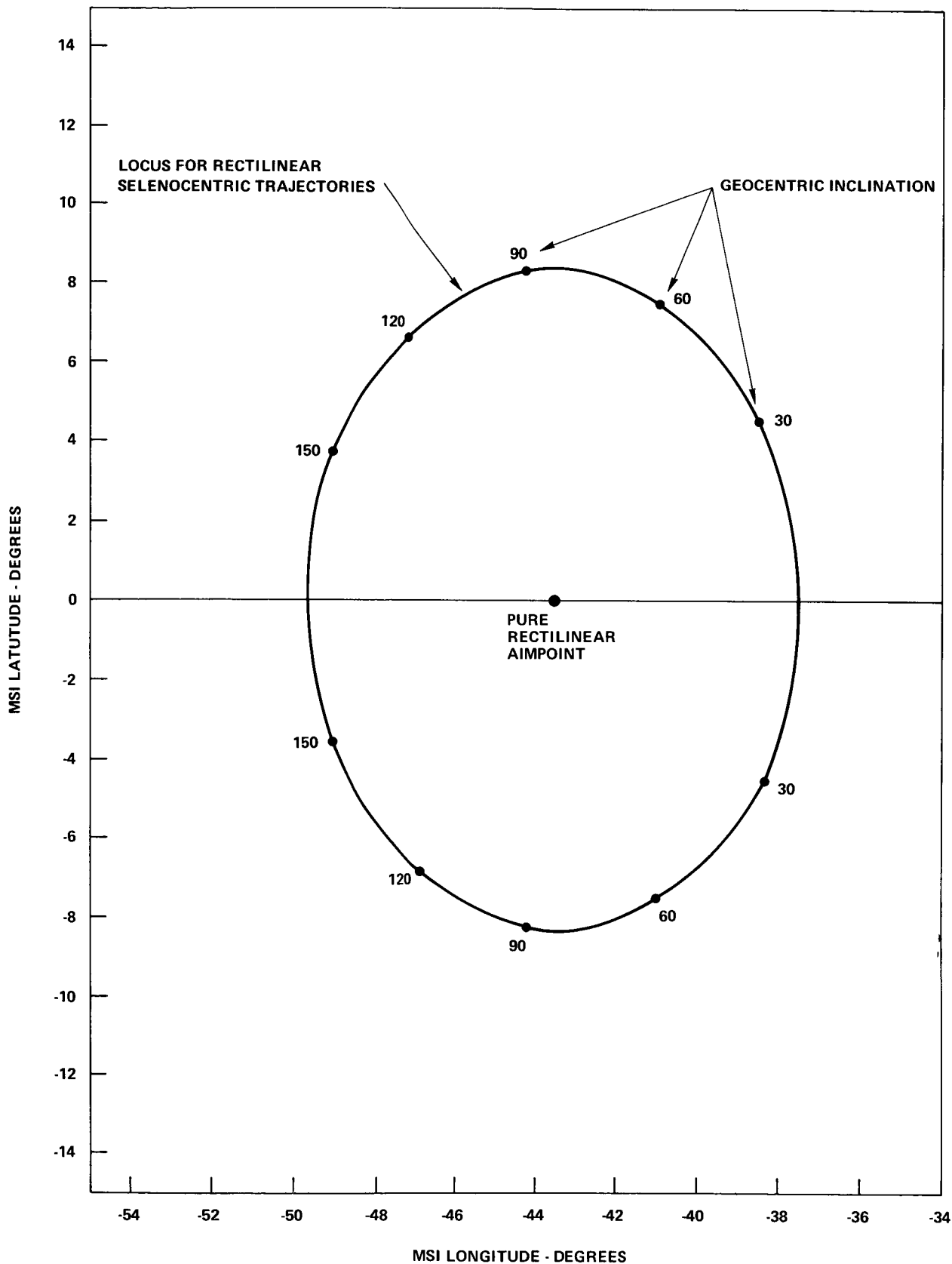


FIGURE 12c



MSI AIMPOINT LOCI INTERRELATIONSHIPS FOR TRANSLUNAR TRAJECTORIES

FIGURE 12a

translunar energy, there are two plot sets, labelled A and B, and any trajectory solution must be taken from only one of the sets, i.e., all points must be taken from set A only or set B only. Even so, the contours on the maps for low energy trajectories cross over one another. In these areas, care must be taken in order to avoid false solutions.

Targeting a Landing Mission

The information on these graphs is sufficient to roughly demonstrate the problem of targeting a lunar landing mission. To simplify the problem, assume that the selenographic coordinate system and the MOP coordinate system are aligned at the time of MSI entry. Also, assume no plane change occurs at lunar orbit insertion and that the trajectory constraints assumed for the plots match the mission. As a demonstration problem, consider a mission to Copernicus (10° N, 20° W).

The site defines a point on the lunar surface which must be in the orbit plane at the time of landing. Consequently, a unique relationship between the inclination and the longitude of the ascending node of the orbit plane is defined as follows:

$$\sin(\text{Long.} + Nt - s) = \tan(\text{Lat.}) \cot(i_s), \quad (4)$$

where i_s = inclination

Ω_s = longitude of the ascending node

N = rate of lunar rotation

t = time from MSI entry to landing

Long = longitude of the site

Lat = latitude of the site

The Nt term accounts for the rotation of the moon between the time of MSI entry and landing. In this case, assume 14 hours as a typical time from MSI entry to lunar orbit insertion and 10 hours waiting time in lunar orbit. The total time from MSI entry to landing then is roughly 24 hours. The average rotational rate of the moon is .549 degrees per hour. Thus,

Equation 4 becomes

$$\sin(6.82^\circ + \Omega_s) + .17633 \cot i_s = 0, \quad (5)$$

taking west longitude as negative. Figure 13 is a plot of this relationship.

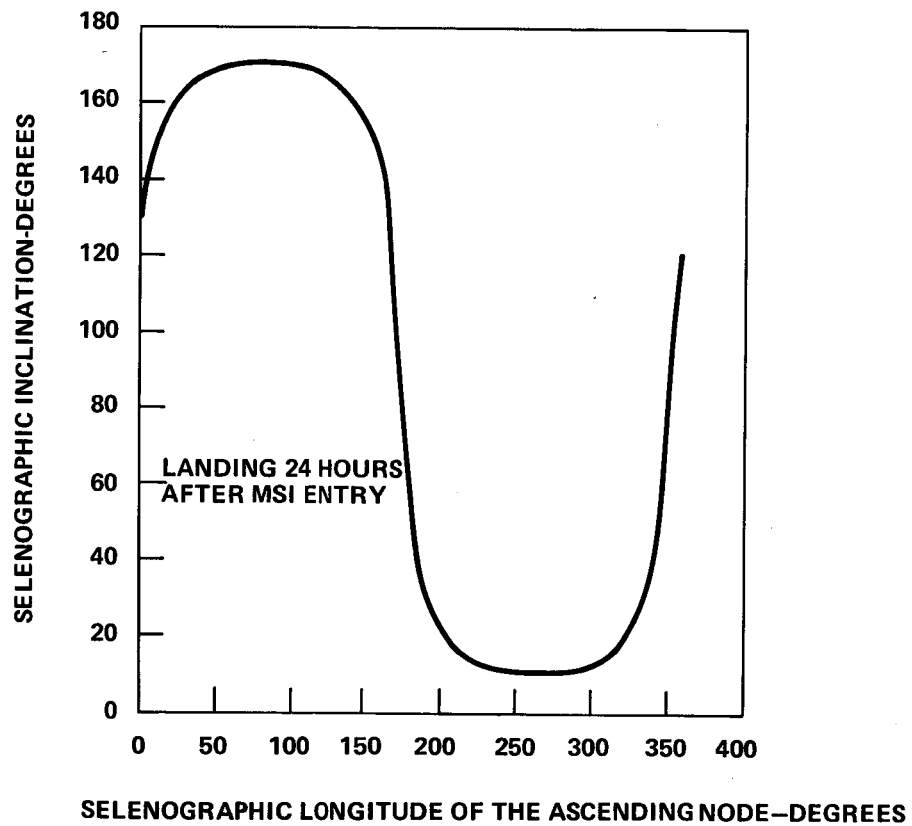


FIGURE 13 - PLANE ORIENTATION FOR A NO PLANE CHANGE LANDING AT COPERNICUS

Comparing the required orbit orientation curve with the aimpoint maps of selenocentric inclination and Ω_s provides the aimpoint loci required to land at Copernicus without a plane change at lunar orbit insertion. Comparison of these loci with the geocentric inclination, node, and argument of perigee maps defines the set of geocentric transfer trajectories. The results of this analysis can be seen in Figure 14 with the resulting orbital elements noted on the loci. In this example, the aimpoint loci is seen to be two separate curves. One curve, B, yields posigrade trajectories. Both curves have a segment requiring posigrade geocentric trajectories and a segment requiring retrograde trajectories. Figure 15 presents the site approach paths to Copernicus produced by the aimpoint loci of Figure 14. Now one can apply any additional constraints on the mission. For example, if only retrograde lunar orbits are of interest, only aimpoint locus A is of use. If, in addition, the geocentric inclination is restricted to less than 57.2° ,* more than half of locus A cannot be used, limiting the range of approach azimuths. The study can be repeated for different geocentric energies and lunar positions to determine the full range of possible trajectories. If the conditions allowed in these analyses are not satisfactory, a plane change at lunar orbit insertion will be required.

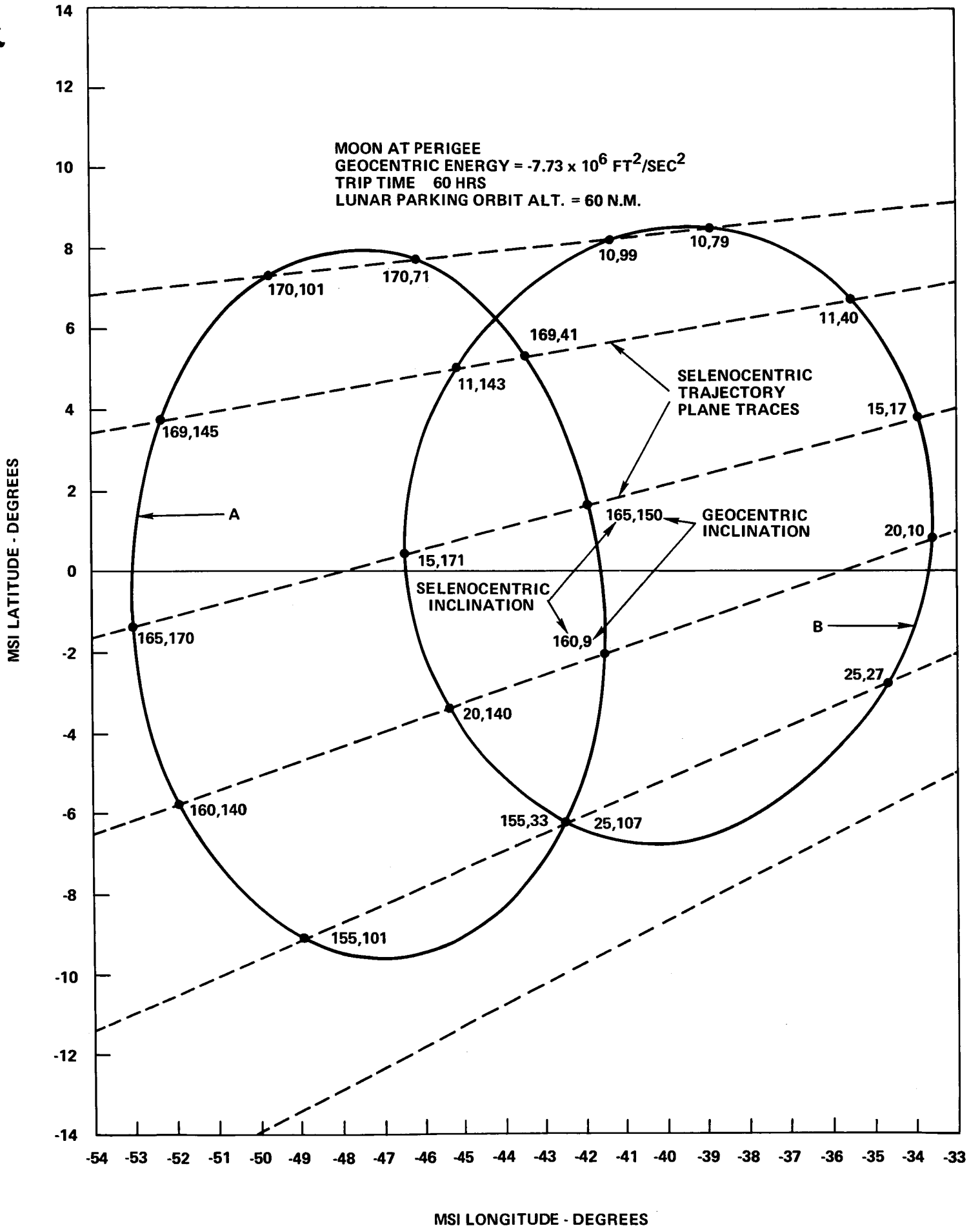
RETURN TRAJECTORIES

The analyses of trajectories from the earth to the moon is directly applicable to the study of trajectories from the moon to the earth, and the results are essentially identical. Figure 16 shows the symmetry of translunar and trans-earth MSI patch points for trajectories in the MOP. Indeed, the aimpoint maps of Figures 26 to 55 may be used as exit point maps, though care must be used in selecting the proper sign of the results. The MSI latitude and longitude change signs, as do the geocentric and selenocentric longitudes of the ascending node and the geocentric argument of perigee. The geocentric and selenocentric inclinations do not change sign.

Free Return Trajectories

A free return trajectory may be defined as a trajectory to the moon, which, after its encounter with the moon,

*The maximum inclination obtainable with a due eastward launch from Cape Kennedy.



MSI LONGITUDE - DEGREES

FIGURE 14

MSI AIMPOINT FOR A LANDING AT COPERNICUS (10°N., 20°W.)

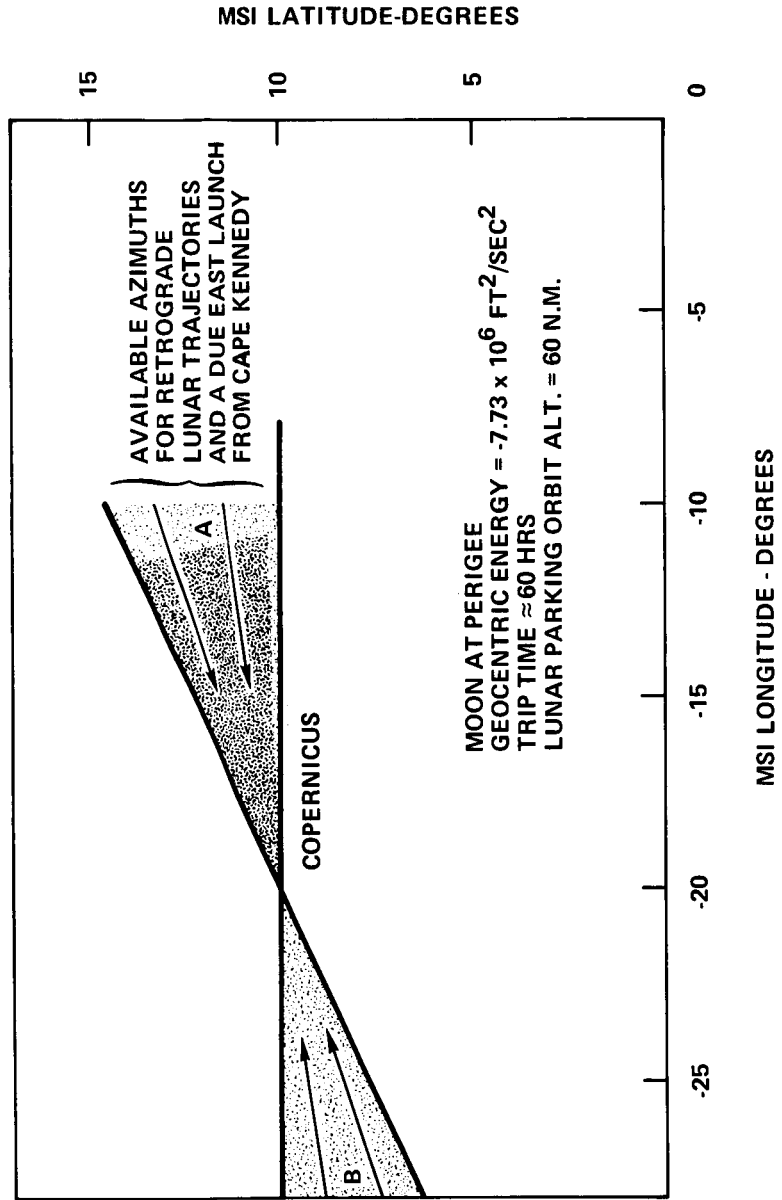


FIGURE 15 - AVAILABLE APPROACH AZIMUTHS FOR A LANDING AT COPERNICUS

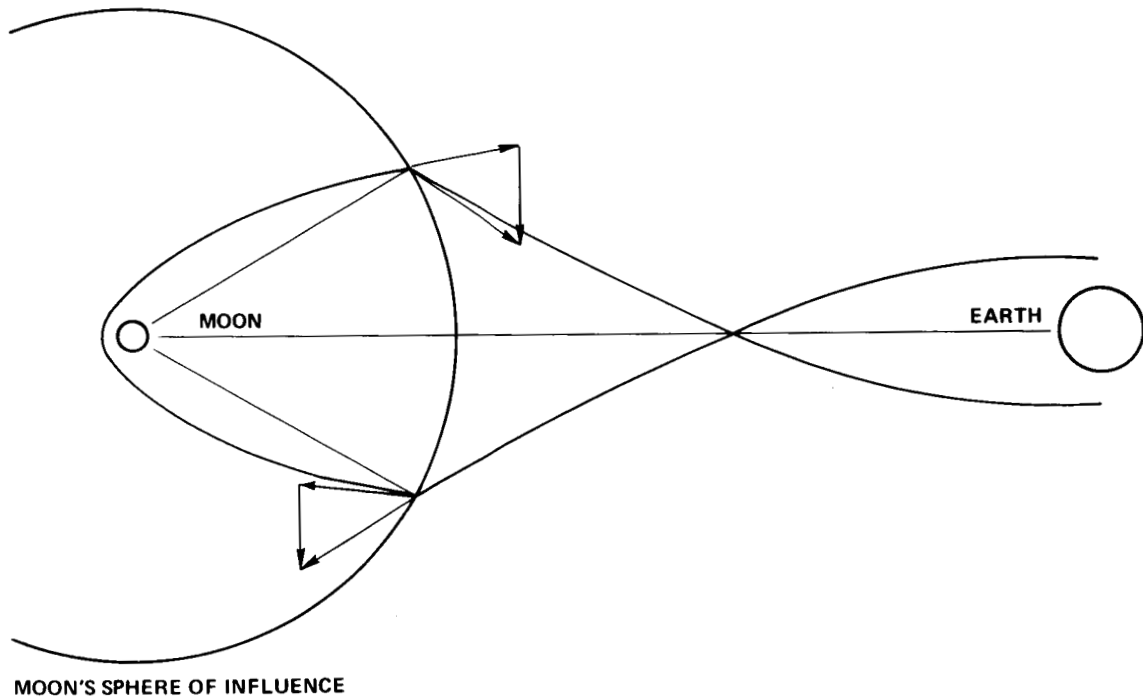


FIGURE 16 - TRANSLUNAR AND TRANSEARTH TRAJECTORIES WITH EQUAL ENERGIES, AND EQUAL PERISELENE AND PERIGEE RADII

will return to the vicinity of the earth in some prescribed fashion and without the use of any powered maneuvers. By this definition, they may be considered to consist of a combination of a translunar and a transearth trajectory which have identical selenocentric orbital elements and the same time of periselene passage.

The previous sections of this study have shown the relationship between translunar or transearth trajectory parameters and MSI entry or exit points. The selenocentric portion of the trajectory must provide the proper "turn angle", ψ_s , to match the translunar and transearth MSI entry and exit points as shown in Figure 17. The turn angle may be expressed as

$$\psi_s = 360 - 2 \cos^{-1} \left\{ \frac{1}{e} \left[\frac{a_s (e^2 - 1)}{r_{MSI}} - 1 \right] \right\} \quad (6)$$

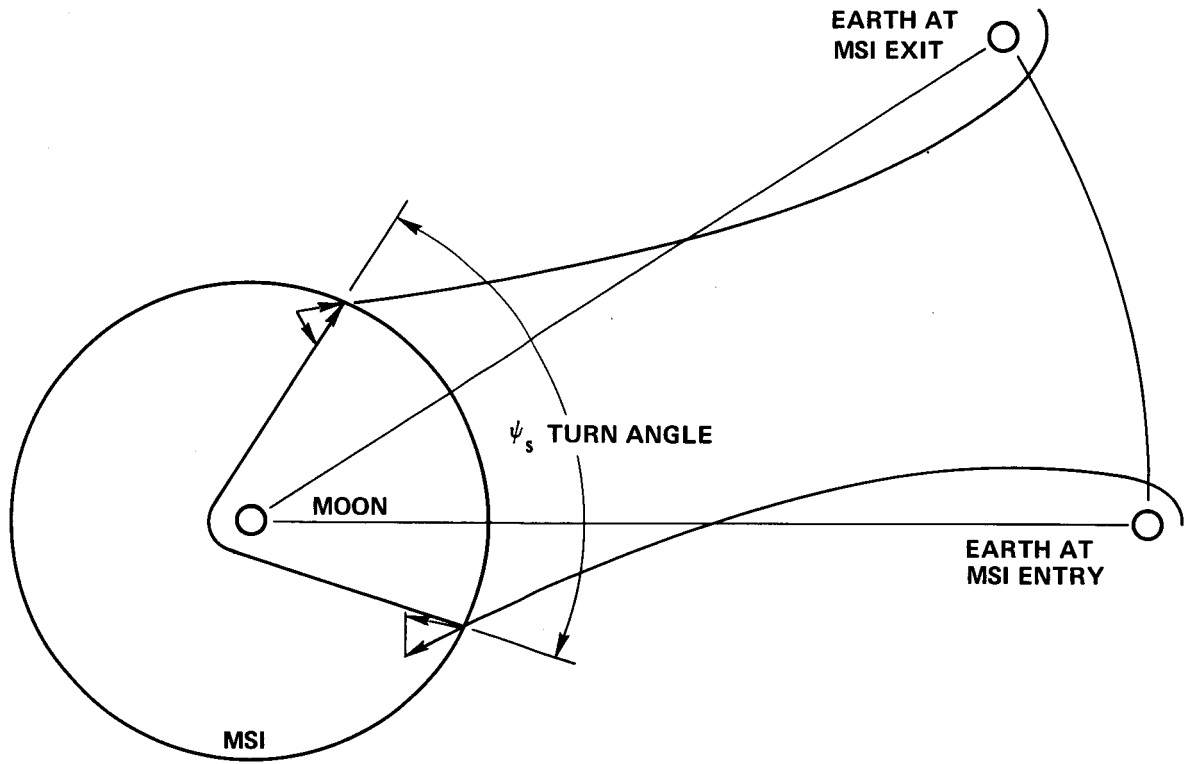


FIGURE 17 - A FREE RETURN TRAJECTORY

where

$$e = \frac{r_{ps}}{a_s} + 1$$

and

a_s = selenocentric semi-major axis

r_{ps} = radius of periselene

r_{MSI} = radius of the MSI

that is, the turn angle is a function of selenocentric energy and radius of periselene only.

Figure 18 presents a graphical solution for a free return trajectory using an MSI entry and exit point map. The initial conditions of the problem presented are fixed translunar and transearth perigee radii, periselene radius, translunar inclination and energy, and time of MSI entry. The solution to the problem goes as follows:

1. From the given geocentric translunar energy, the pure rectilinear entry point is established (i.e., the entry point for trajectories which ascend vertically on the earth and descend vertically to the moon).
2. From the given translunar perigee radius, the RST aimpoint locus is established (i.e., the aimpoint locus for trajectories with rectilinear selenocentric positions).
3. From the given translunar geocentric inclination, which is derived from the launch azimuth and lunar declination, the RST entry point for this case is found.
4. From the given radius of periselene, the true entry point locus is drawn around the RST entry point.
5. The traces on the MSI of possible selenocentric trajectory planes may be drawn, remembering that they approximately pass through the RST entry point. Since the selenocentric plane must pass through the MSI exit point, the range of selenocentric planes is limited.
6. Since the selenocentric energy is constant, the exit selenocentric velocity and flight path angle will be constant. Since only a small range of selenocentric inclinations is possible and exit point longitude does not vary greatly, it is sufficiently accurate for this analysis to say that geocentric transearth energy is constant. Then the pure rectilinear exit point for that energy can be found. (It would be laborious to actually do this).

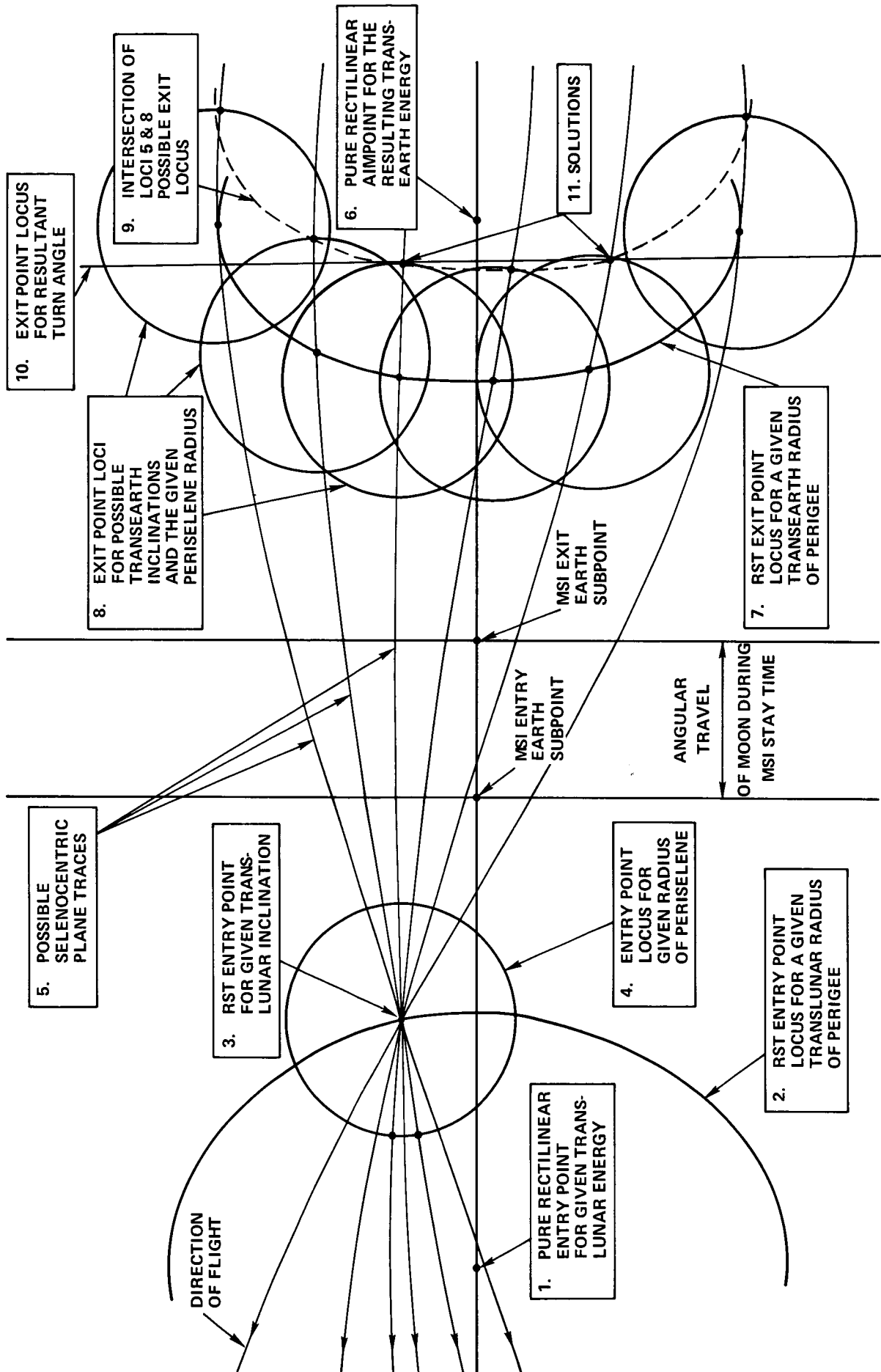


FIGURE 18 - FREE RETURN TRAJECTORY ANALYSIS

7. The RST exit locus for the desired transearth perigee radius may now be drawn about the pure rectilinear exit point.
8. The selenocentric plane trace must pass through the RST exit point for the transearth trajectory geocentric inclination associated with it. Thus, each intersection of the RST exit point locus with a possible plane trace defines the center of a locus of exit points for the given periselene radius.
9. The selenocentric orbit must exit then at the intersection of its plane trace (step 5) and the matching locus of step 8. The points of locus 9 are the required exit points.
10. The exit points must also satisfy the turn angle obtained from Equation 6. The locus of possible exit points satisfying the turn angle condition is obtained by measuring off this angle on the selenocentric plane traces. The selenocentric energy required by Equation 6 may be obtained from the geocentric translunar energy and inclination and aimpoint longitude, though it would be laborious. For the purpose of this study it is sufficient to note that since entry point longitude is nearly constant, selenocentric energy is nearly constant. The exit point locus is roughly a vertical straight line on the scale of the figure.
11. Steps 9 and 10 produce two exit loci, both of which must be satisfied to have a solution to the free return problem. Thus, the intersections of lines 9 and 10 on the figure are valid solutions.

Since there are two possible entry point loci for a given translunar geocentric inclination, one above and one below the MOP, there will be two more solutions in addition to those just found. In summary, if the values of:

- i) geocentric translunar energy
- ii) geocentric translunar inclination
- iii) translunar perigee radius
- iv) periselene radius
- v) transearth perigee radius

are fixed, four distinct solutions for the free return problem exist. Figure 19, which was originally produced in Reference 1, presents a perspective view of the four solutions (with assumed posigrade transearth portions).

It should be noted that while the five parameters listed above are nominally independent, in fact, they interact and produce limitations on one another. Since the MSI entry and exit regions must be separated by the "turn angle" of the selenocentric portion of the trajectory, only those combinations of perigee radii, periselene radius, and energy which produce intersections of loci 9 and 10 on Figure 18 will be free return trajectories. As a consequence, if the perigee radii and periselene radius are fixed by mission constraints, only a narrow band of energies are available to the mission planner for free return trajectories. Figures 20 and 21 show the approximate ranges of translunar energy and turn angle which will produce free return trajectories* for different lunar positions. Since the range of free return translunar energy is limited, the range of possible free return trip times is also limited. Figure 22 shows the variation of trip time (from translunar perigee to periselene) with energy for general translunar trajectories (both free and non-free return). Comparison of Figure 22 with Figure 20 gives a free return trip time range of 63 to 78 hours during a lunar month.

The available range of selenocentric inclinations is also severely limited. From Figure 18, it can be seen that the maximum MSI entry and exit latitudes are about the same as the maximum latitude attained by the RST loci for entry and exit. Figure 8 shows that this is always less than 11° . The relationship between turn angle and MSI entry and exit latitude is shown in Figure 23. Since the maximum turn angle from Figure 21 is 91° , the maximum inclination is approximately 15° (or, more correctly 165° , since the trajectory is in the retrograde sense).

*For this example, trajectories with equal translunar and transearth perigee radii and energies were used due to their ease of calculation. For the same reason, only trajectories lying in the MOP were calculated. Comparison was made of Figure 2D with a number of BCMASP generated free return trajectories which meet Apollo atmospheric entry requirements. The energies in Figure 21 are from 10% to 25% lower than the BCMASP trajectory energies.

CROSS-HATCHED AREAS LIE BELOW THE MOON'S ORBIT PLANE
SHADED AREAS LIE ABOVE THE MOON'S ORBIT PLANE

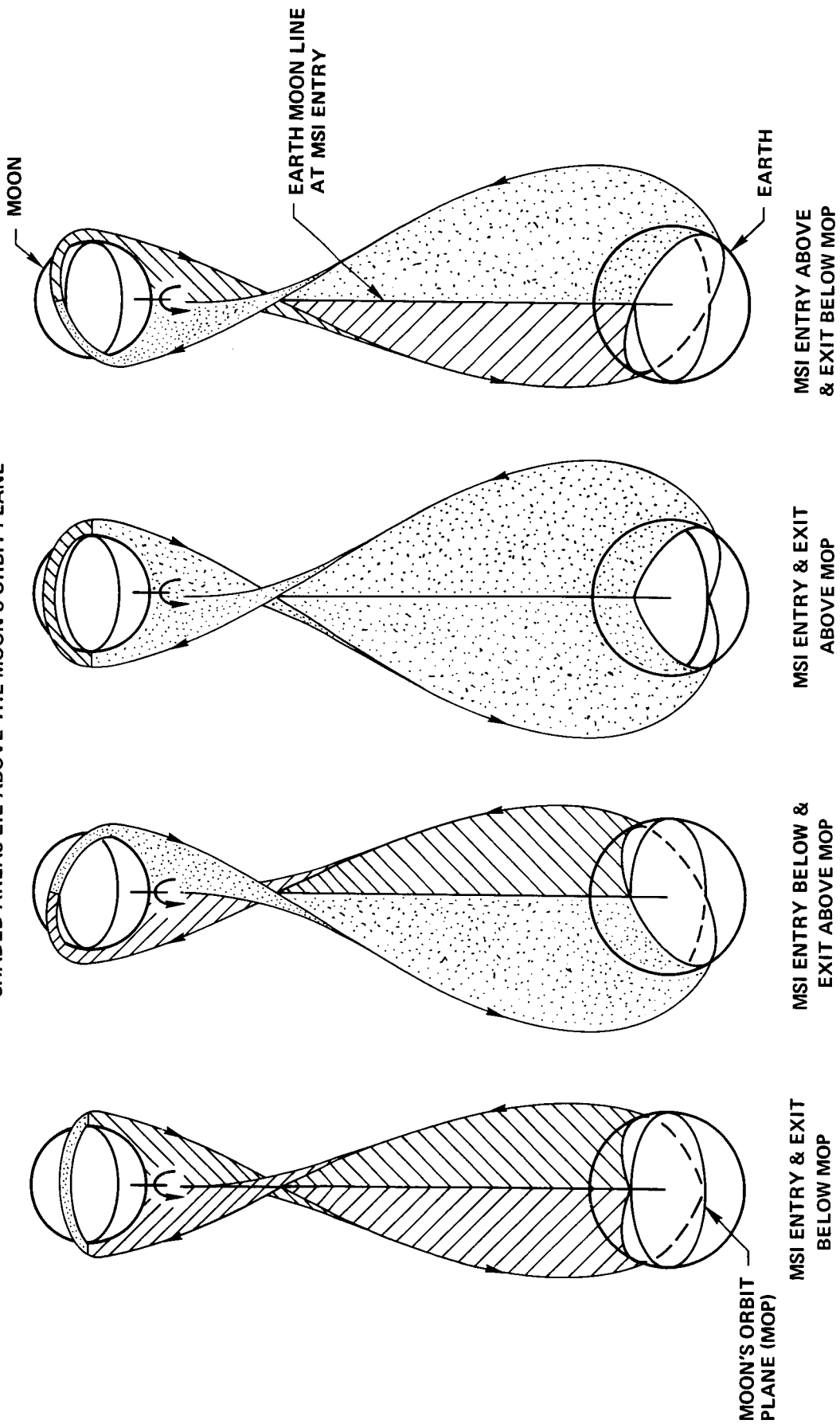


FIGURE 19 - FREE RETURN TRAJECTORY CONFIGURATIONS

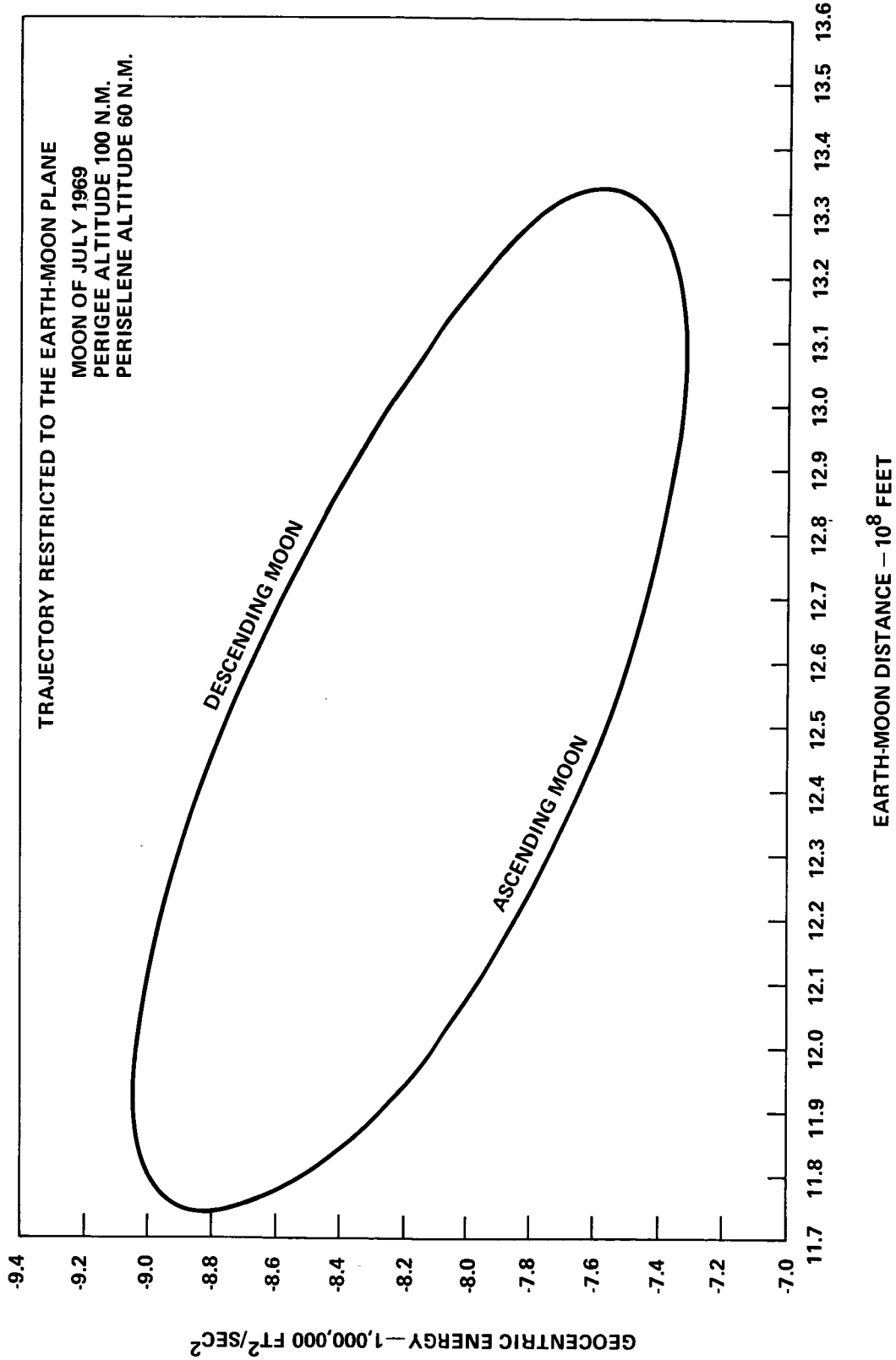


FIGURE 20 - FREE RETURN ENERGY FOR EQUAL TRANSLUNAR AND TRANSEARTH ENERGY AND PERIGEE RADIUS

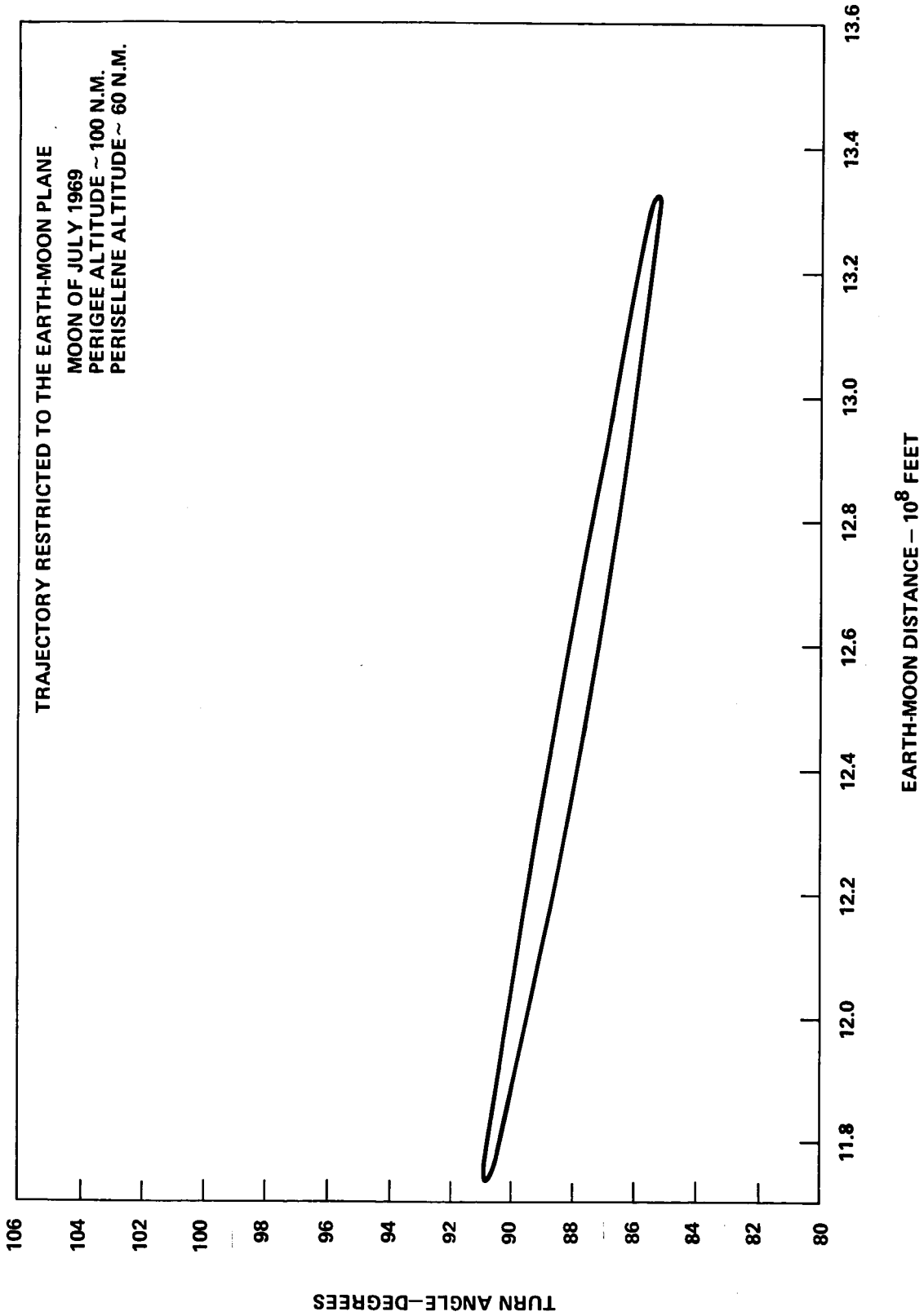


FIGURE 21 - FREE RETURN TURN ANGLE FOR EQUAL TRANSLUNAR AND TRANSEARTH ENERGY AND PERIGEE RADIUS

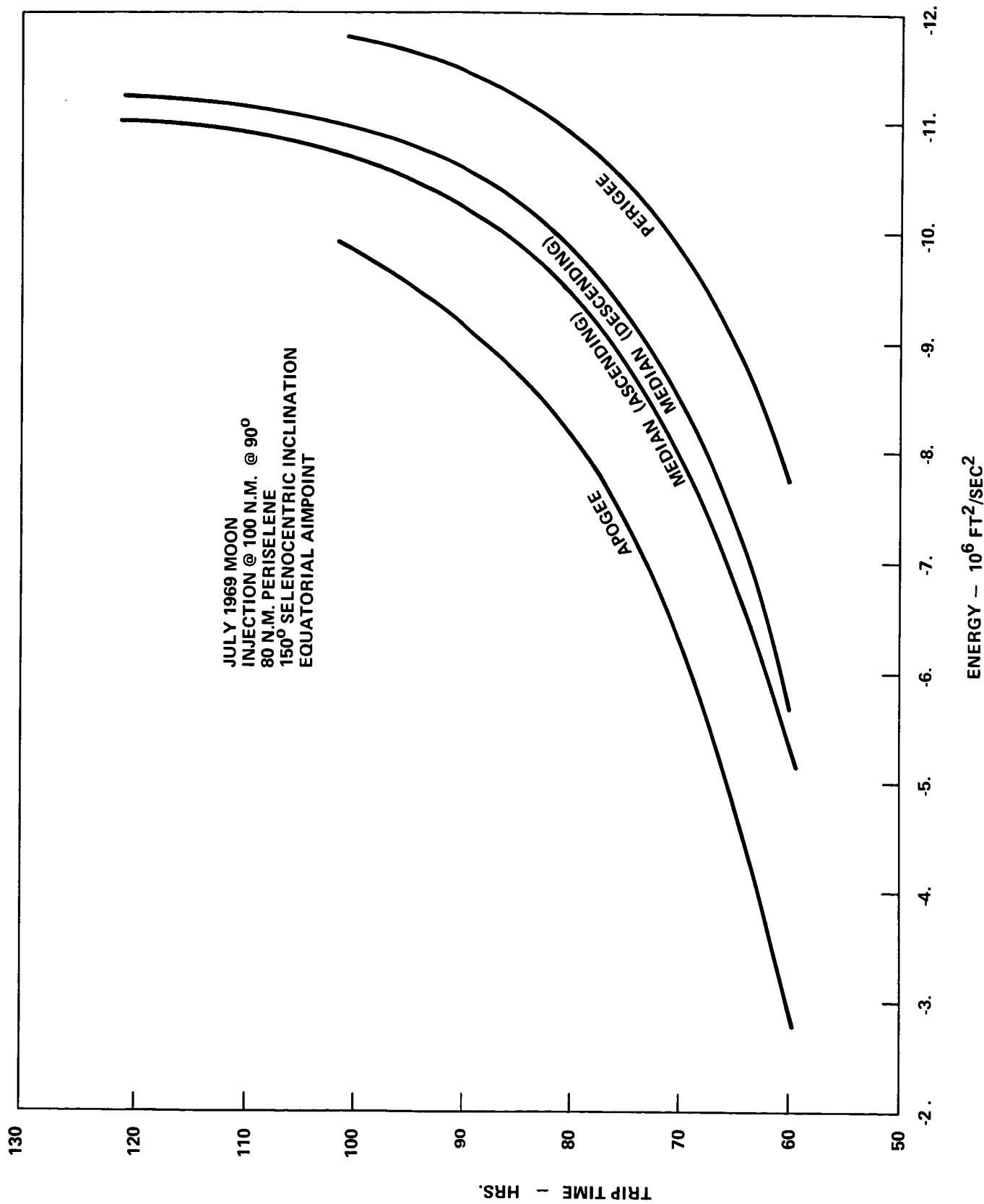


FIGURE 22 - TRANSLUNAR TRIP TIME VS. GEOCENTRIC ENERGY

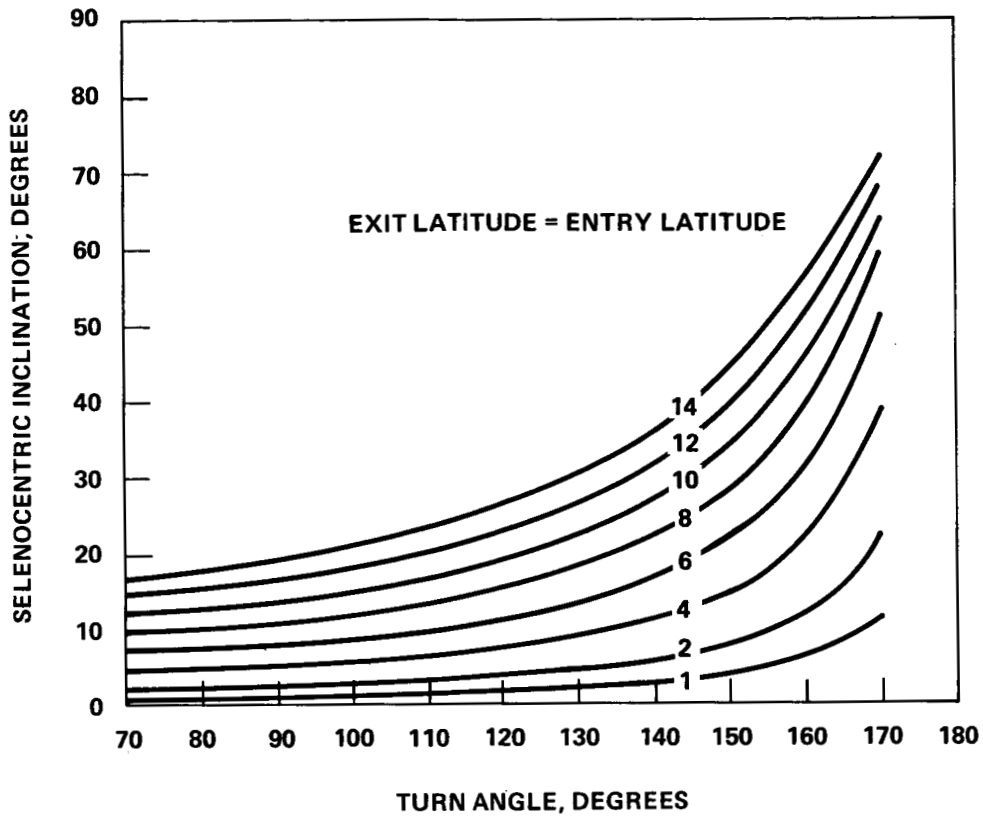


FIGURE 23 - SELENOCENTRIC INCLINATION VS TURN ANGLE FOR VARIOUS MSI ENTRY/EXIT LATITUDES

The range of selenocentric inclination available can be influenced by changing periselene altitude. Figure 24 shows the variation of turn angle with periselene altitude for free return trajectories of equal translunar and transearth geocentric energy and equal perigee radii. Comparison of Figures 23 and 24 indicates the increase in inclination available. For example, a free return trajectory with a 4000 N.M. periselene altitude to a moon at perigee could have an inclination of up to 24°.

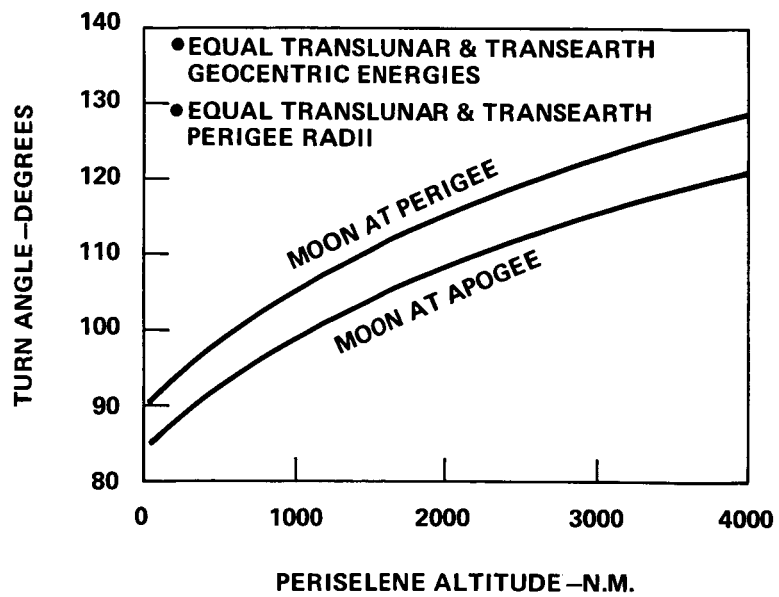
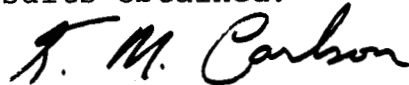


FIGURE 24 - FREE RETURN TURN ANGLE VS PERISELENE ALTITUDE

Summary

This study provides insights into the basic nature of lunar trajectories. The geometry establishing the variation of the aimpoint on the MSI is shown to consist of a set of simple figures, each influenced by a single parameter. The major influencing parameters are geocentric energy, geocentric inclination, radius of perigee and radius of periselene. MSI aimpoint contours for the last three parameters consist of nearly elliptical curves. The aimpoint region is centered on the intersection of the MOP on the MSI and around the aimpoint for pure rectilinear trajectories. MSI aimpoint curves for varying Keplerian elements of the translunar trajectory complete the picture.

These aimpoint curves are not suitable for precision targeting analysis, nor were they intended to be. The true value of this study lies in the demonstration of the functional relationships between significant parameters and their limits, thus providing the analyst with the understanding required to effectively conduct more precise analyses using computer simulations and to interpret the results obtained.



K. M. Carlson

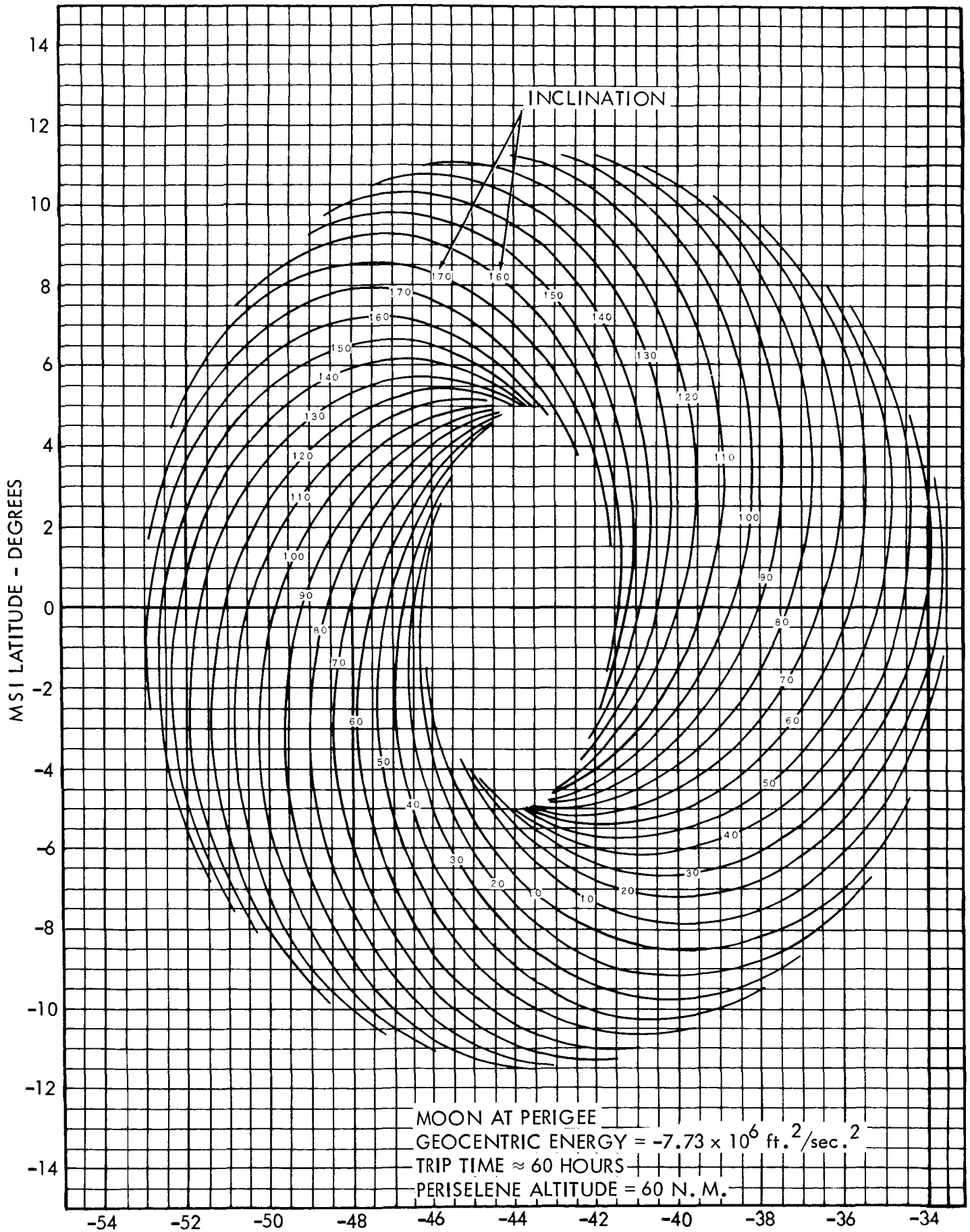
2011-KMC-vh

Attachments
Figures 25A thru 54B

BELLCOMM, INC.

REFERENCES

1. North American Aviation, Inc., "Circumlunar Trajectory Analysis", SID-62-1430, December 14, 1962.
2. Tolson, Robert H., "Geometrical Characteristics of Lunar Orbits Established from Earth-Moon Trajectories", NASA TN-D-1780, April 1963.
3. Roy, Archie E., The Foundations of Astrodynamics, MacMillan, 1965.



MSI LONGITUDE - DEGREES

FIGURE 25A - LOCUS OF MSI AIM POINTS FOR VARIOUS SELENOCENTRIC INCLINATIONS

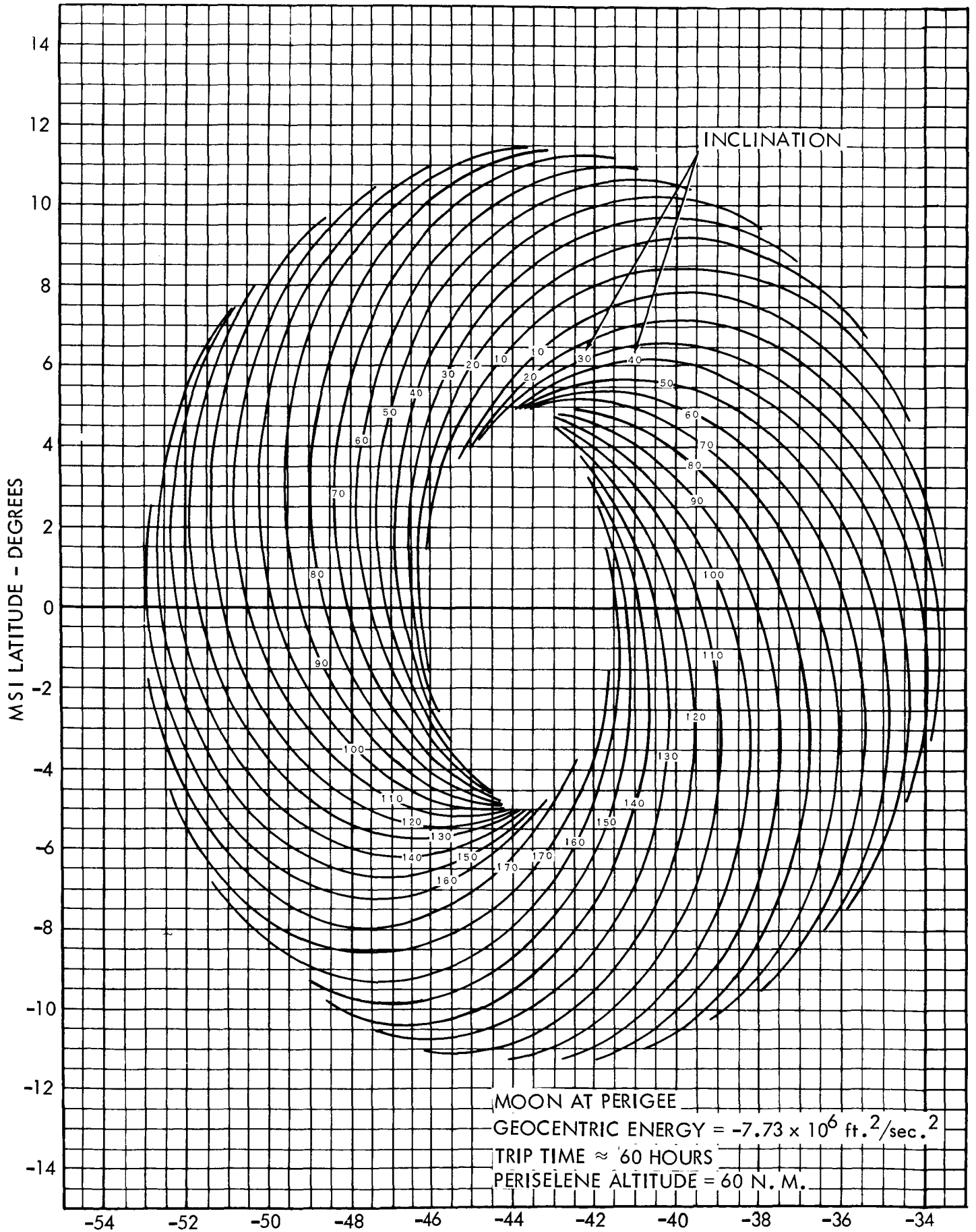
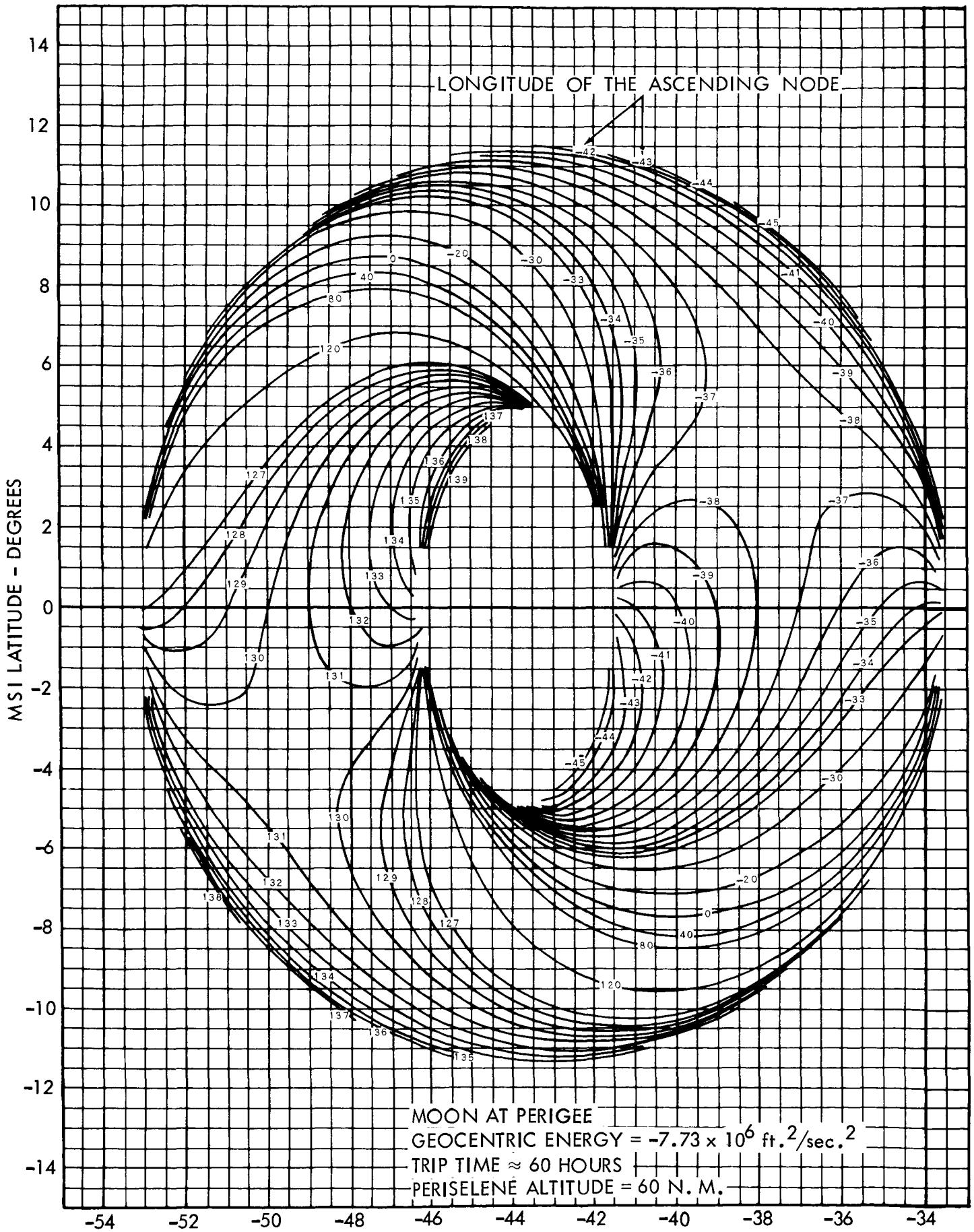
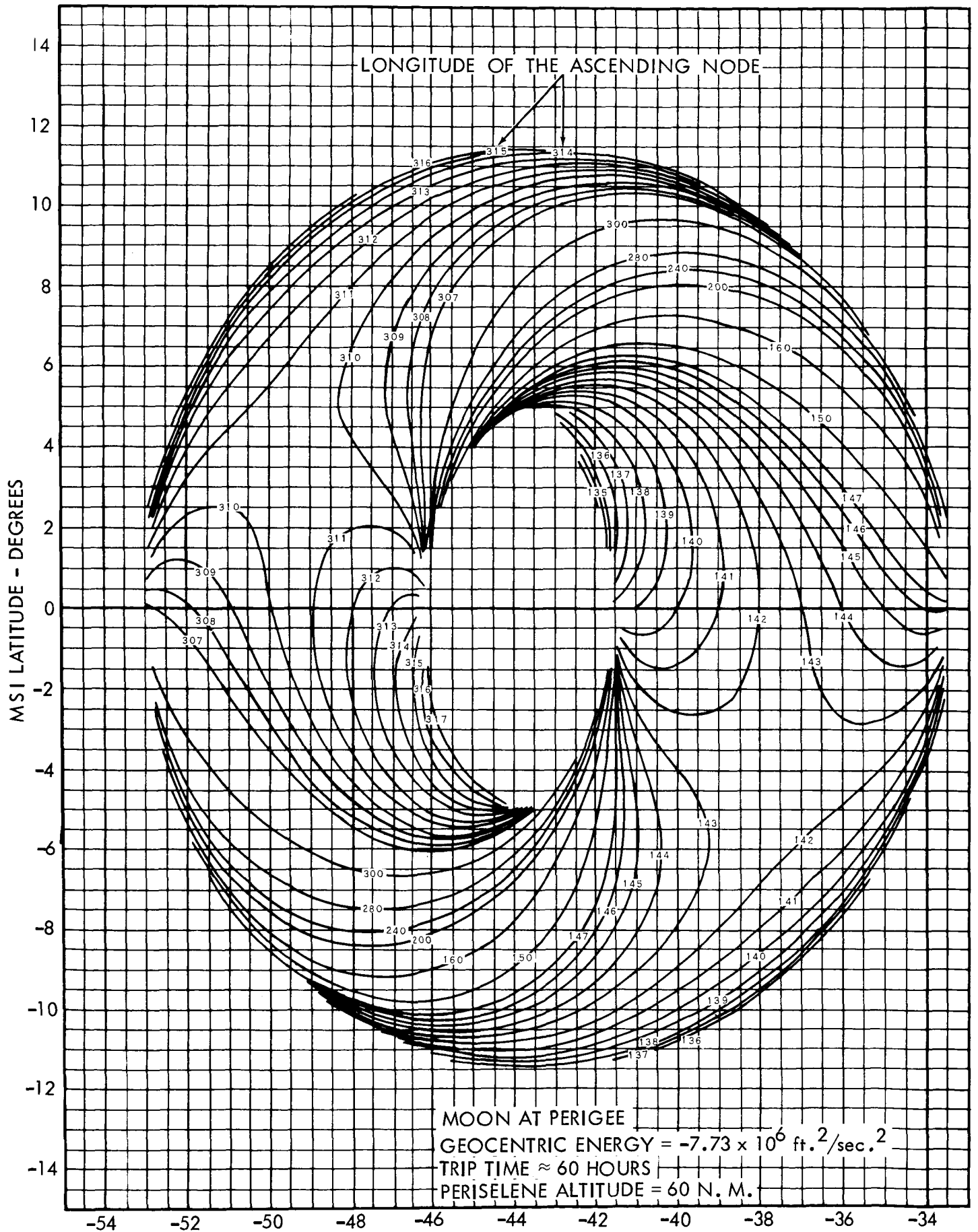


FIGURE 25B - LOCUS OF MSI AIMPOINTS FOR VARIOUS SELENOCENTRIC INCLINATIONS



MOON AT PERIGEE
 GEOCENTRIC ENERGY = $-7.73 \times 10^6 \text{ ft.}^2/\text{sec.}^2$
 TRIP TIME \approx 60 HOURS
 PERISELENÉ ALTITUDE = 60 N. M.

MSI LONGITUDE - DEGREES
 FIGURE 26A - LOCUS OF MSI AIM POINTS FOR VARIOUS SELENOCENTRIC
 LONGITUDES OF THE ASCENDING NODE



MSI LONGITUDE - DEGREES
**FIGURE 26B - LOCUS OF MSI AIM POINTS FOR VARIOUS SELENOCENTRIC
 LONGITUDES OF THE ASCENDING NODE**

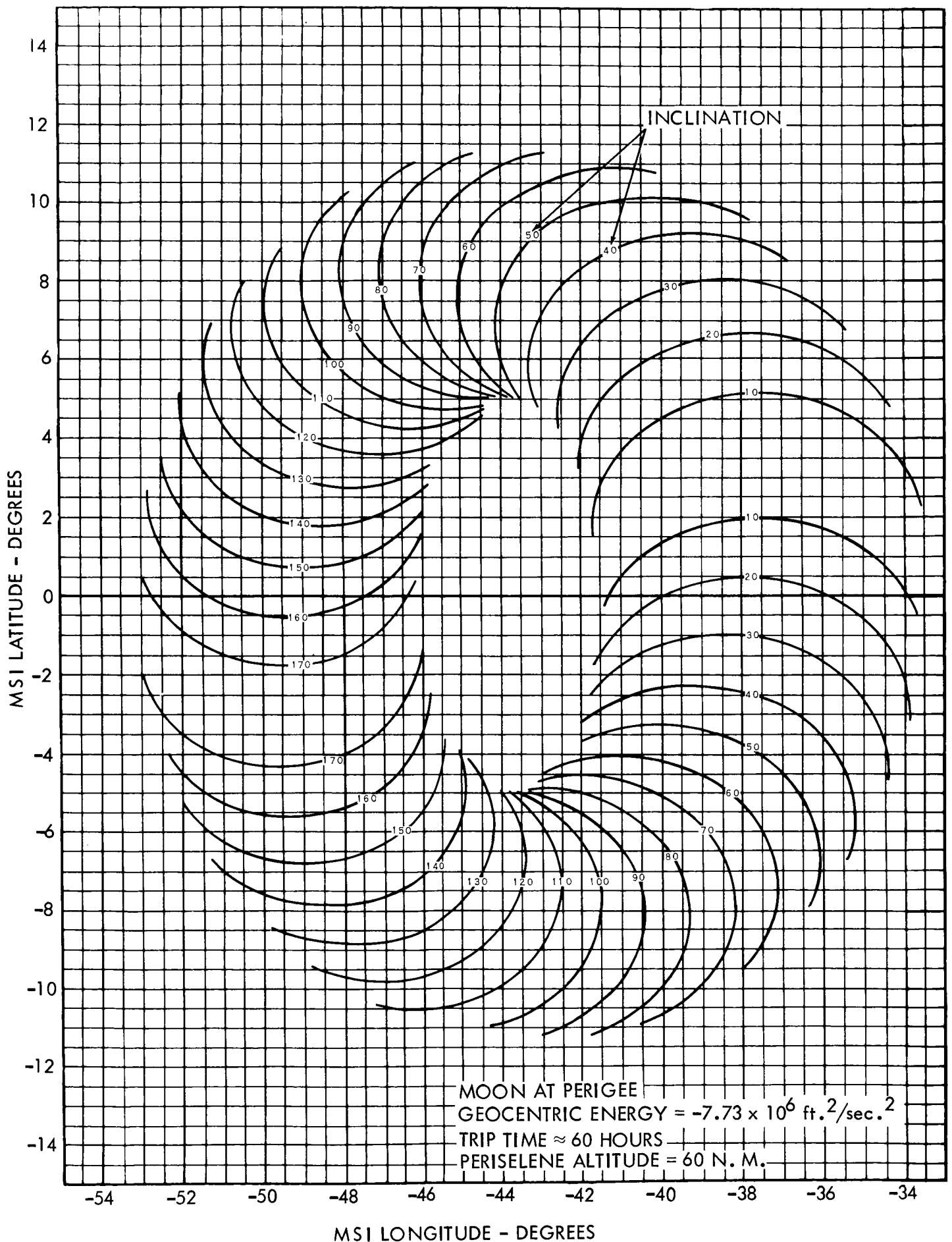


FIGURE 27A - LOCUS OF MSI AIM POINTS FOR VARIOUS GEOCENTRIC INCLINATIONS

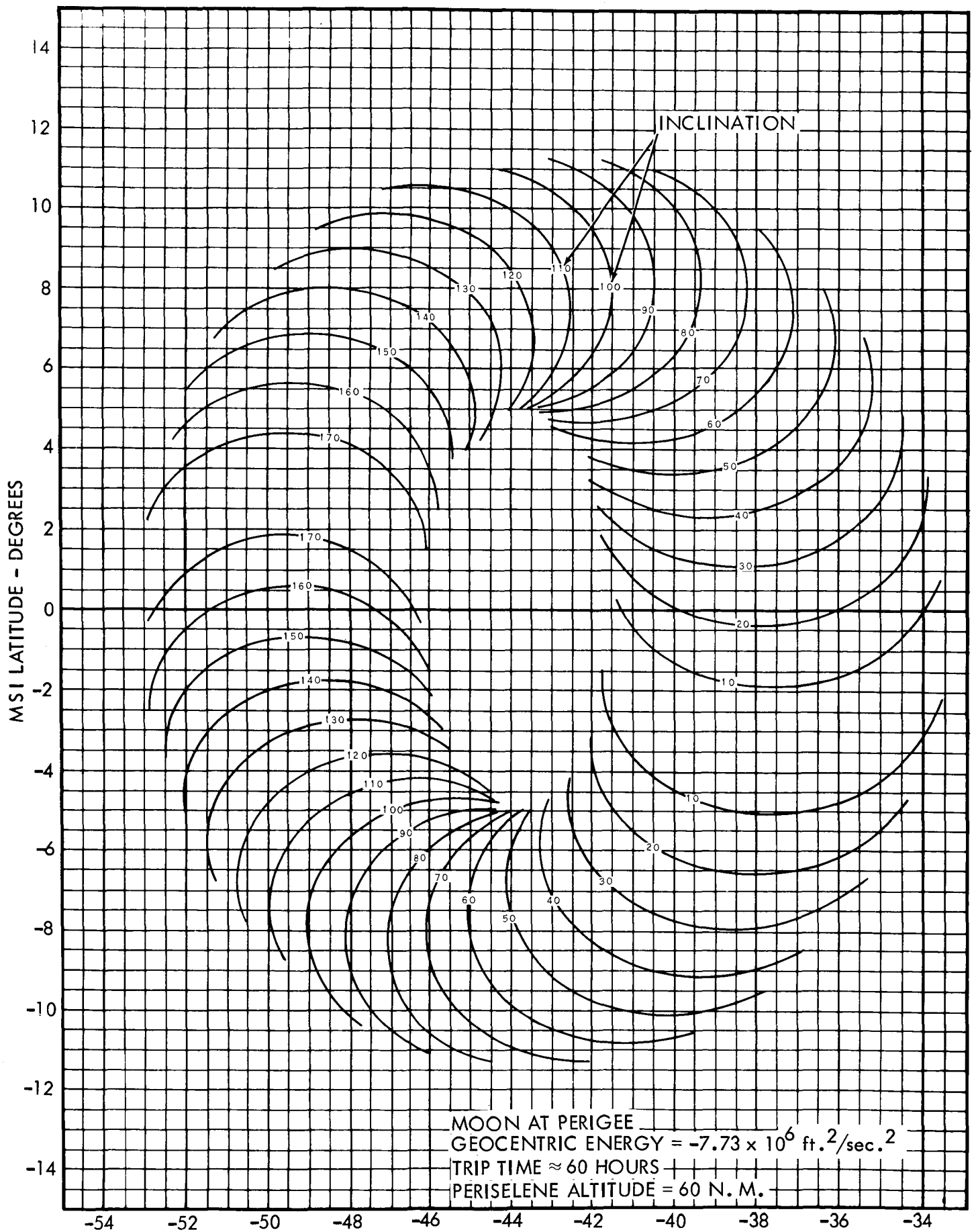
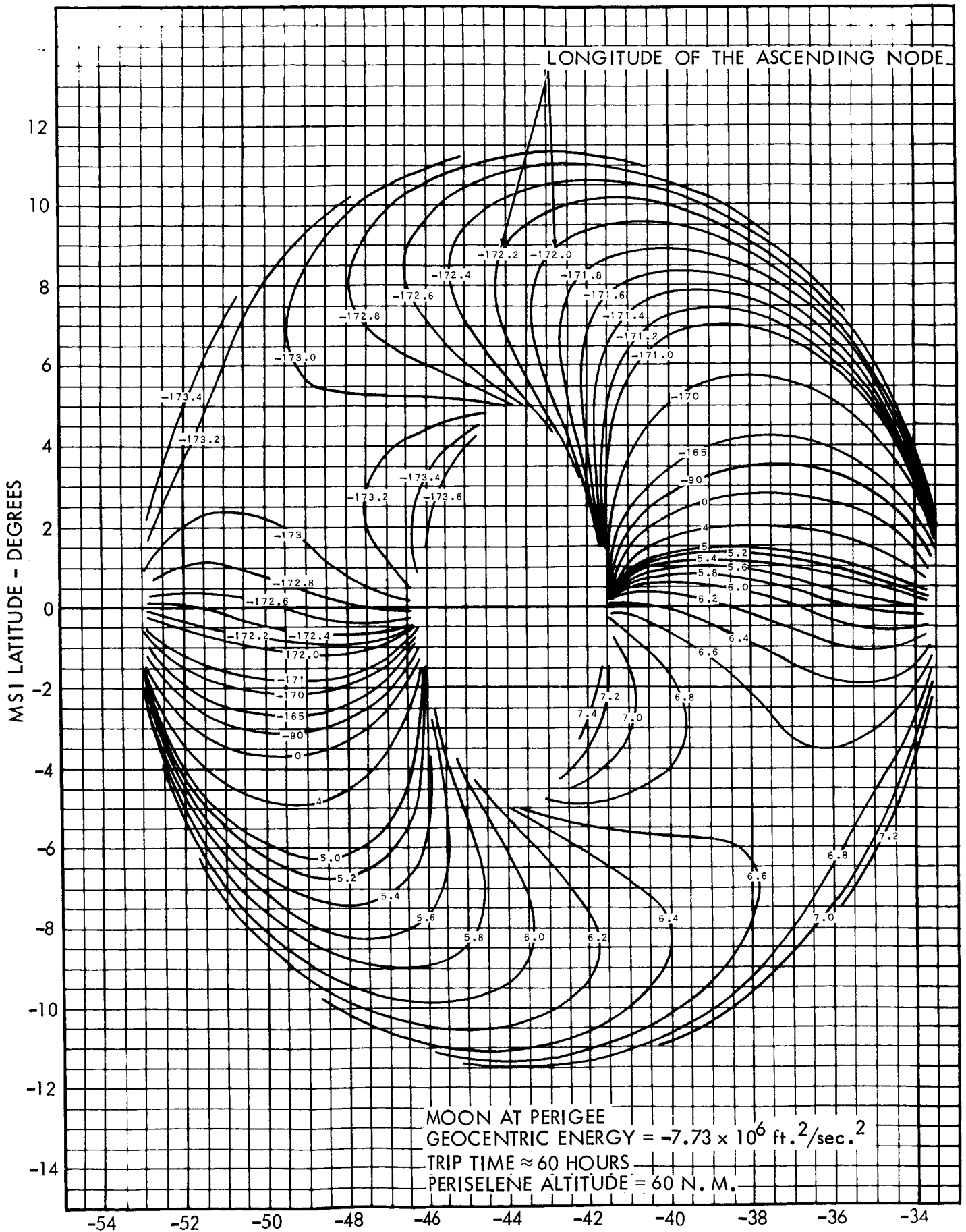
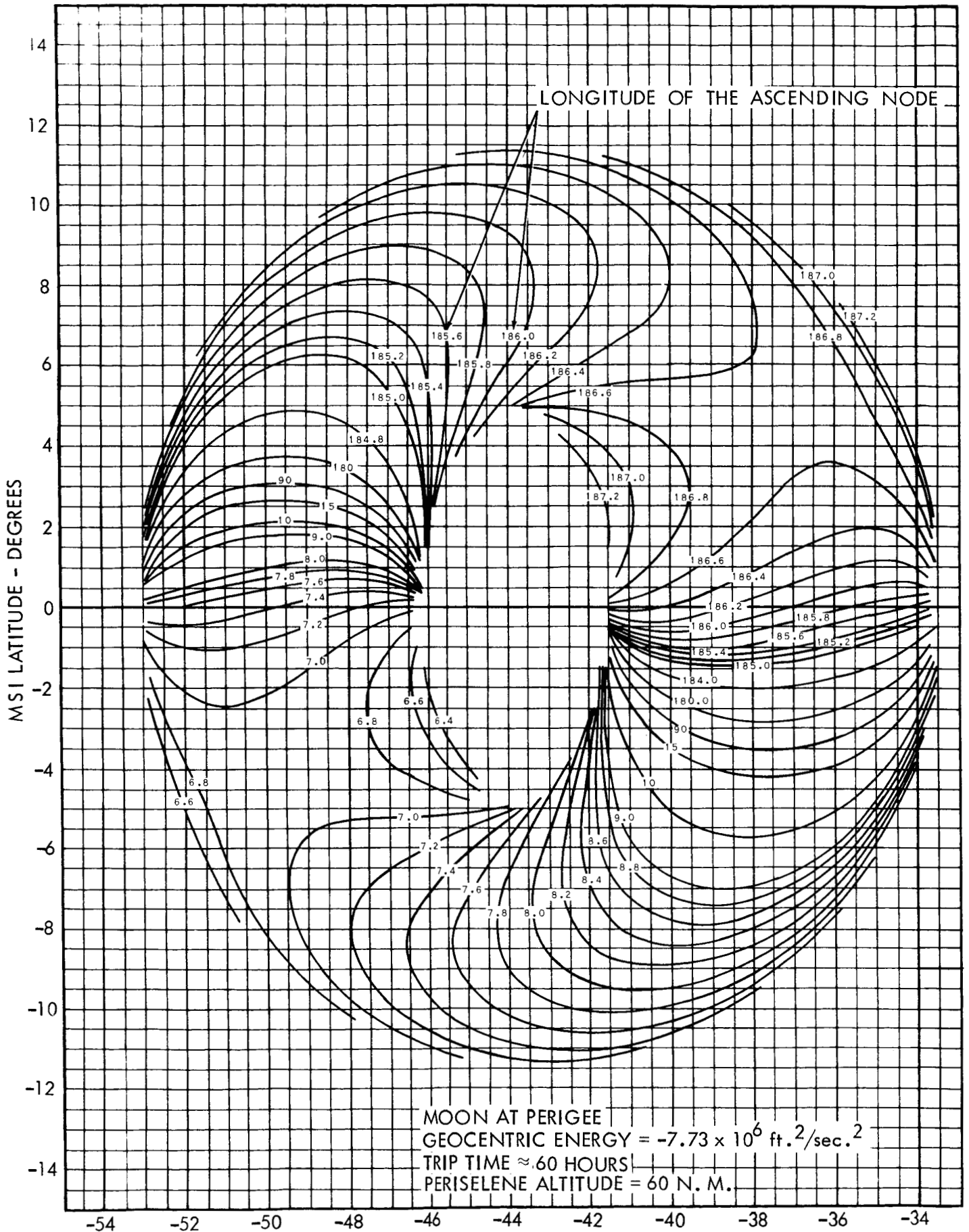


FIGURE 27B - LOCUS OF MSI AIM POINTS FOR VARIOUS GEOCENTRIC INCLINATIONS



MSI LONGITUDE - DEGREES
FIGURE 28A - LOCUS OF MSI AIM POINTS FOR VARIOUS GEOCENTRIC LONGITUDES OF THE ASCENDING NODE



MSI LONGITUDE - DEGREES
**FIGURE 28B - LOCUS OF MSI AIM POINTS FOR VARIOUS GEOCENTRIC LONGITUDES
 OF THE ASCENDING NODE**

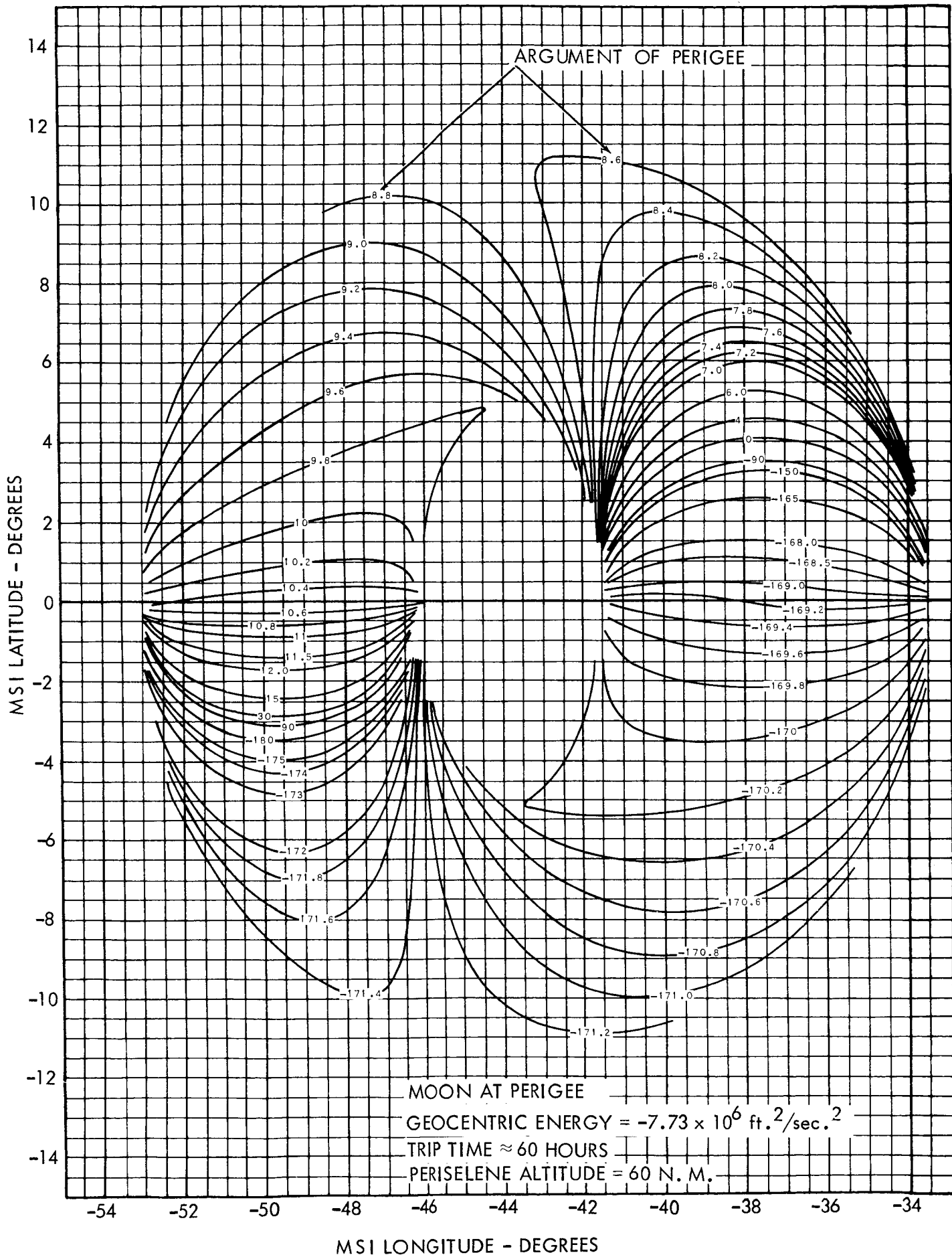


FIGURE 29A - LOCUS OF MSI AIM POINTS FOR VARIOUS GEOCENTRIC ARGUMENTS OF PERIGEE

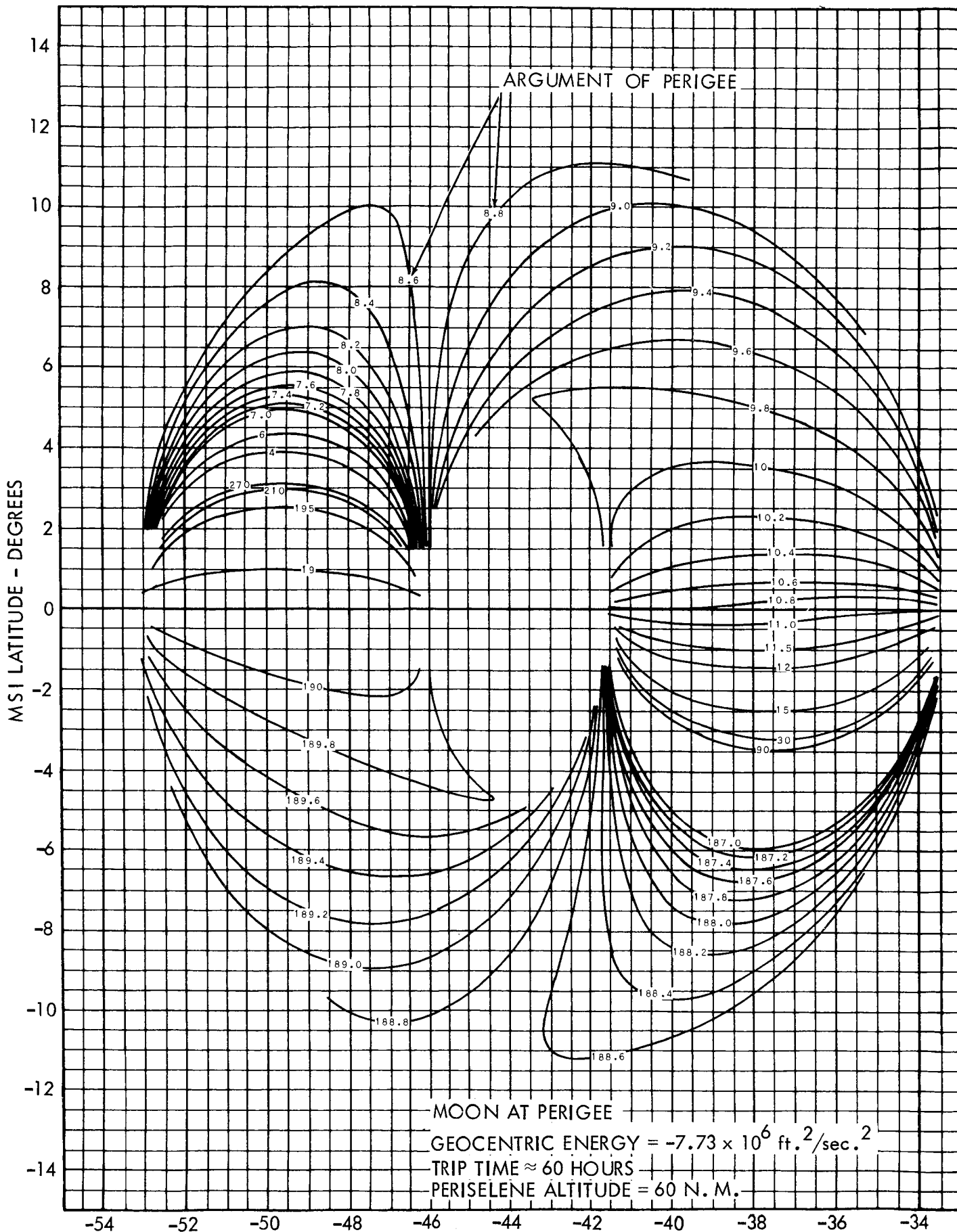


FIGURE 29B - LOCUS OF MSI AIM POINTS FOR VARIOUS GEOCENTRIC ARGUMENTS OF PERIGEE

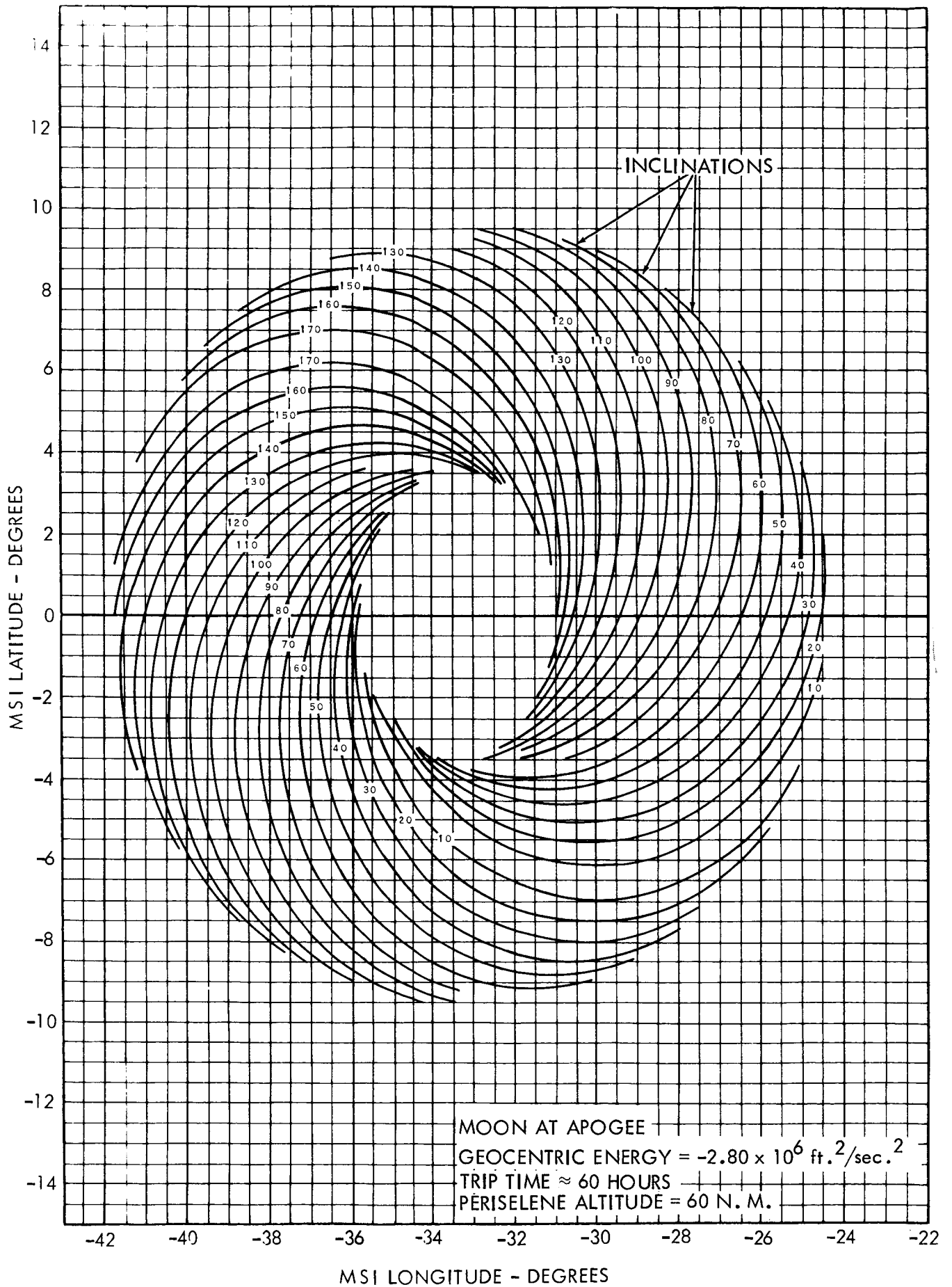


FIGURE 30A - LOCUS OF MSI AIM POINTS FOR VARIOUS SELENOCENTRIC INCLINATIONS

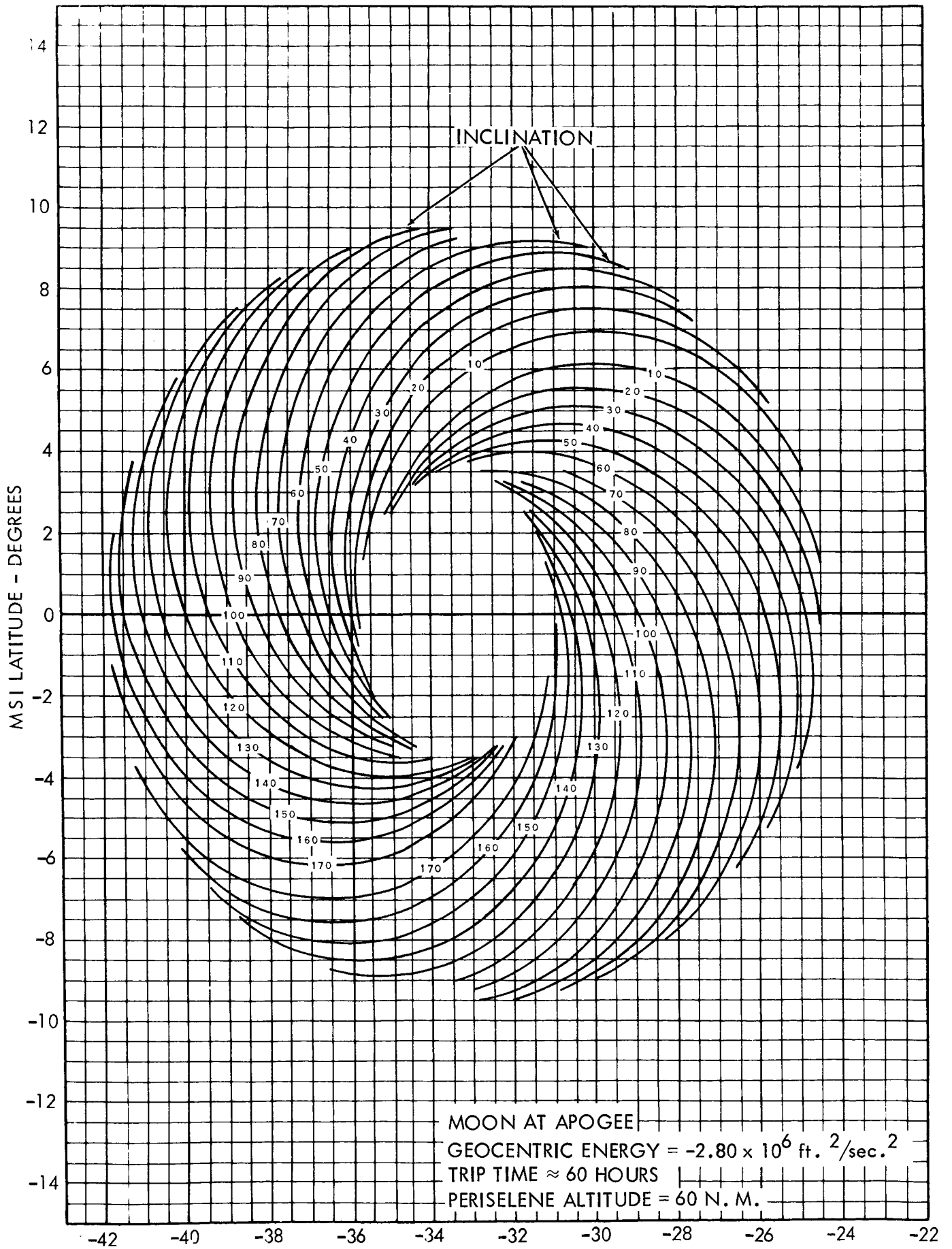


FIGURE 30B - LOCUS OF MSI AIM POINTS FOR VARIOUS SELENOCENTRIC INCLINATIONS

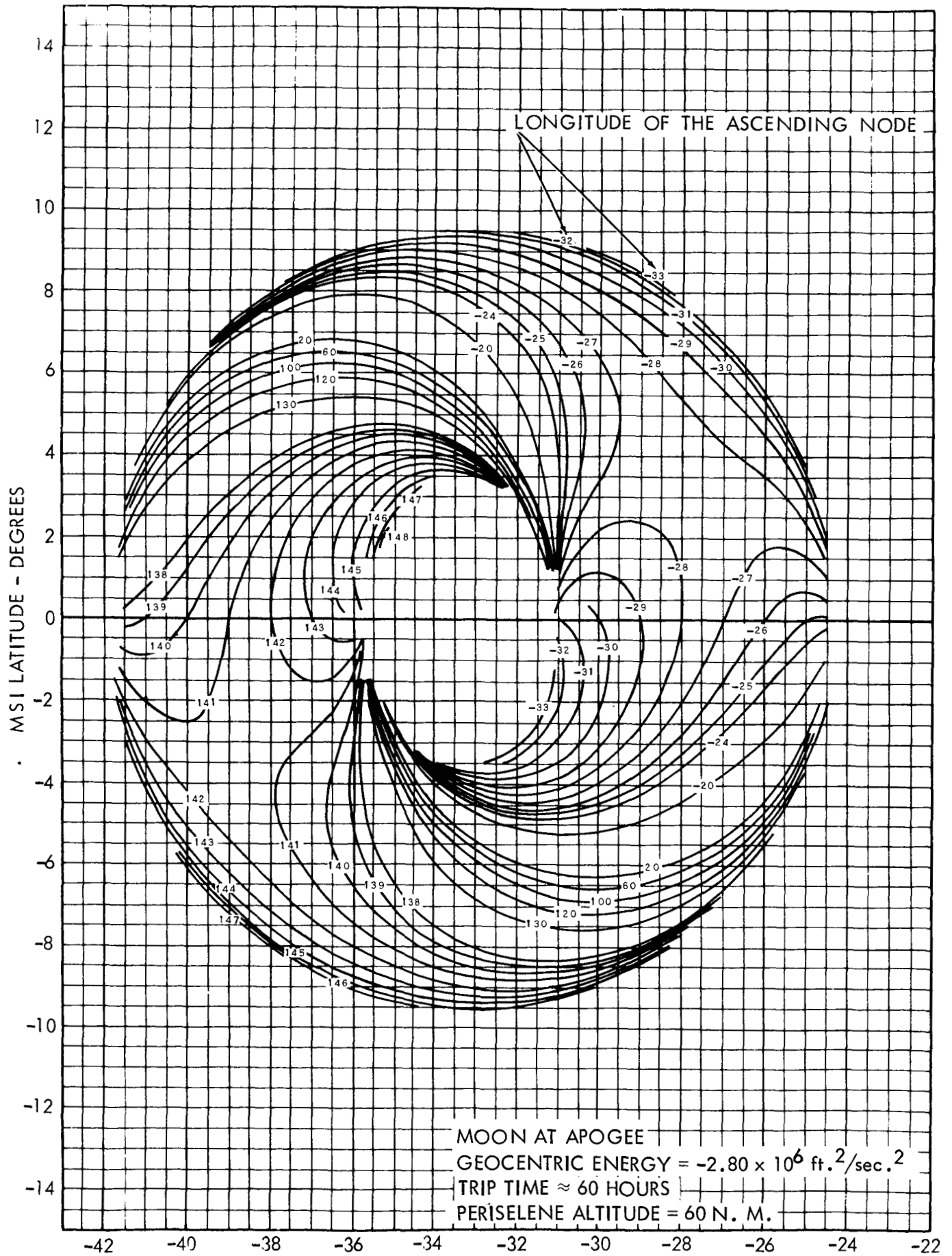


FIGURE 31A - LOCUS OF MSI AIM POINTS FOR VARIOUS LONGITUDES OF THE ASCENDING NODES

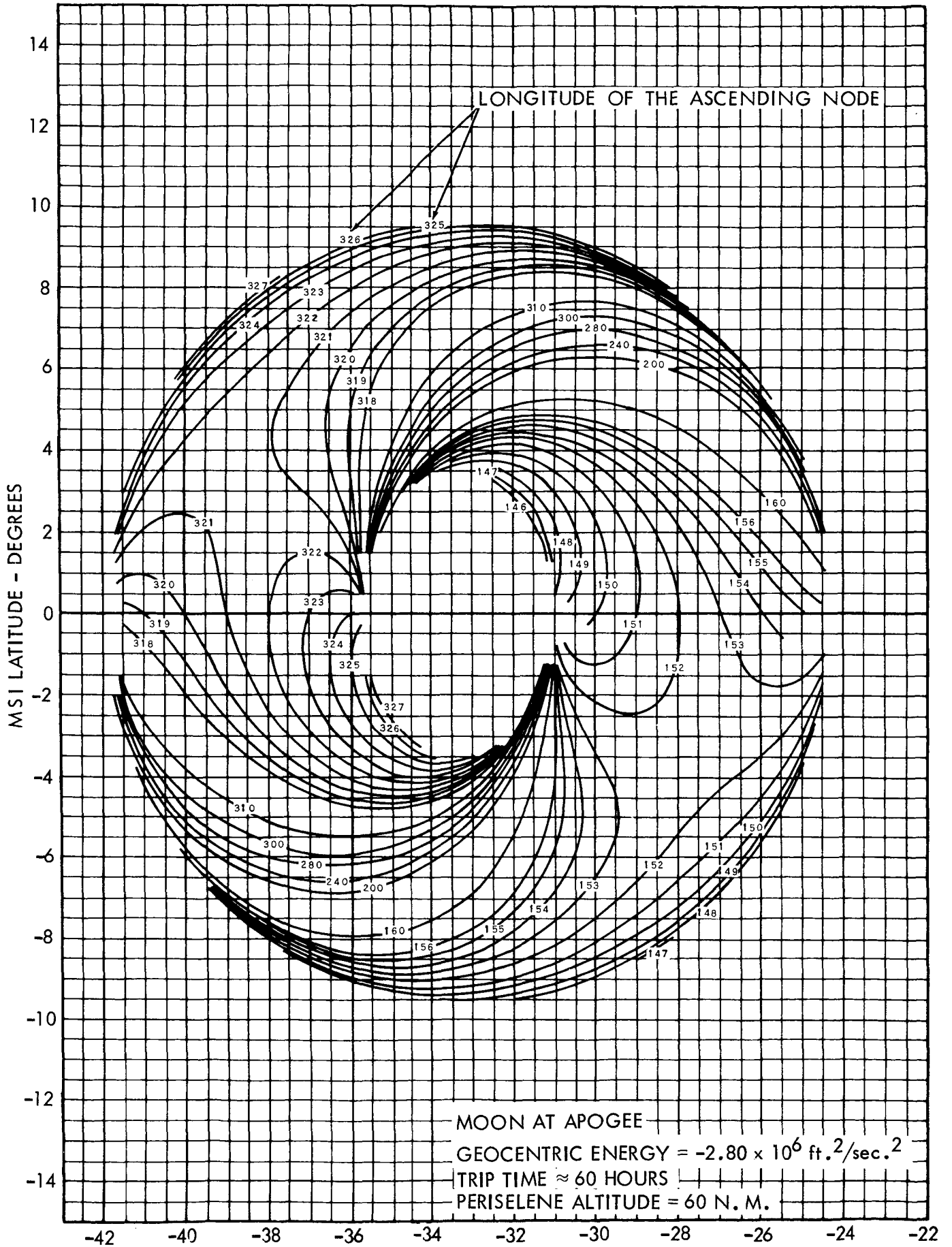


FIGURE 31B - LOCUS OF MSI AIM POINTS FOR VARIOUS SELENOCENTRIC LONGITUDES OF THE ASCENDING NODE

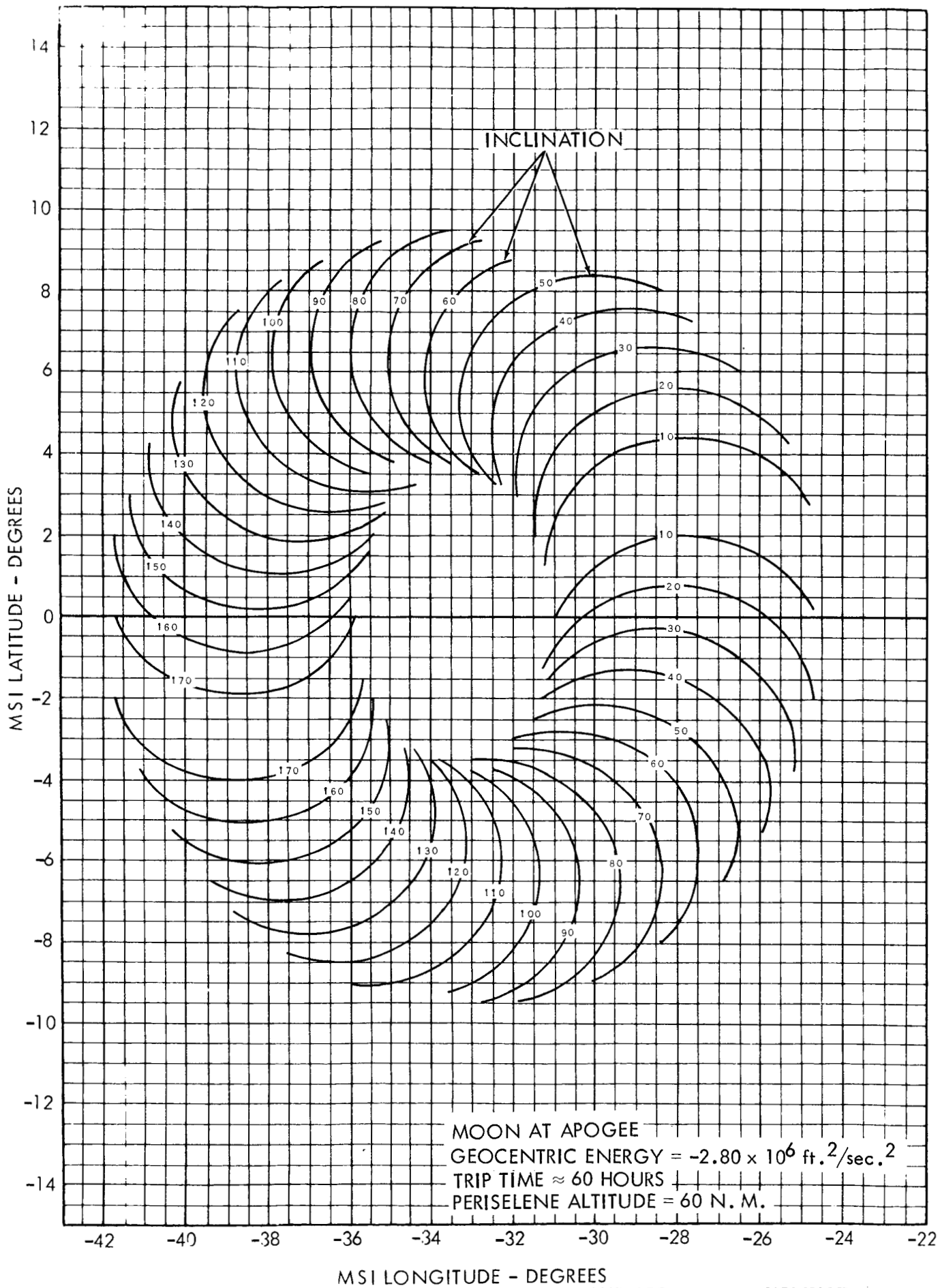


FIGURE 32A - LOCUS OF MSI AIM POINTS FOR VARIOUS GEOCENTRIC INCLINATIONS

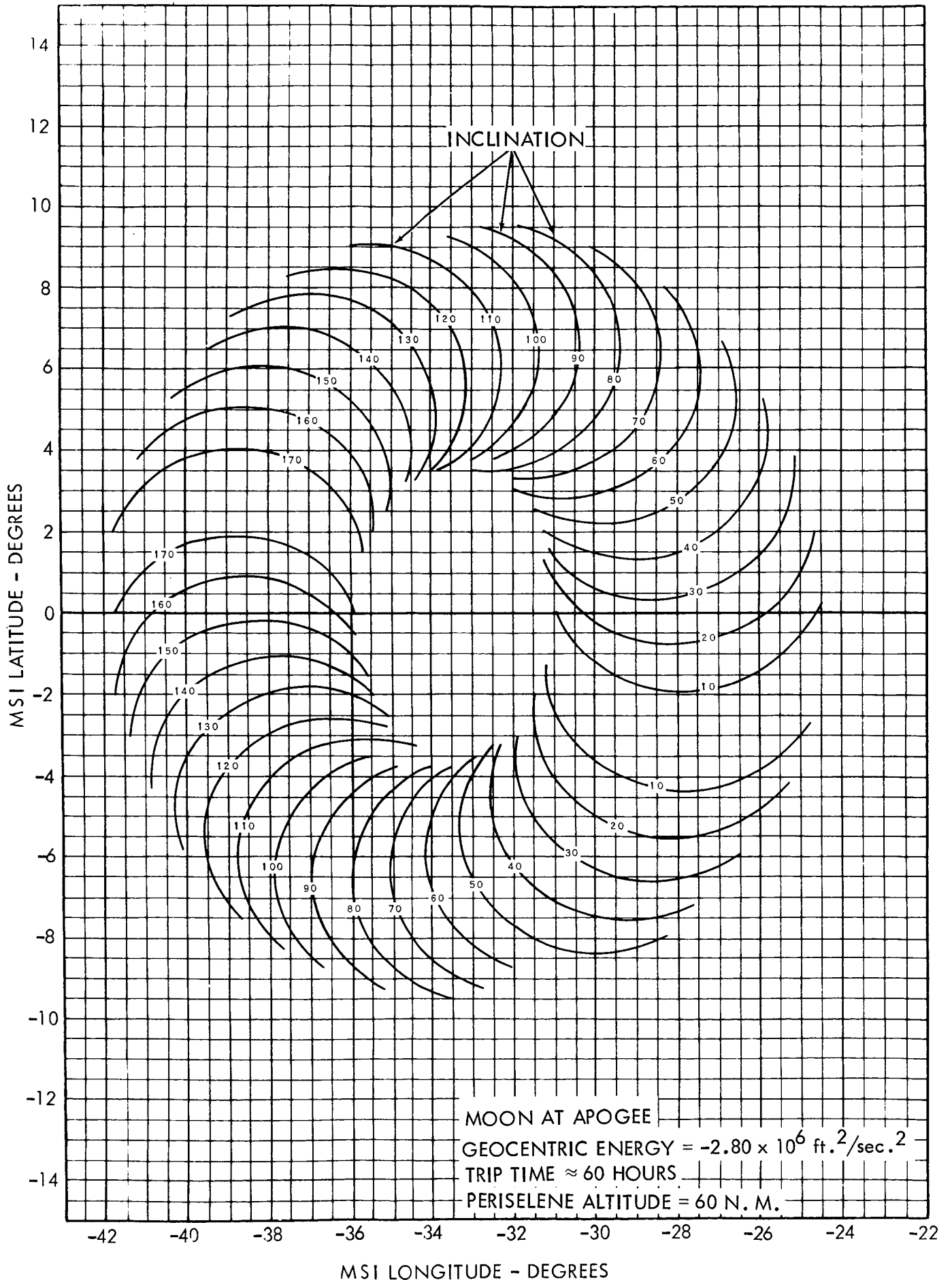


FIGURE 32B - LOCUS OF MSI AIM POINTS FOR VARIOUS GEOCENTRIC INCLINATIONS

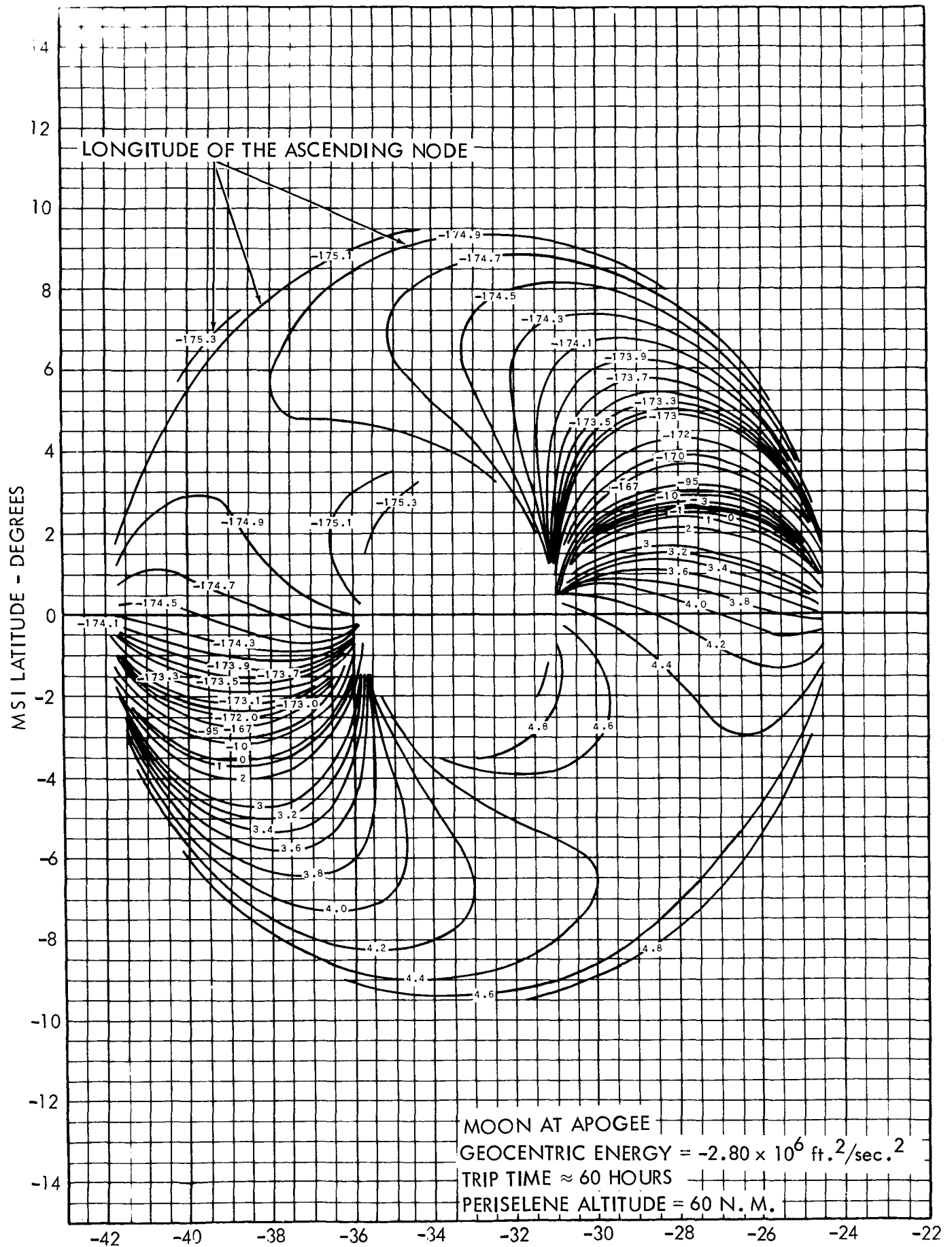


FIGURE 33A - LOCUS OF MSI AIM POINTS FOR VARIOUS GEOCENTRIC LONGITUDES OF THE ASCENDING NODE

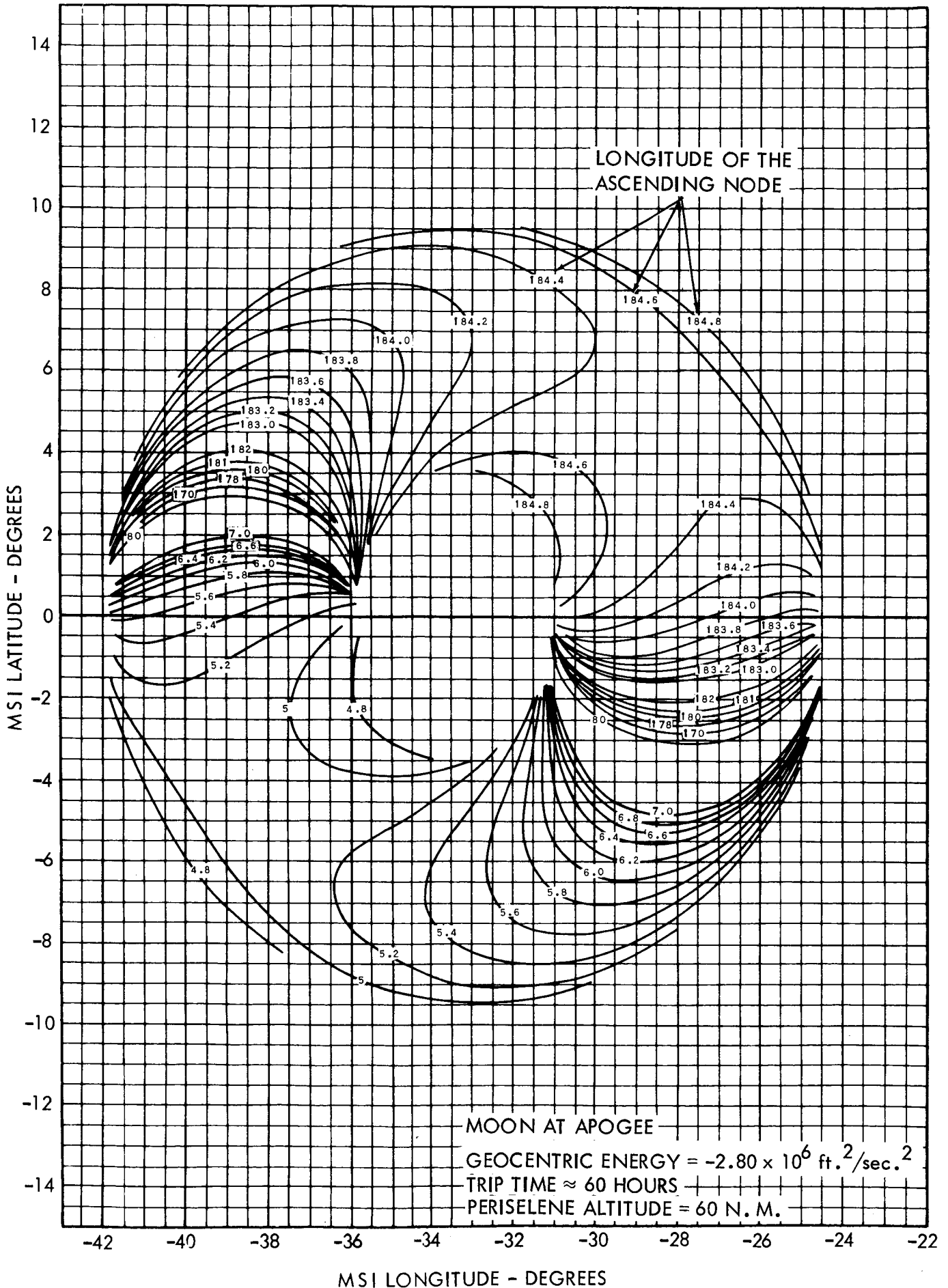
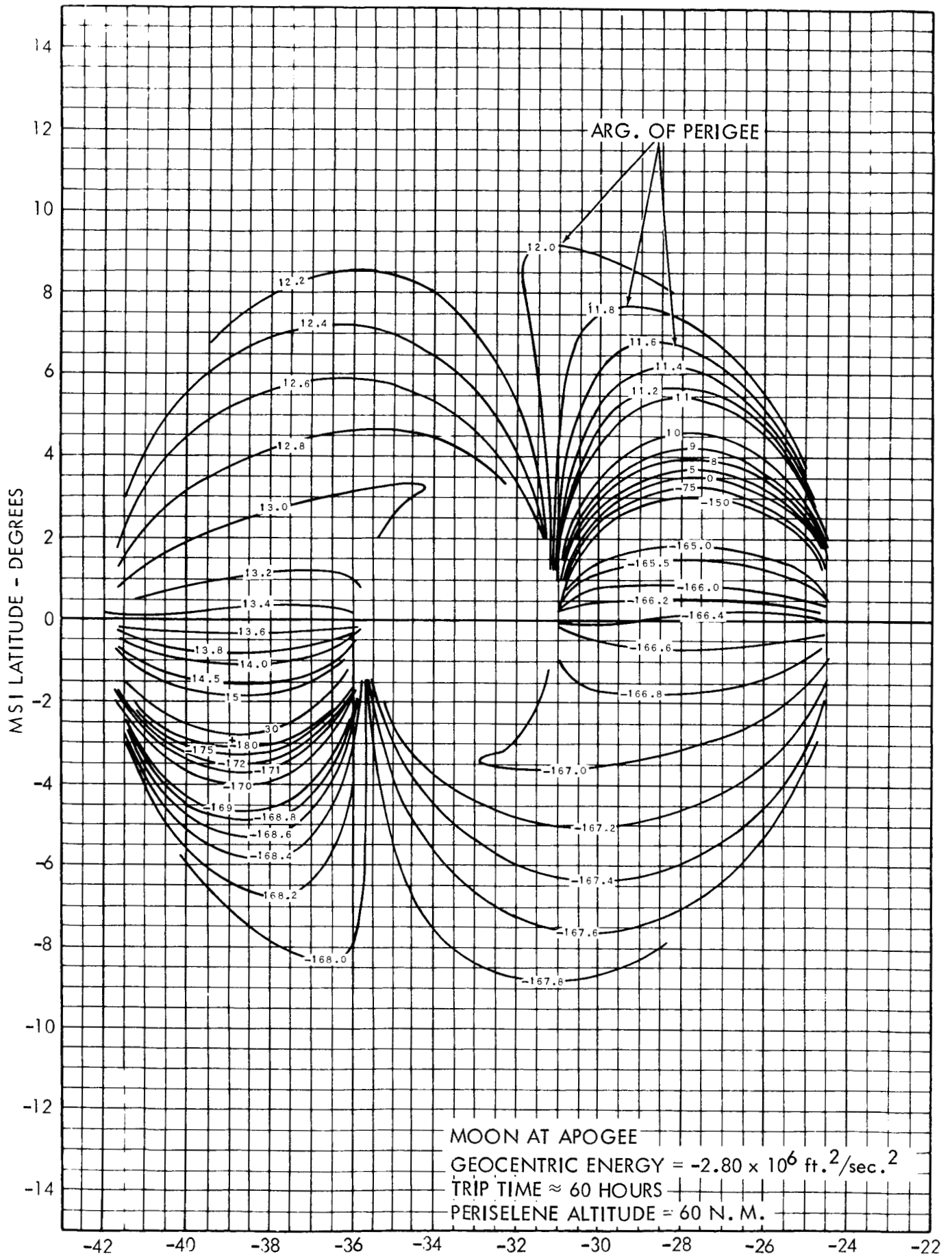


FIGURE 33B - LOCUS OF MSI AIM POINTS FOR VARIOUS GEOCENTRIC LONGITUDES OF THE ASCENDING NODE



MSI LONGITUDE - DEGREES
 FIGURE 34A - LOCUS OF MSI AIM POINTS FOR VARIOUS GEOCENTRIC ARG. OF PERIGEE

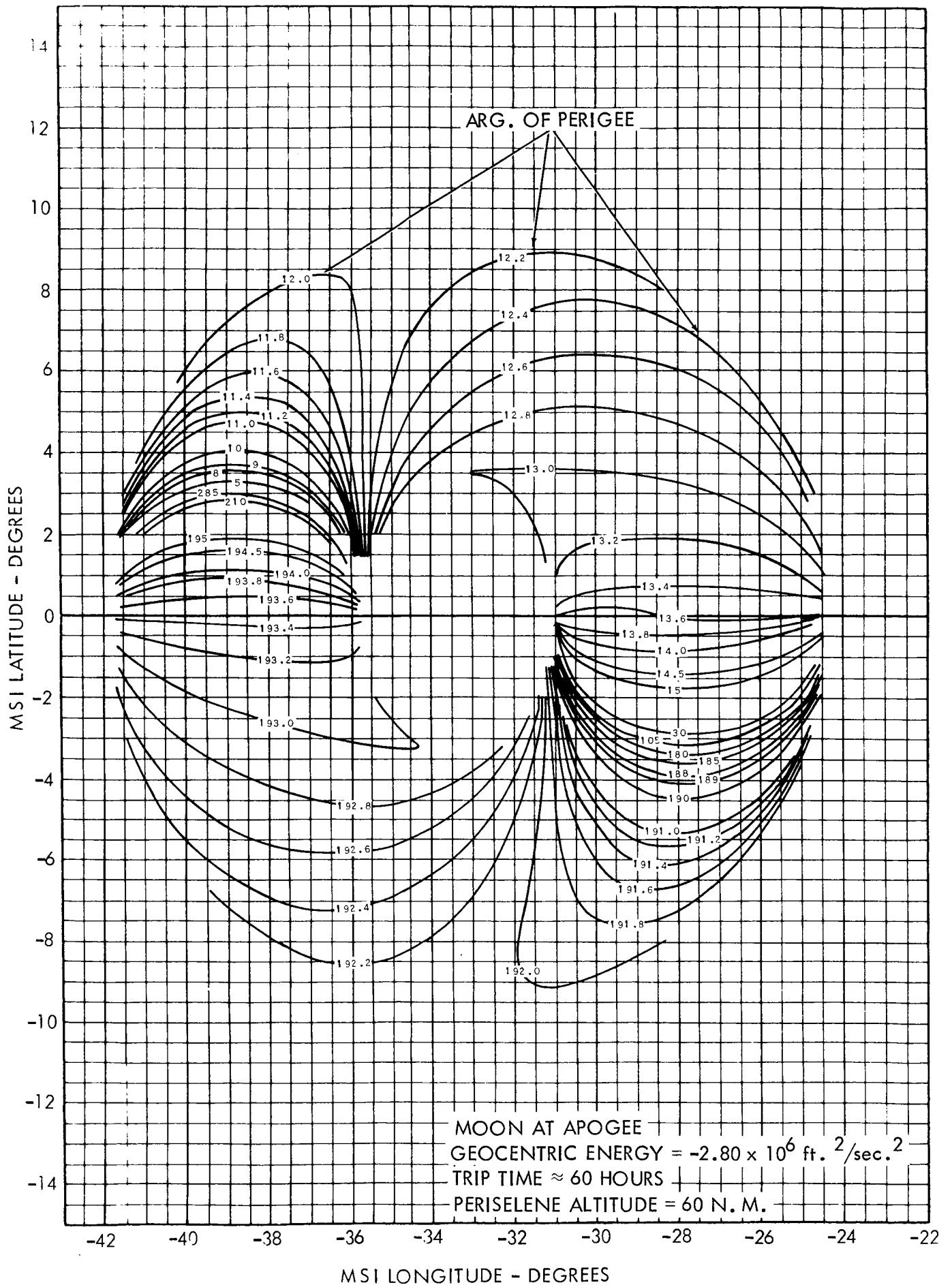


FIGURE 34B - LOCUS OF MSI AIM POINTS FOR VARIOUS GEOCENTRIC ARG. OF PERIGEE

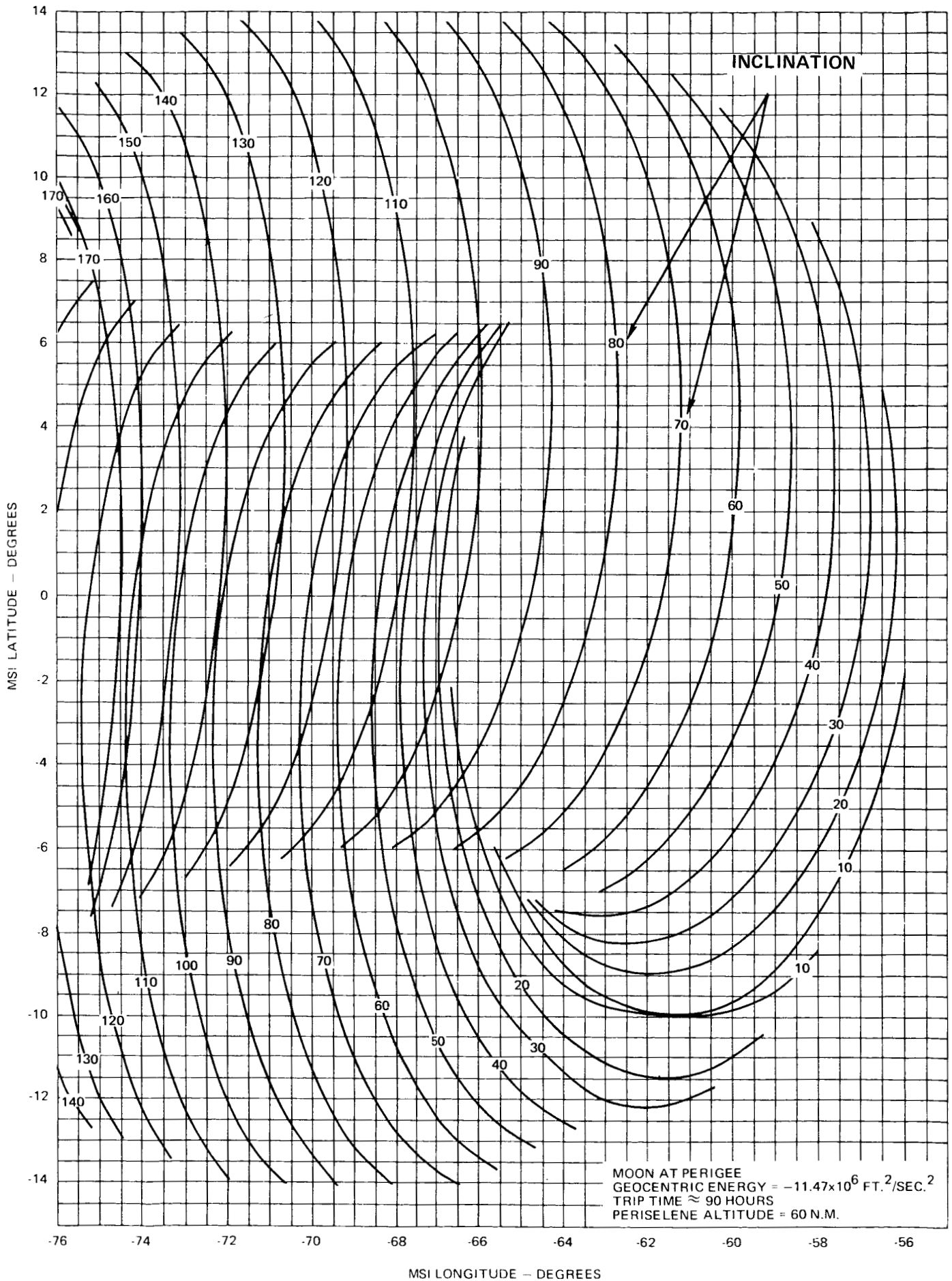


FIGURE 35A - LOCUS OF MSI AIMPOINTS FOR VARIOUS SELENOCENTRIC INCLINATIONS

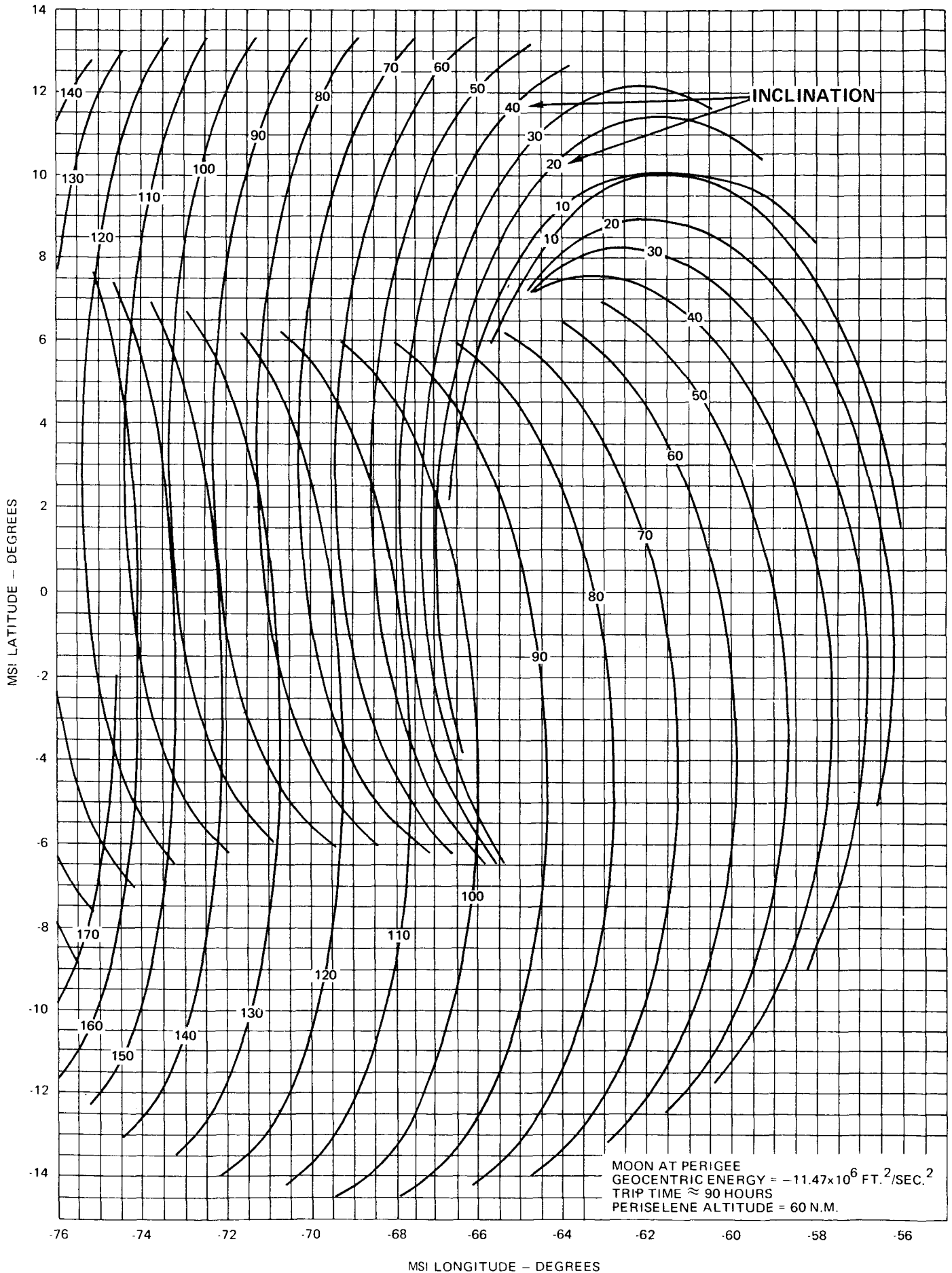


FIGURE 35B - LOCUS OF MSI AIMPOINTS FOR VARIOUS SELENOCENTRIC INCLINATIONS

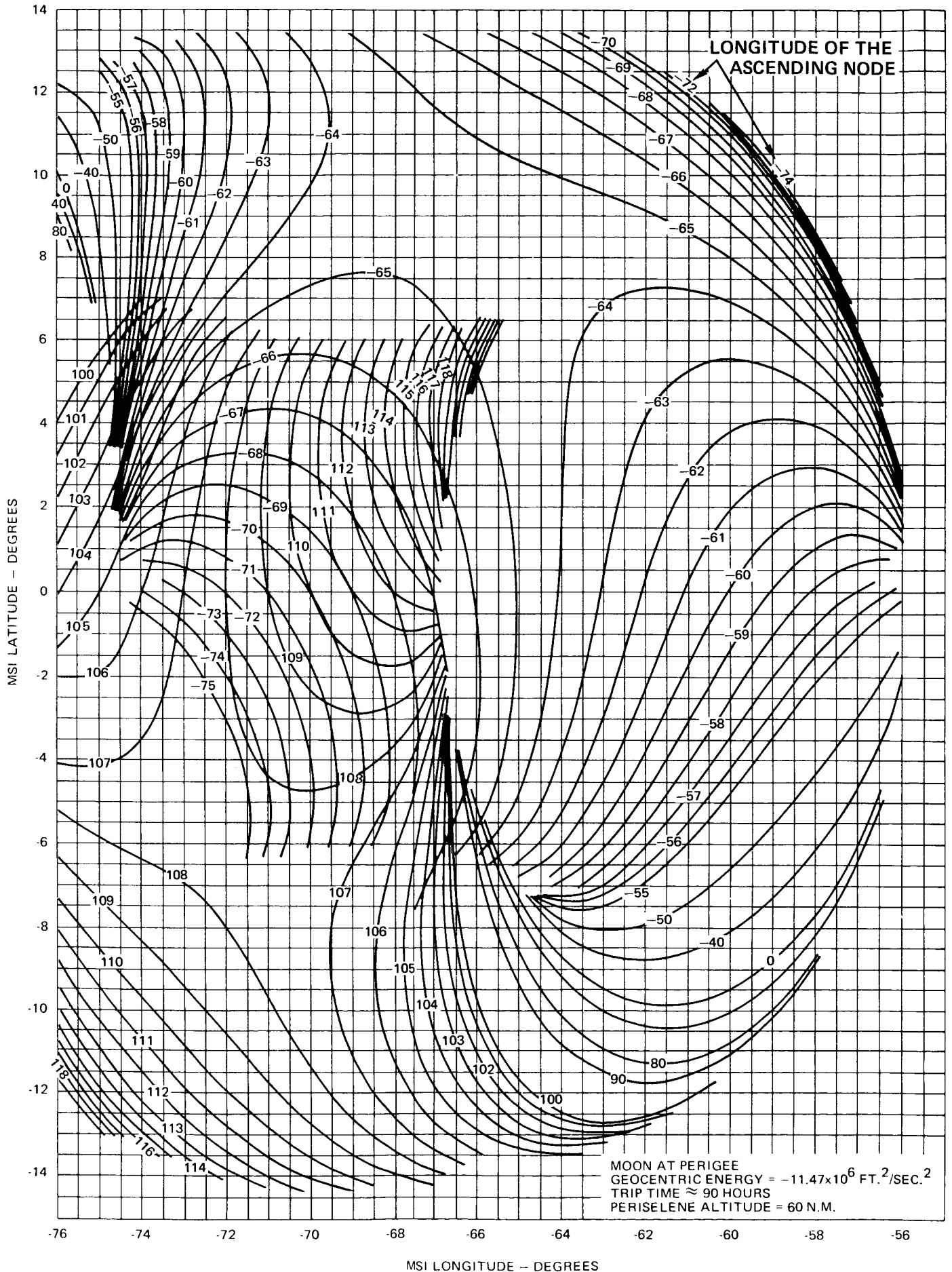


FIGURE 36A - LOCUS OF MSI AIMPOINTS FOR VARIOUS SELENOCENTRIC LONGITUDES OF THE ASCENDING NODE

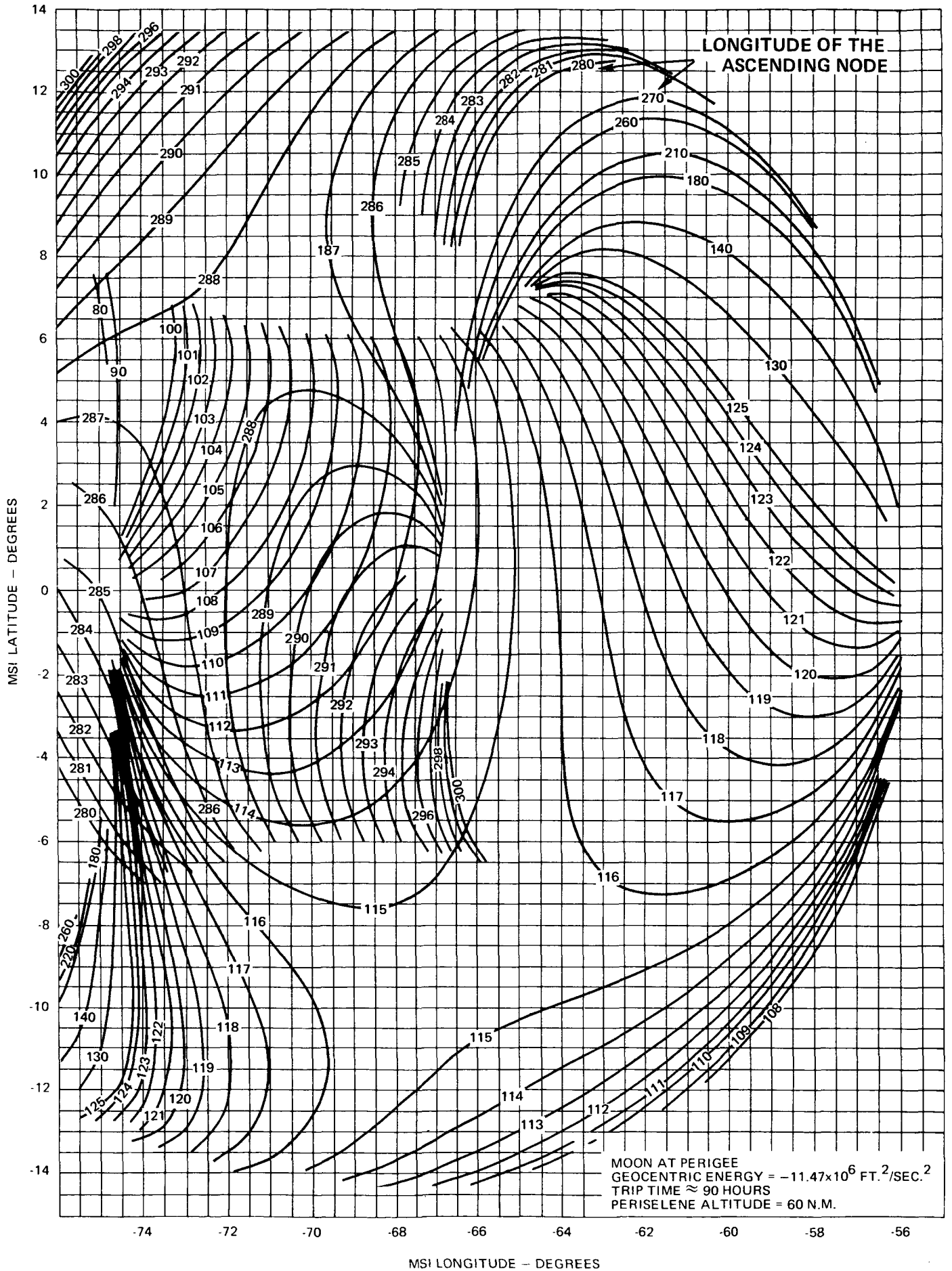


FIGURE 36B - LOCUS OF MSI AIMPOINTS FOR VARIOUS SELENOCENTRIC LONGITUDES OF THE ASCENDING NODE

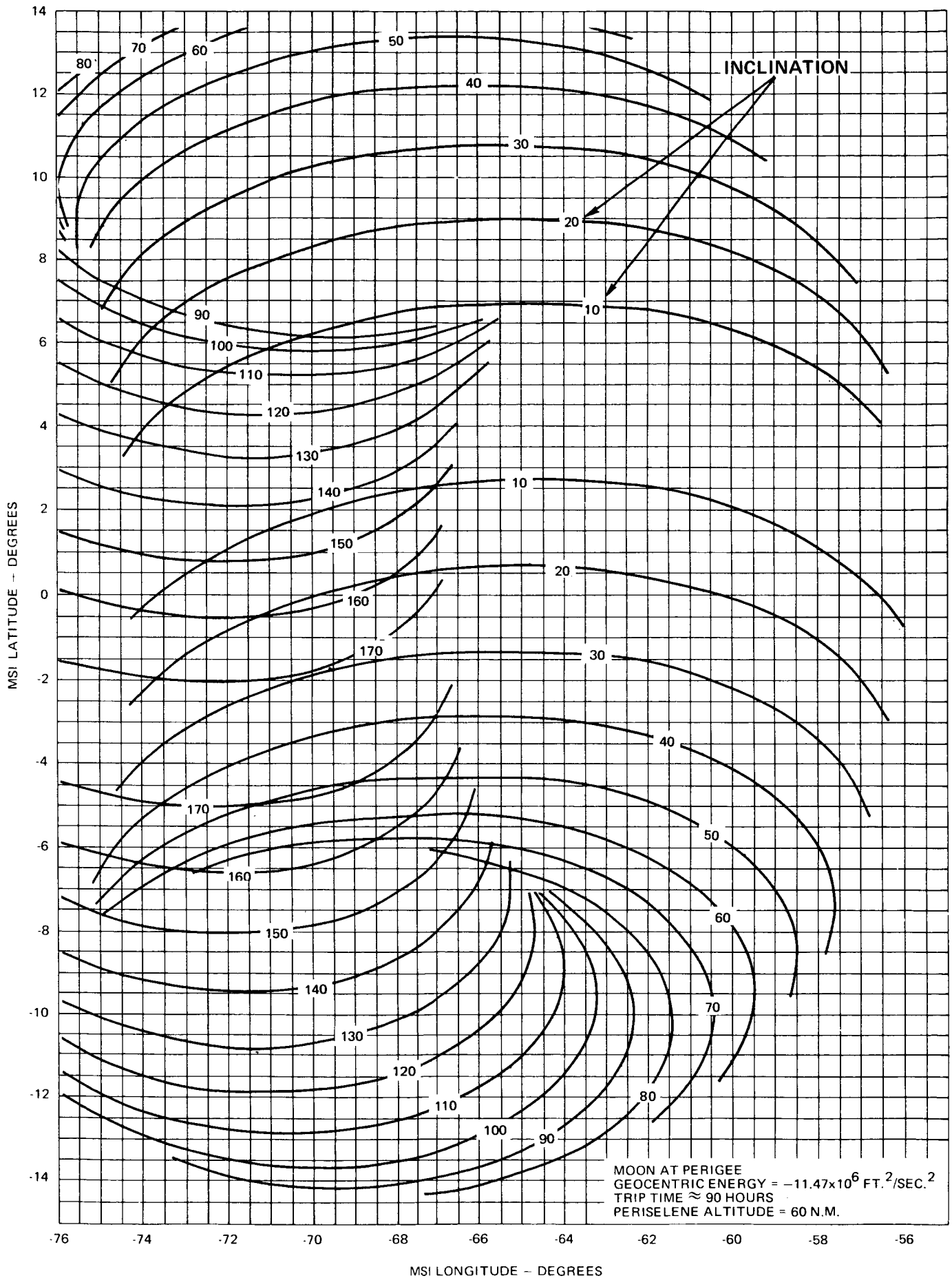
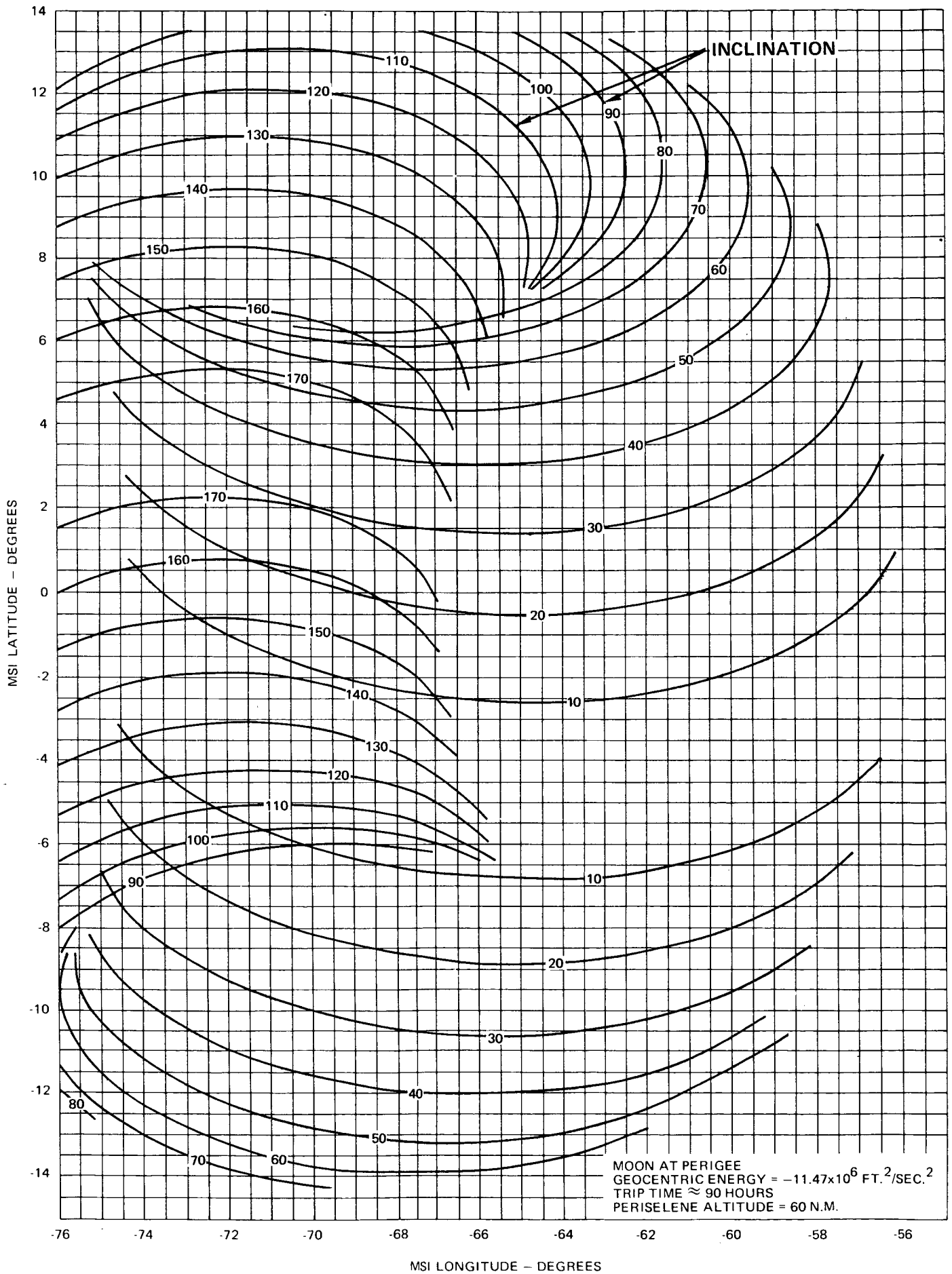


FIGURE 37A - LOCUS OF MSI AIMPOINTS FOR VARIOUS
 GEOCENTRIC INCLINATIONS



**FIGURE 37B - LOCUS OF MSI AIMPOINTS FOR VARIOUS
 GEOCENTRIC INCLINATIONS**

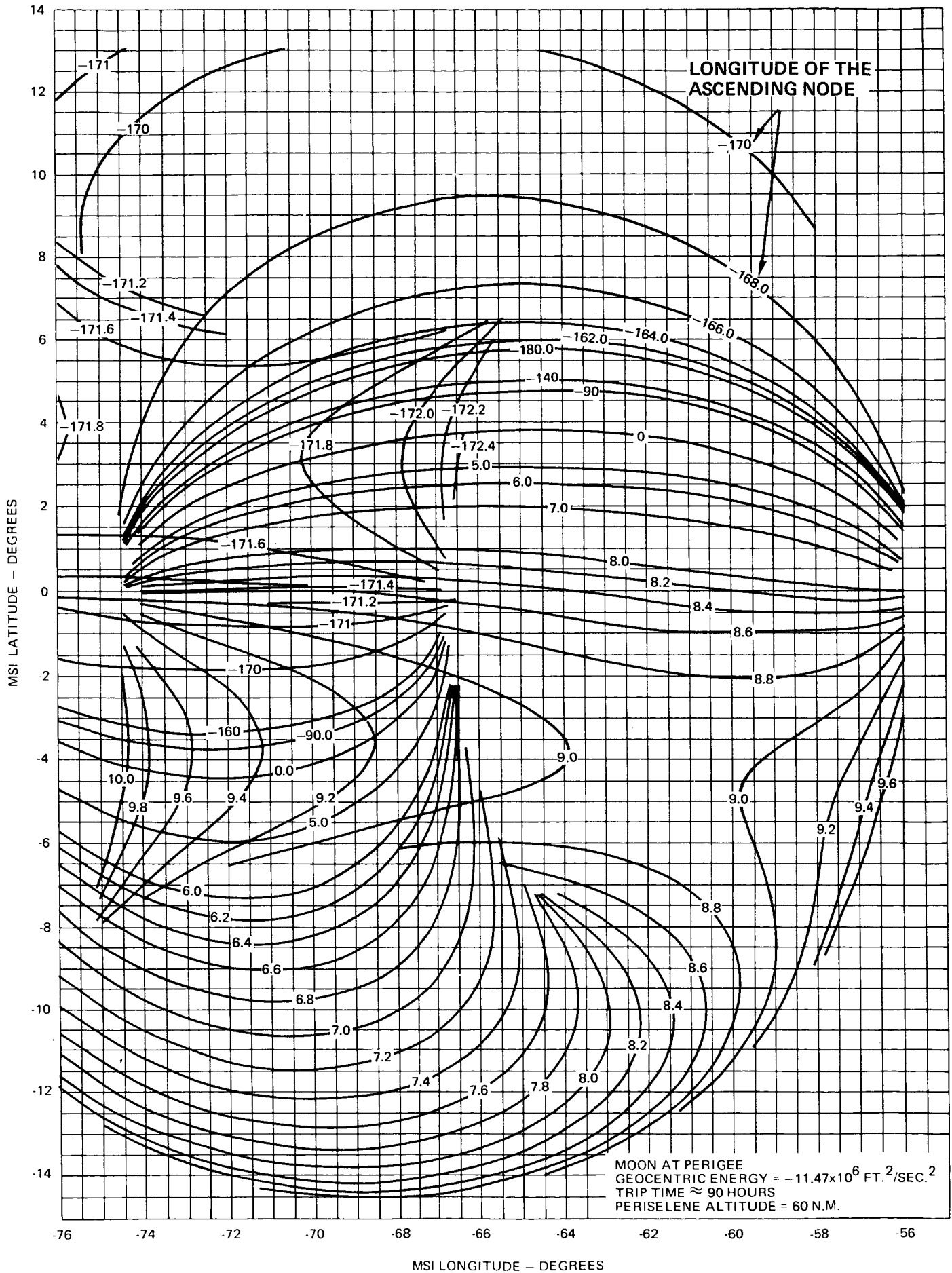
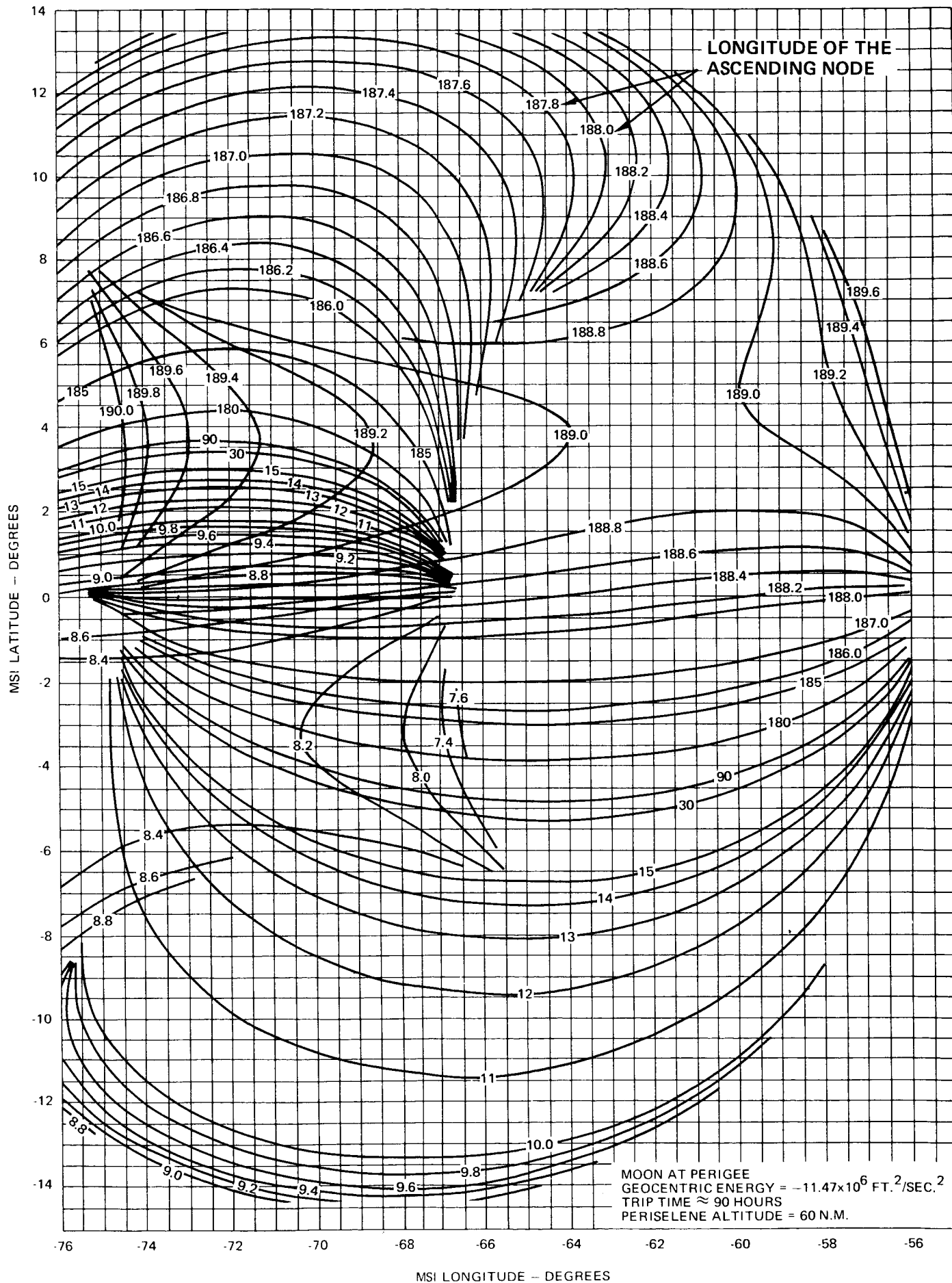


FIGURE 38A - LOCUS OF MSI AIMPOINTS FOR VARIOUS GEOCENTRIC LONGITUDES OF THE ASCENDING NODE



**FIGURE 38B - LOCUS OF MSI AIMPOINTS FOR VARIOUS GEOCENTRIC
LONGITUDES OF THE ASCENDING NODE**

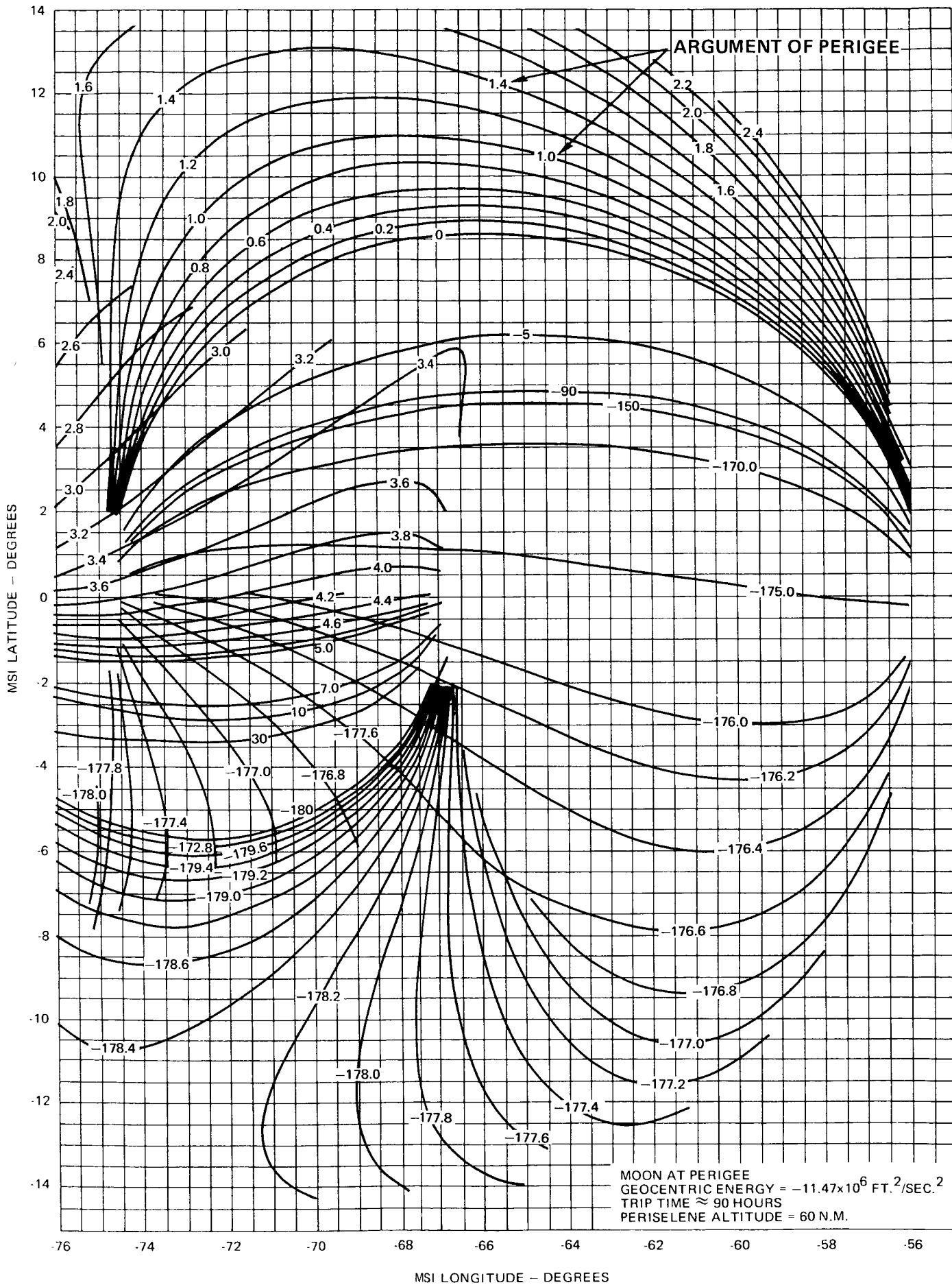


FIGURE 39A - LOCUS OF MSI AIMPOINTS FOR VARIOUS GEOCENTRIC ARGUMENTS OF PERIGEE

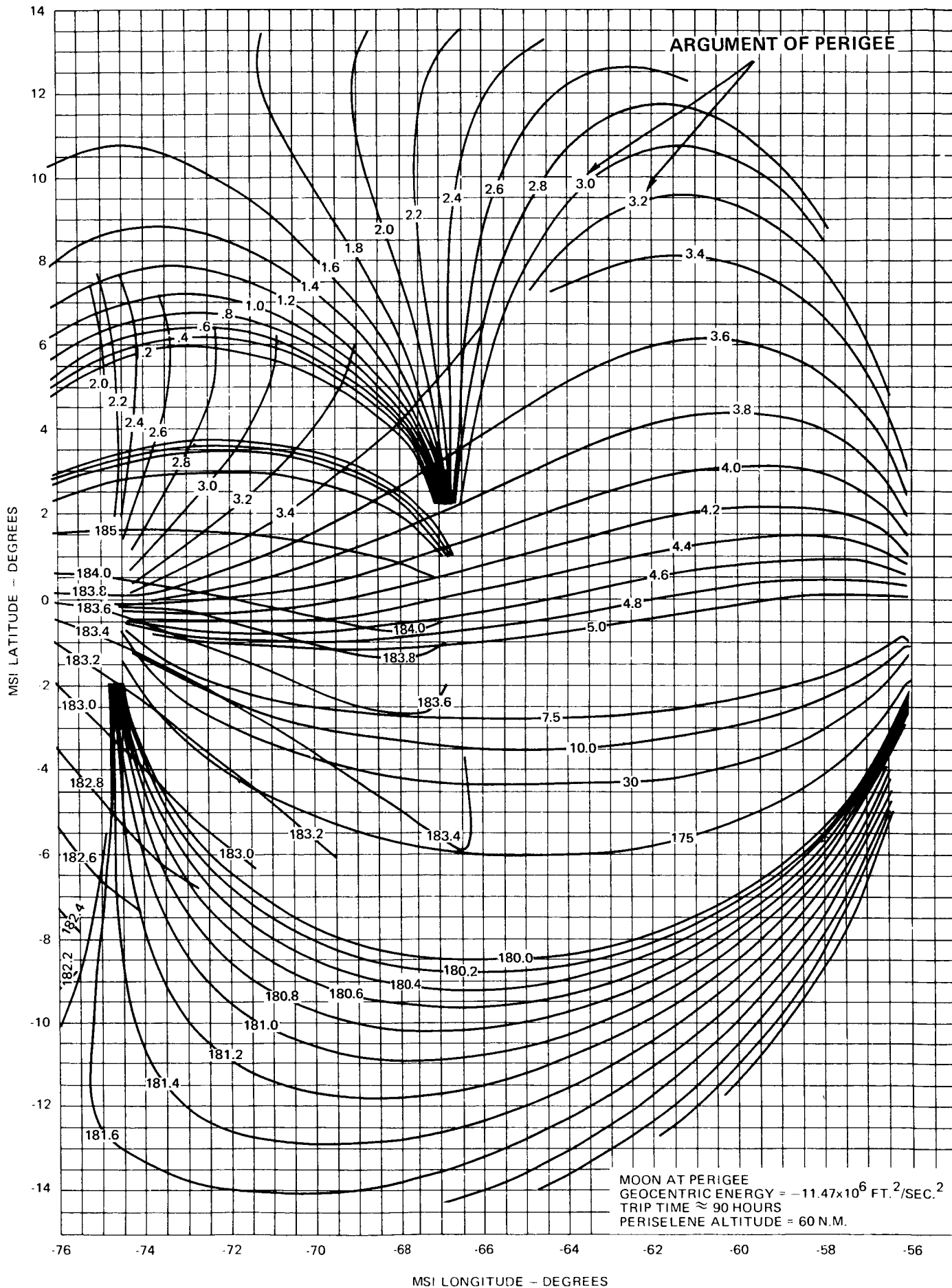


FIGURE 39B - LOCUS OF MSI AIMPOINTS FOR VARIOUS GEOCENTRIC ARGUMENTS OF PERIGEE

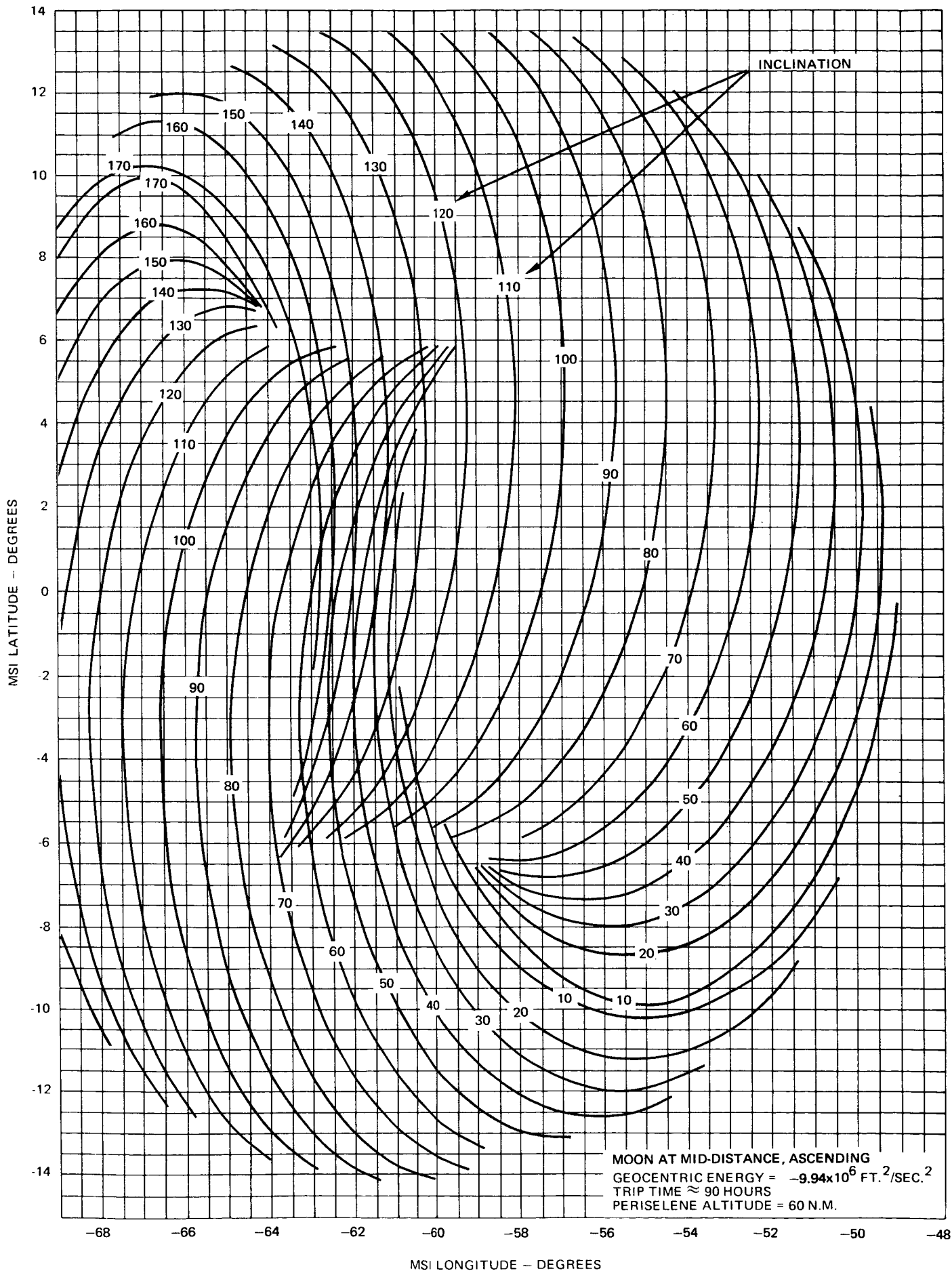


FIGURE 40A - LOCUS OF MSI AIMPOINTS FOR VARIOUS SELENOCENTRIC INCLINATIONS

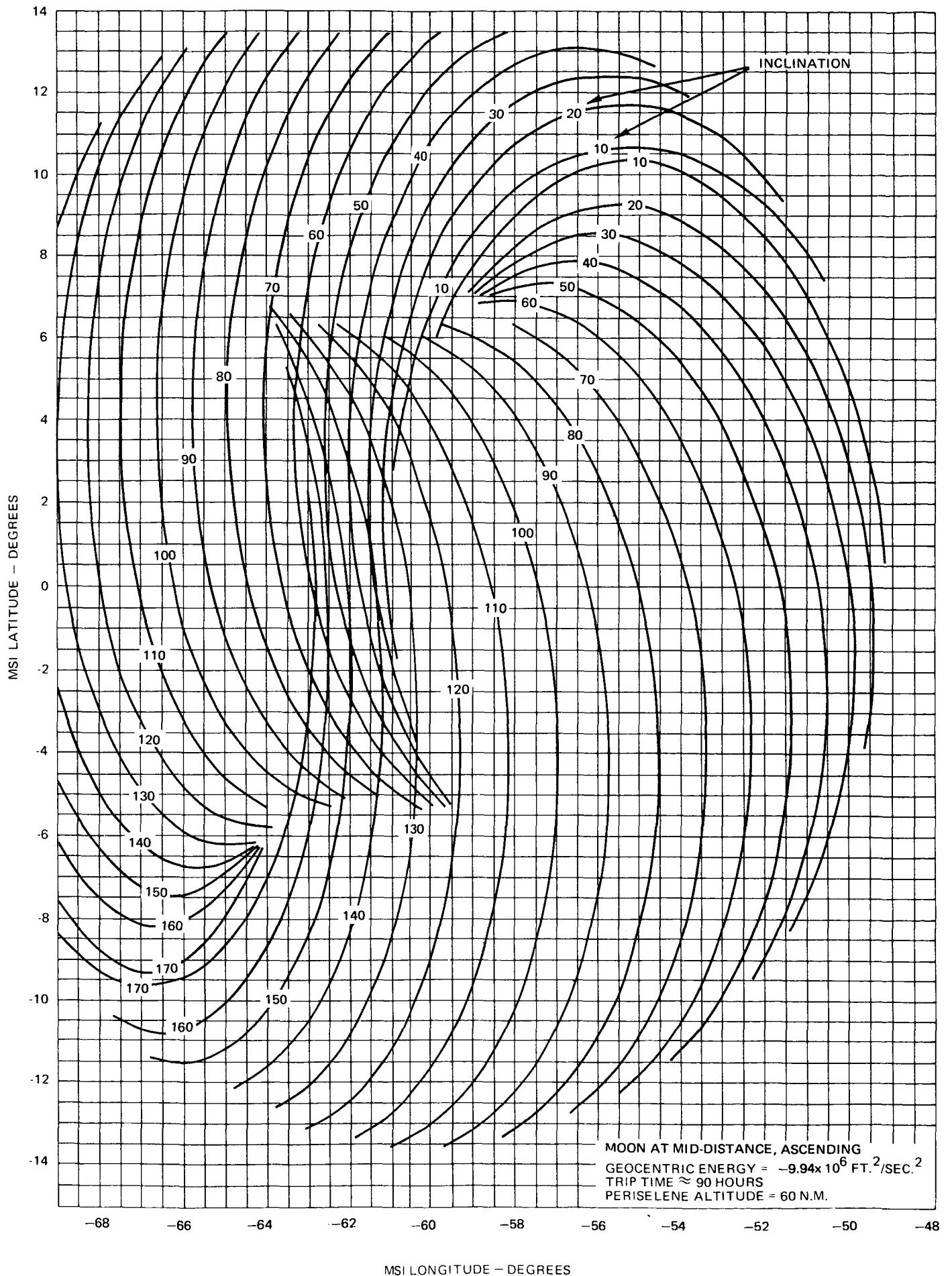


FIGURE 40B - LOCUS OF MSI AIMPOINTS FOR VARIOUS SELENOCENTRIC INCLINATIONS

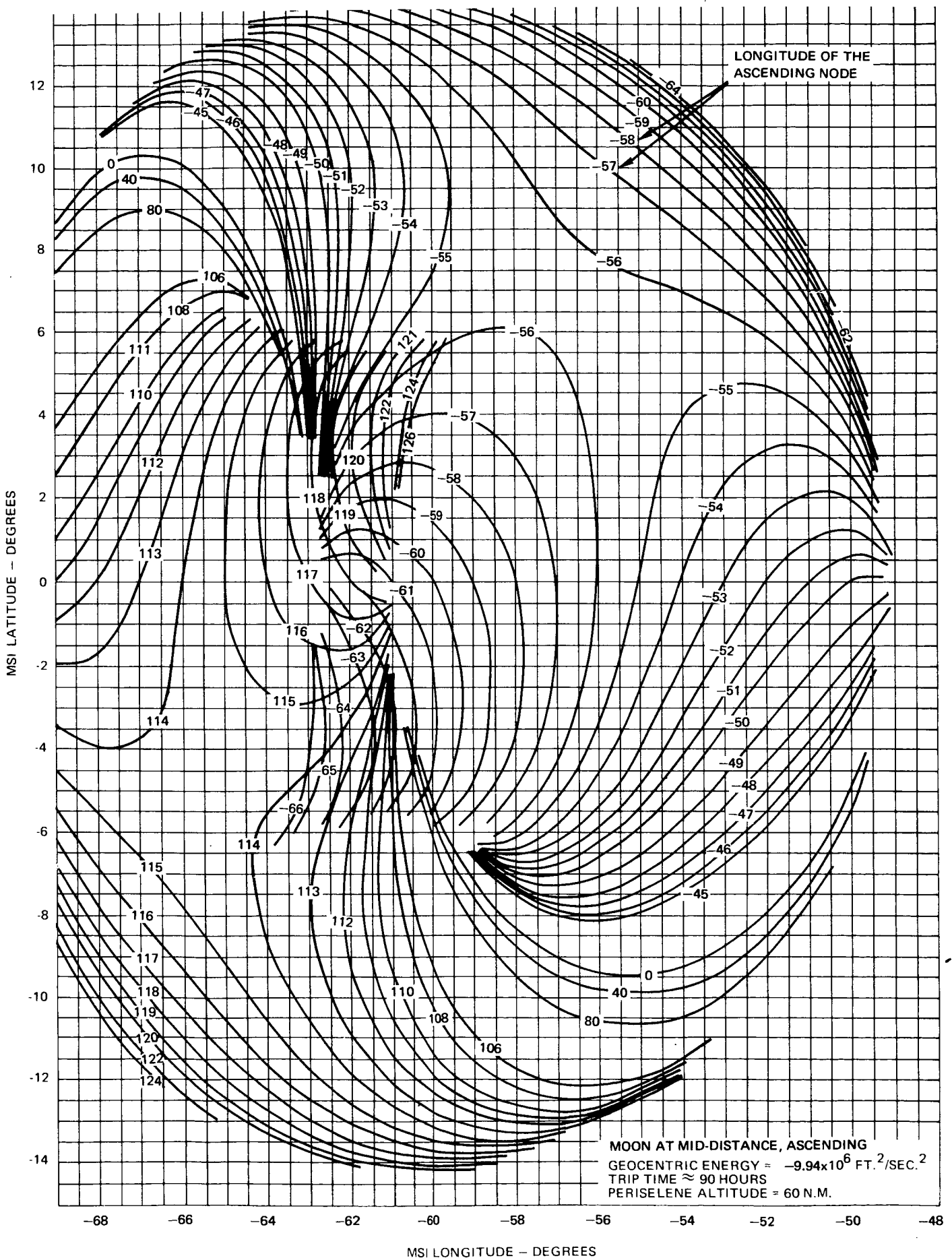


FIGURE 41A - LOCUS OF MSI AIMPOINTS FOR VARIOUS SELENOCENTRIC LONGITUDES OF THE ASCENDING NODE

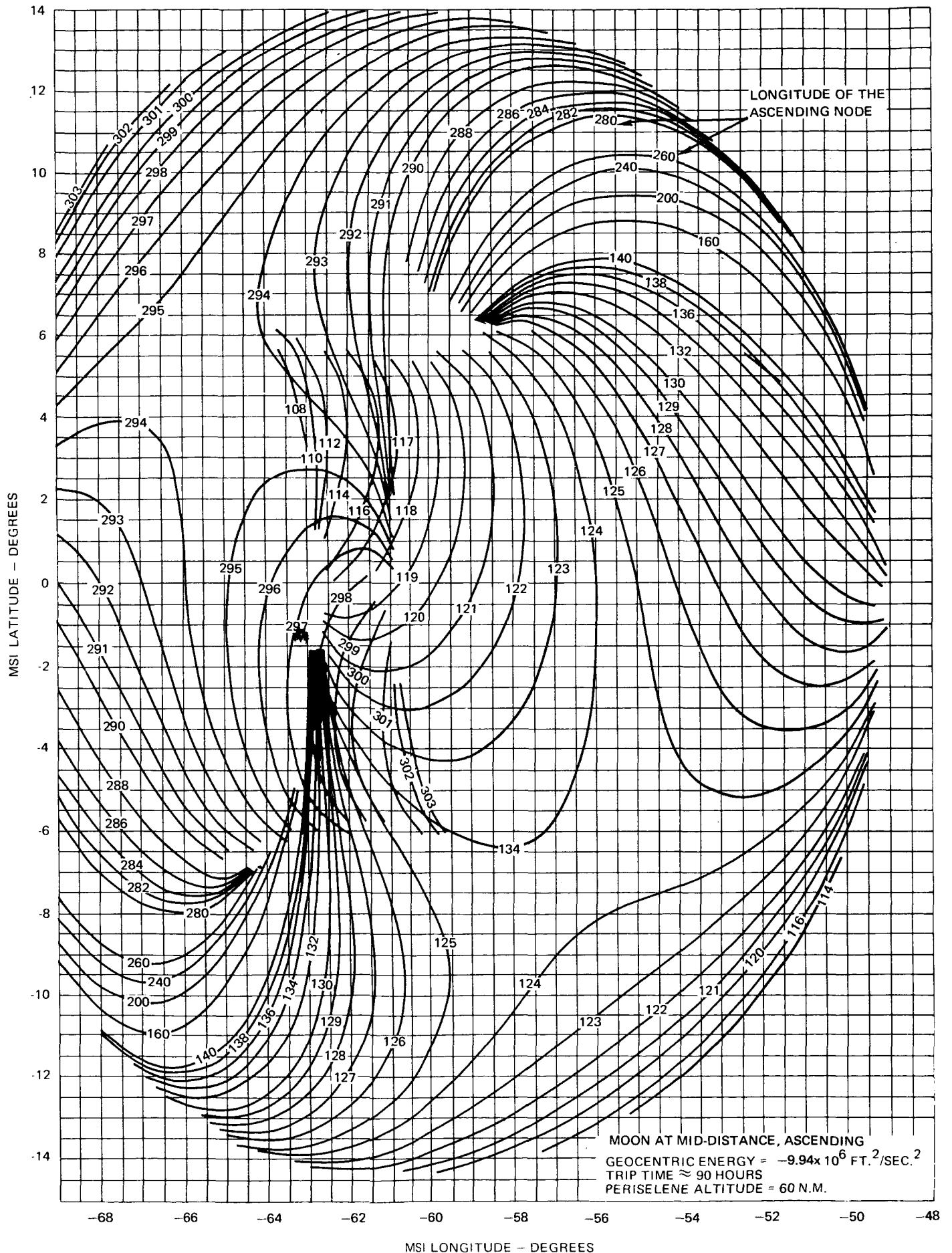


FIGURE 41B - LOCUS OF MSI AIMPOINTS FOR VARIOUS SELENOCENTRIC LONGITUDES OF THE ASCENDING NODE

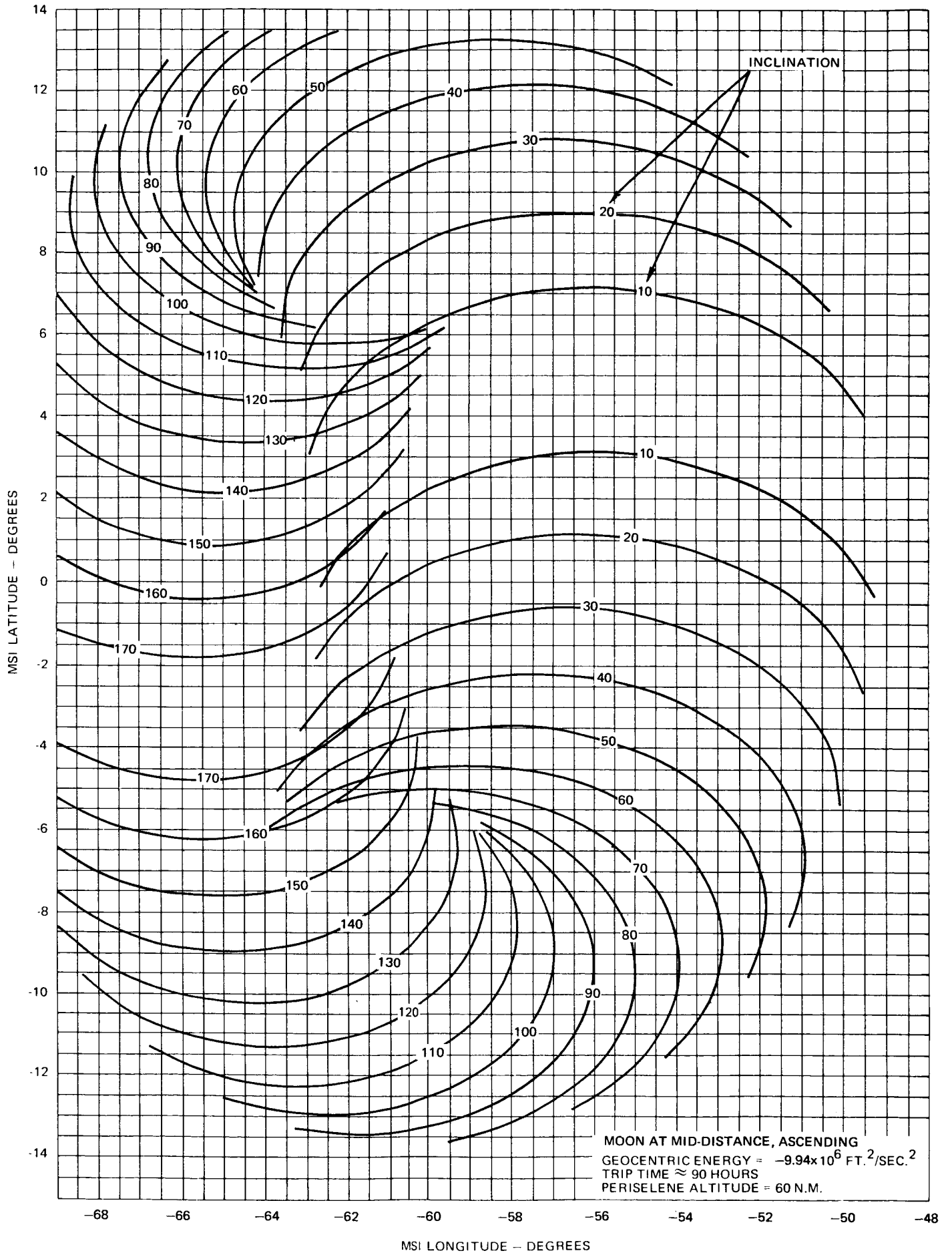


FIGURE 42A - LOCUS OF MSI AIMPOINTS FOR VARIOUS GEOCENTRIC INCLINATIONS

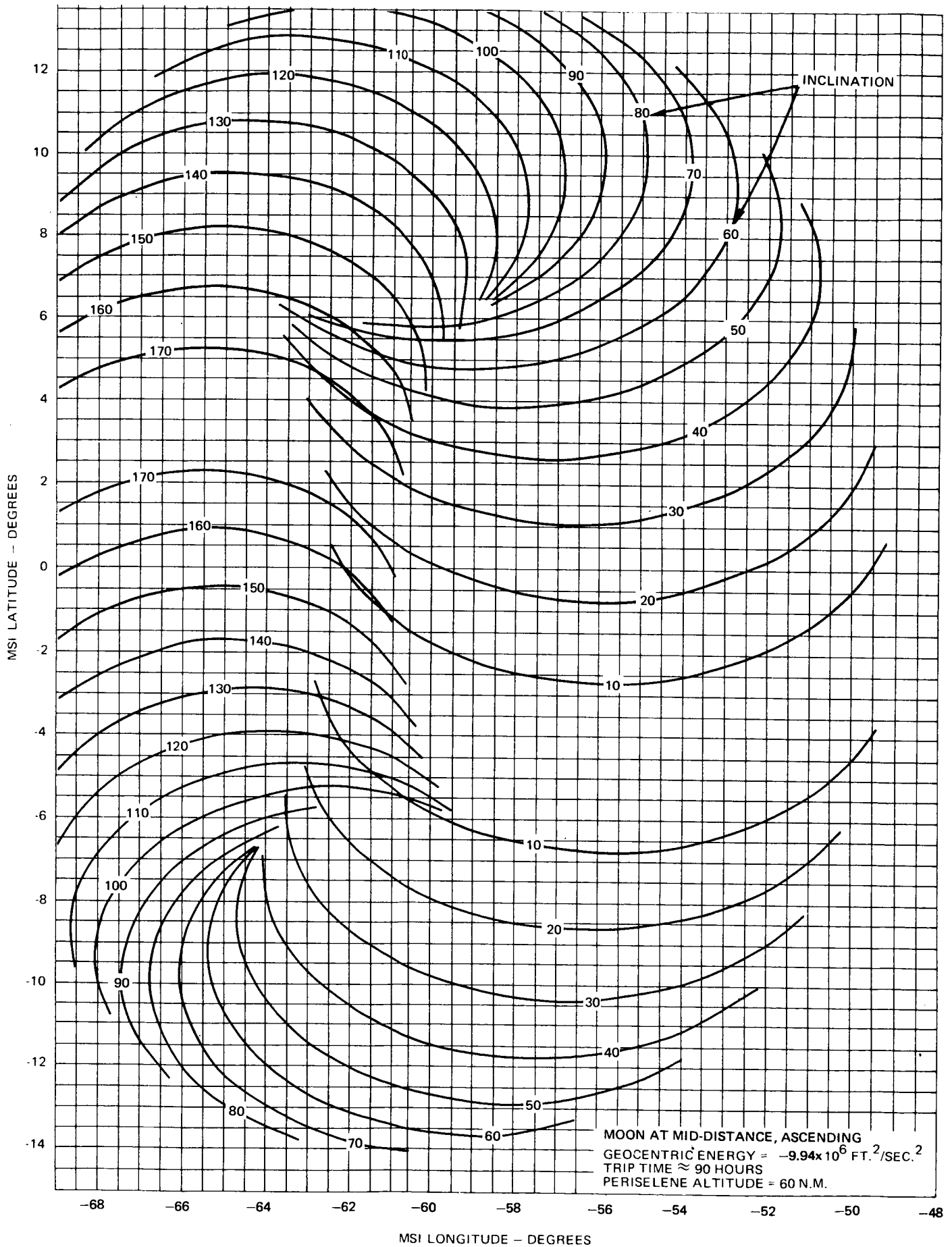


FIGURE 42B - LOCUS OF MSI AIMPOINTS FOR VARIOUS GEOCENTRIC INCLINATIONS

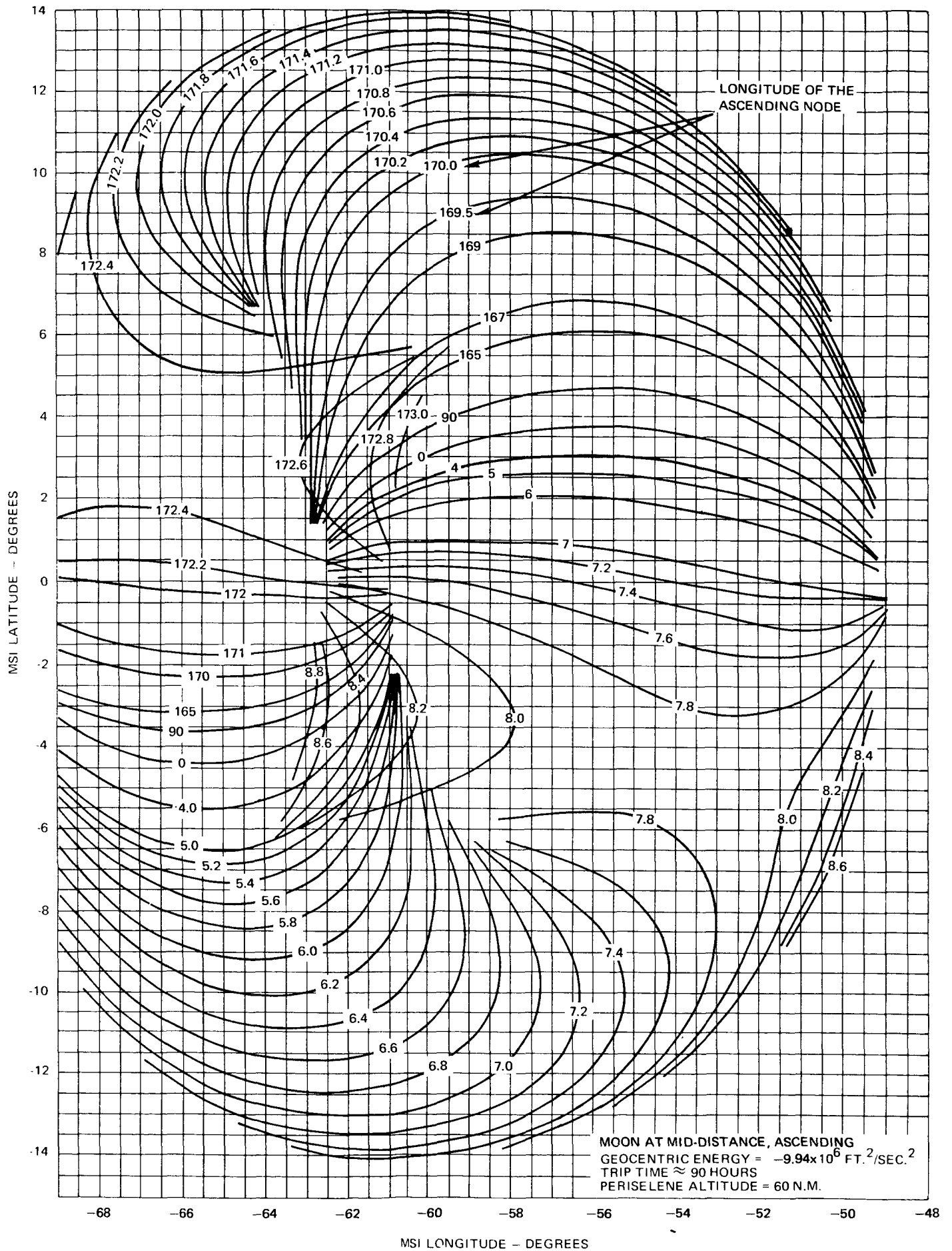


FIGURE 43A - LOCUS OF MSI AIMPOINTS FOR VARIOUS GEOCENTRIC LONGITUDES OF THE ASCENDING NODE

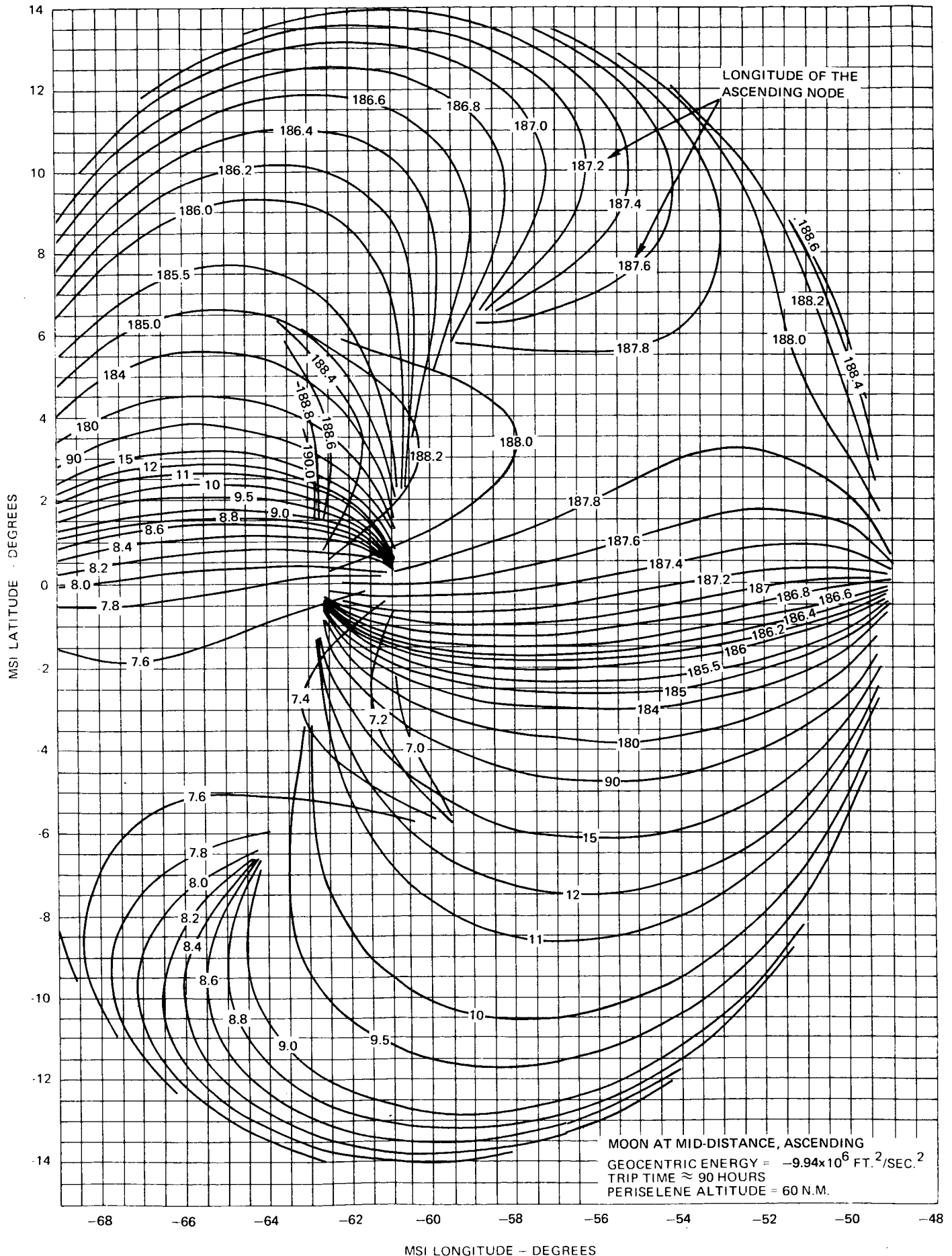


FIGURE 43B - LOCUS OF MSI AIMPOINTS FOR VARIOUS GEOCENTRIC LONGITUDES OF THE ASCENDING NODE

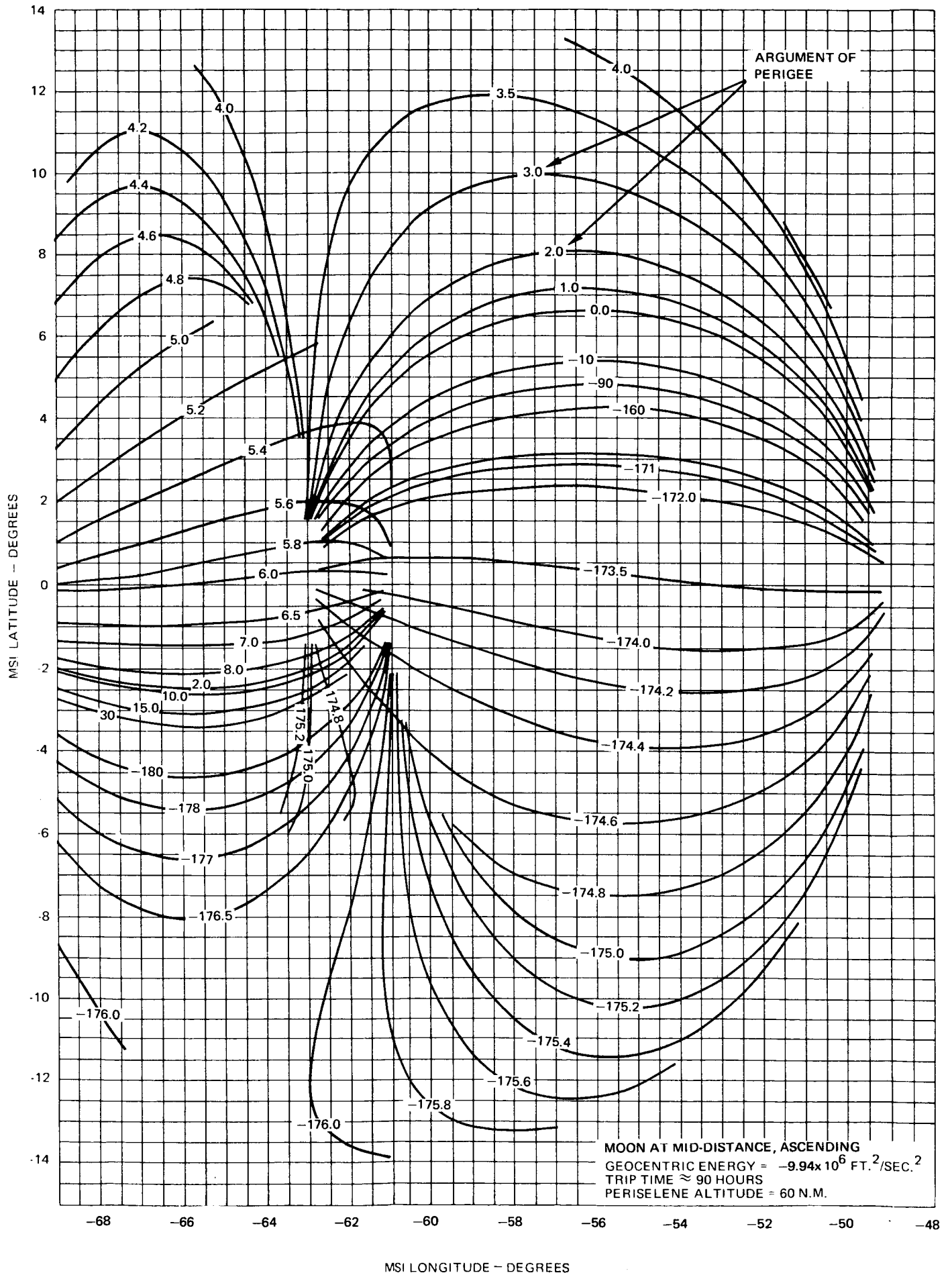


FIGURE 44A - LOCUS OF MSI AIM POINTS FOR VARIOUS GEOCENTRIC ARGUMENTS OF PERIGEE

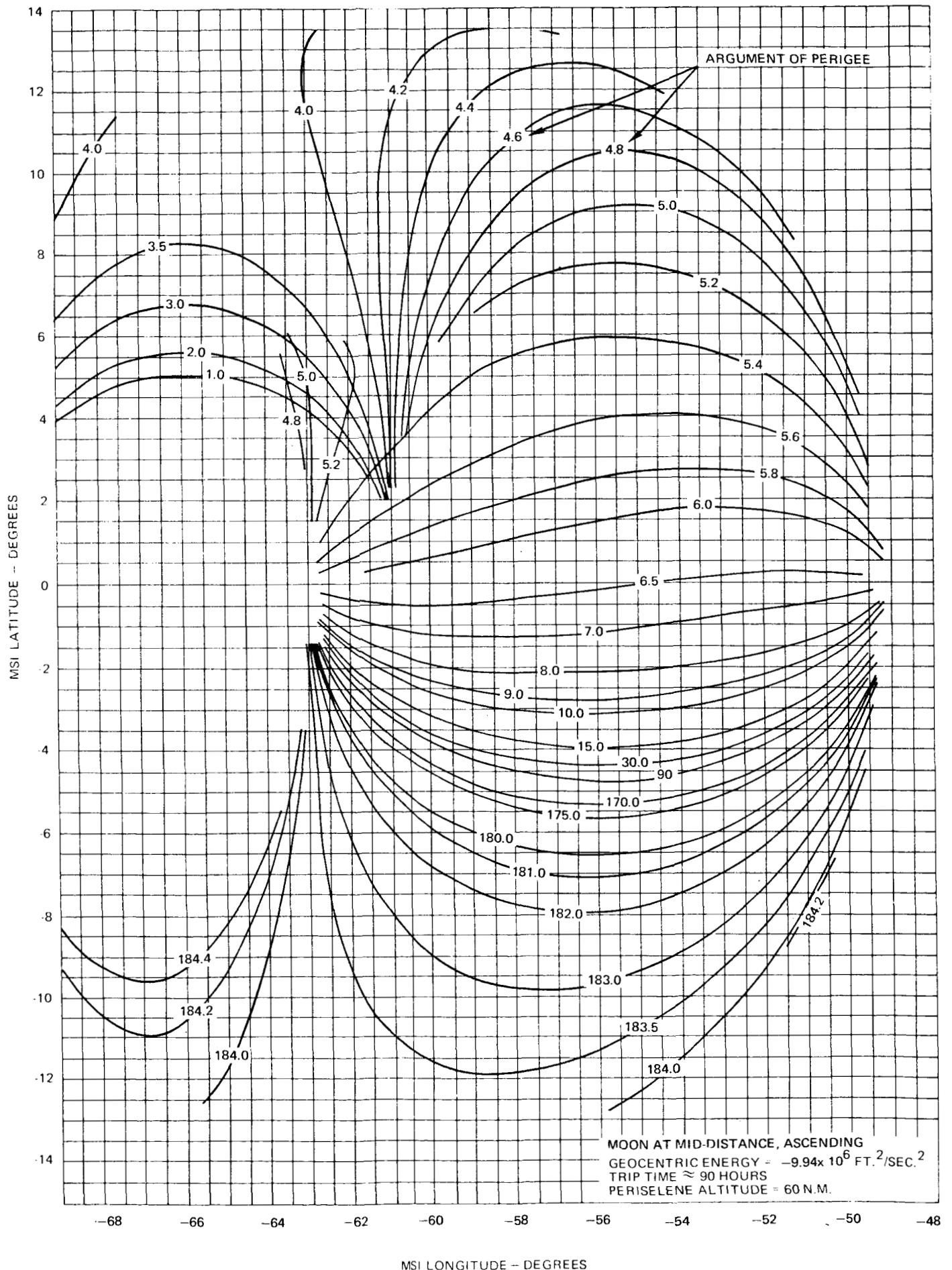


FIGURE 44B - LOCUS OF MSI AIM POINTS FOR VARIOUS GEOCENTRIC ARGUMENTS OF PERIGEE

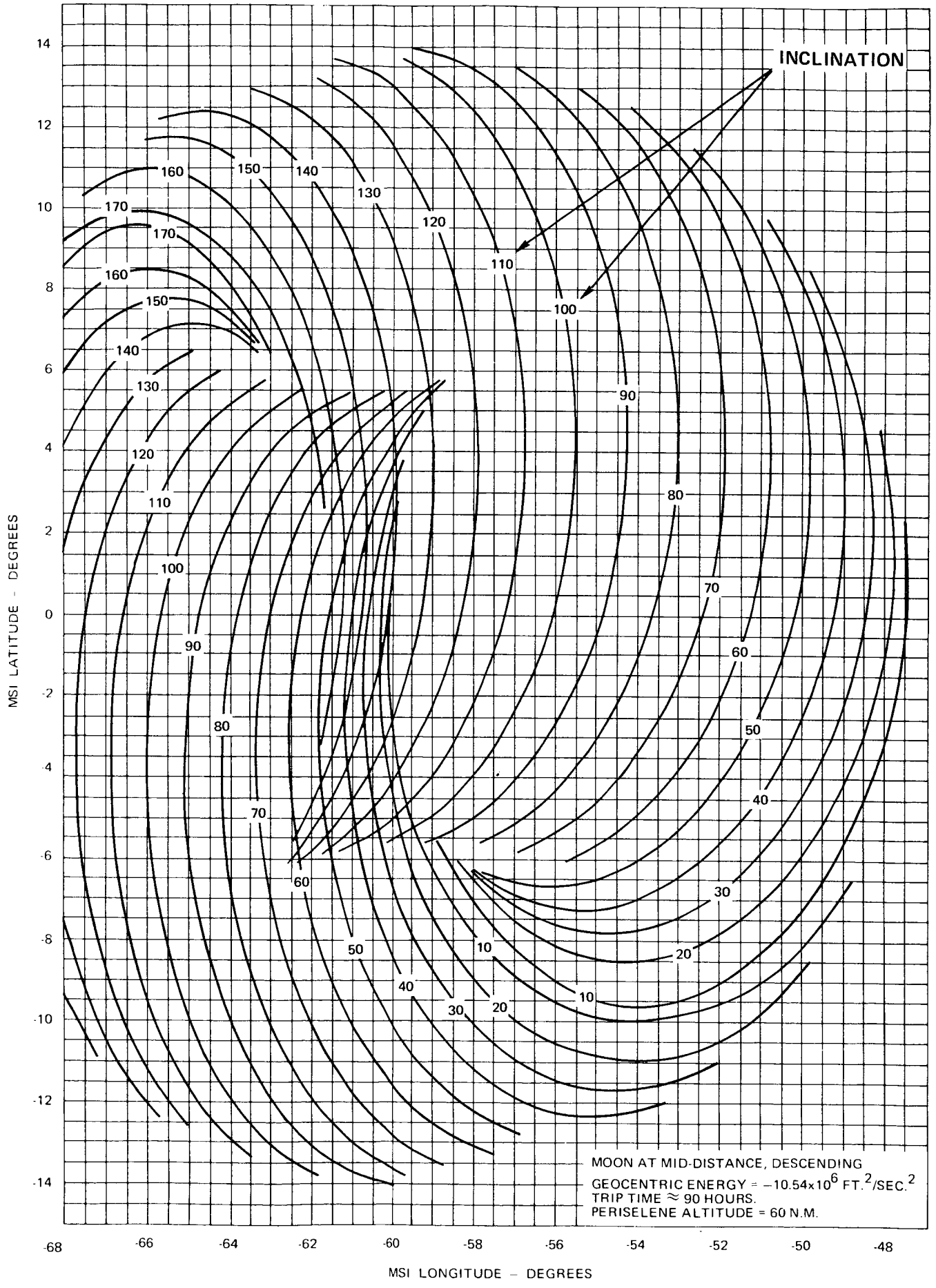


FIGURE 45A - LOCUS OF MSI AIMPOINTS FOR VARIOUS SELENOCENTRIC INCLINATIONS

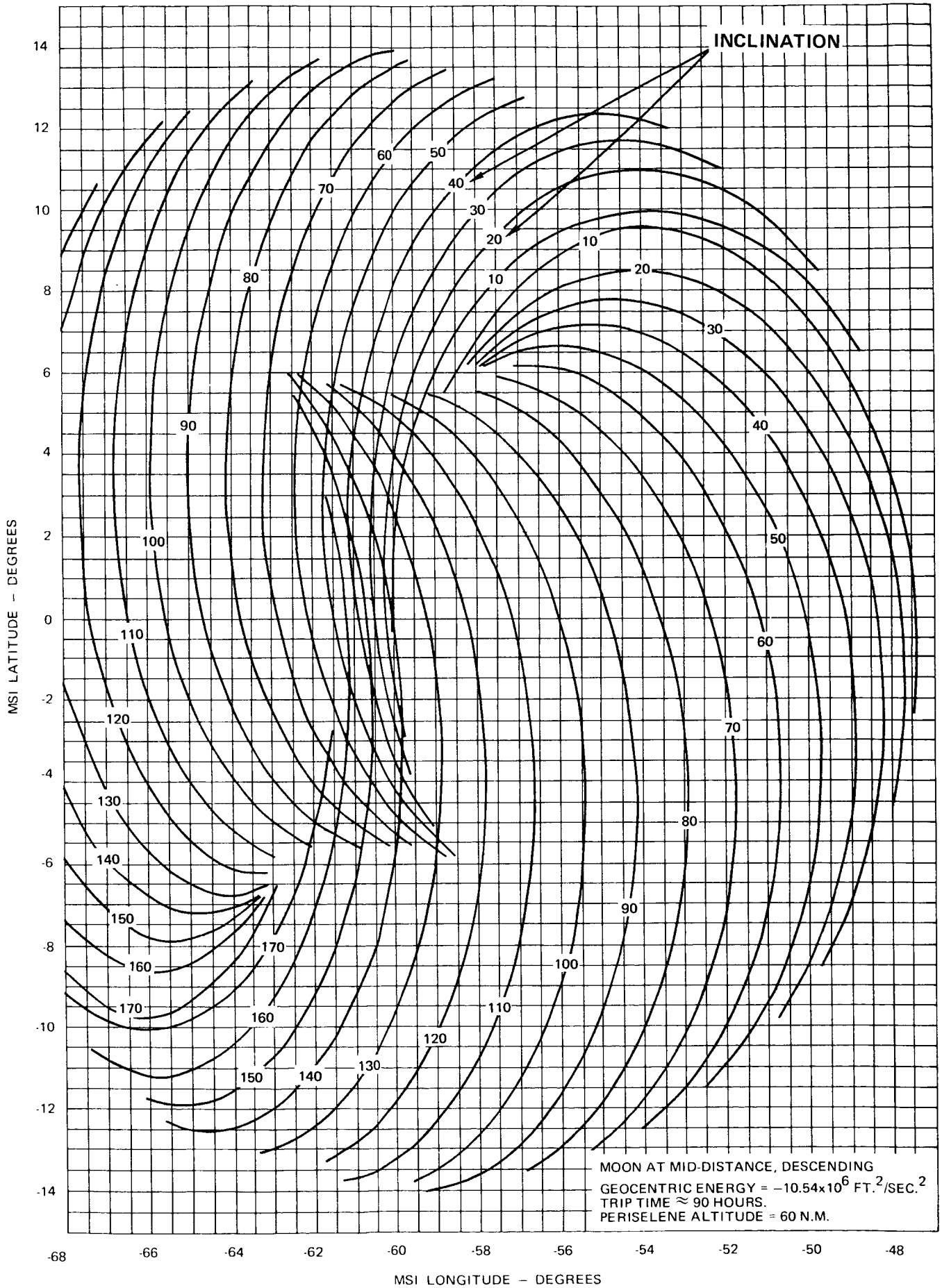


FIGURE 45B - LOCUS OF MSI AIMPOINTS FOR VARIOUS SELENOCENTRIC INCLINATIONS

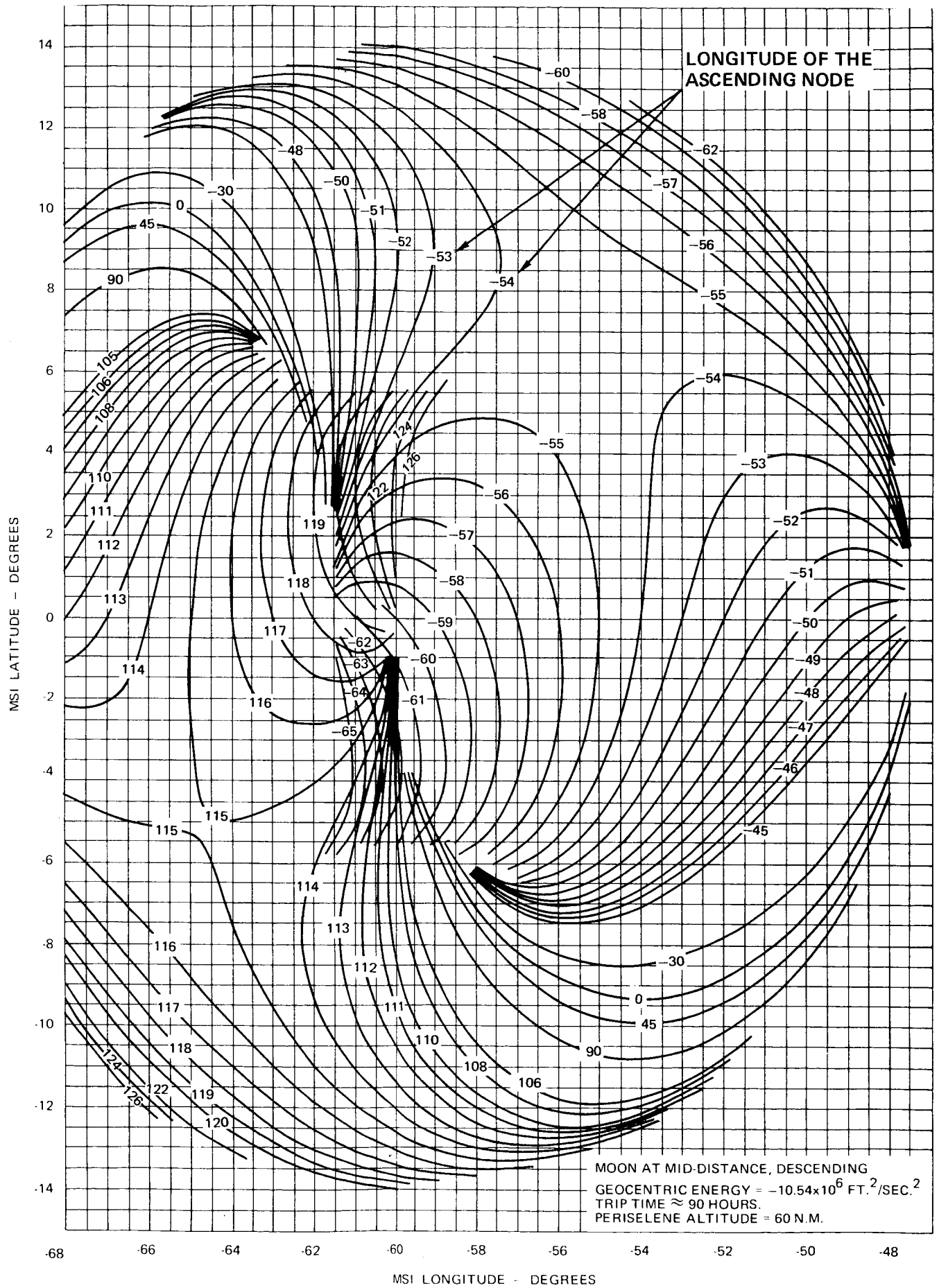


FIGURE 46A - LOCUS OF MSI AIMPOINTS FOR VARIOUS SELENOCENTRIC LONGITUDES OF THE ASCENDING NODE

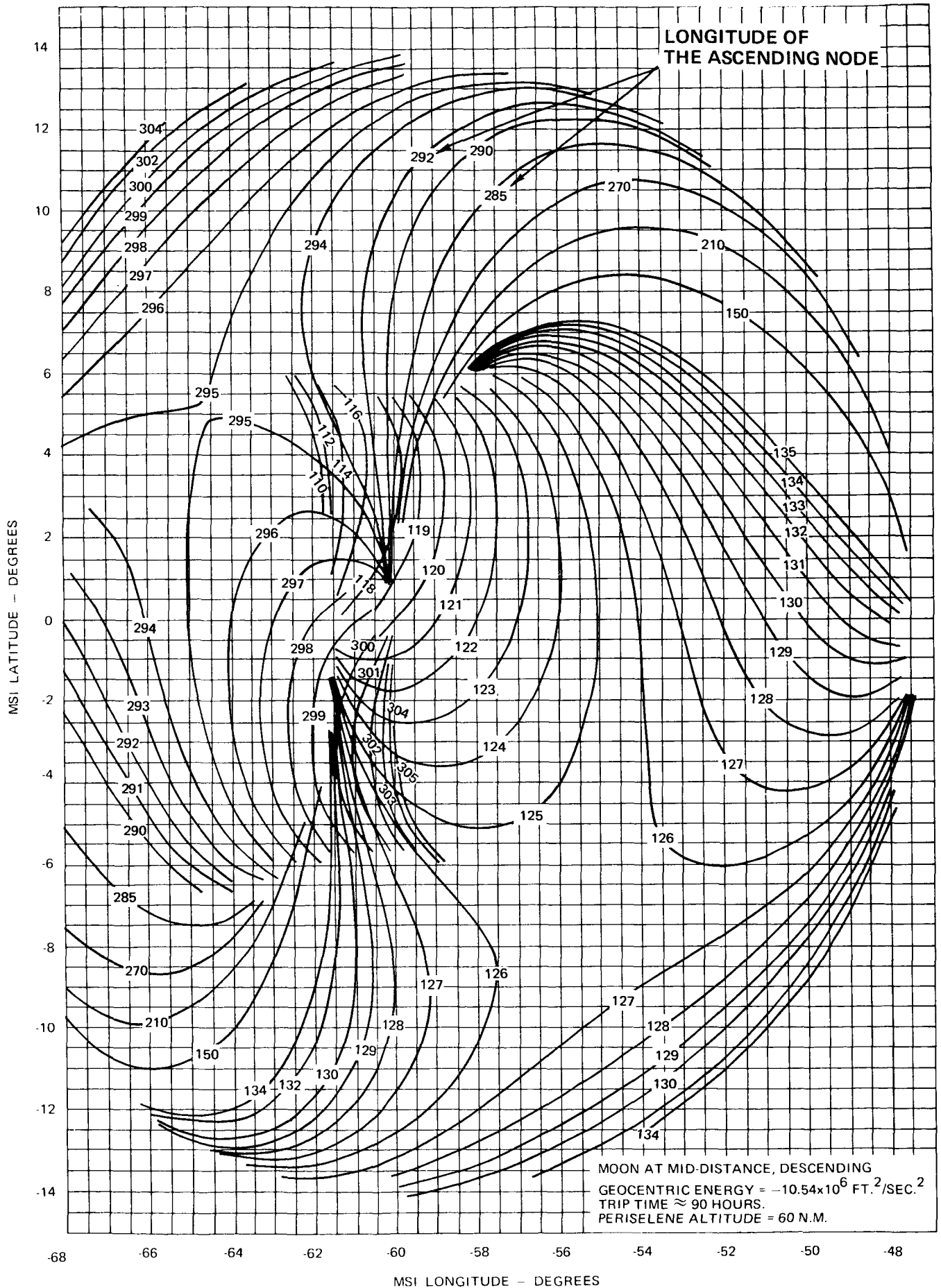


FIGURE 46B - LOCUS OF MSI AIMPOINTS FOR VARIOUS SELENOCENTRIC LONGITUDES OF THE ASCENDING NODE

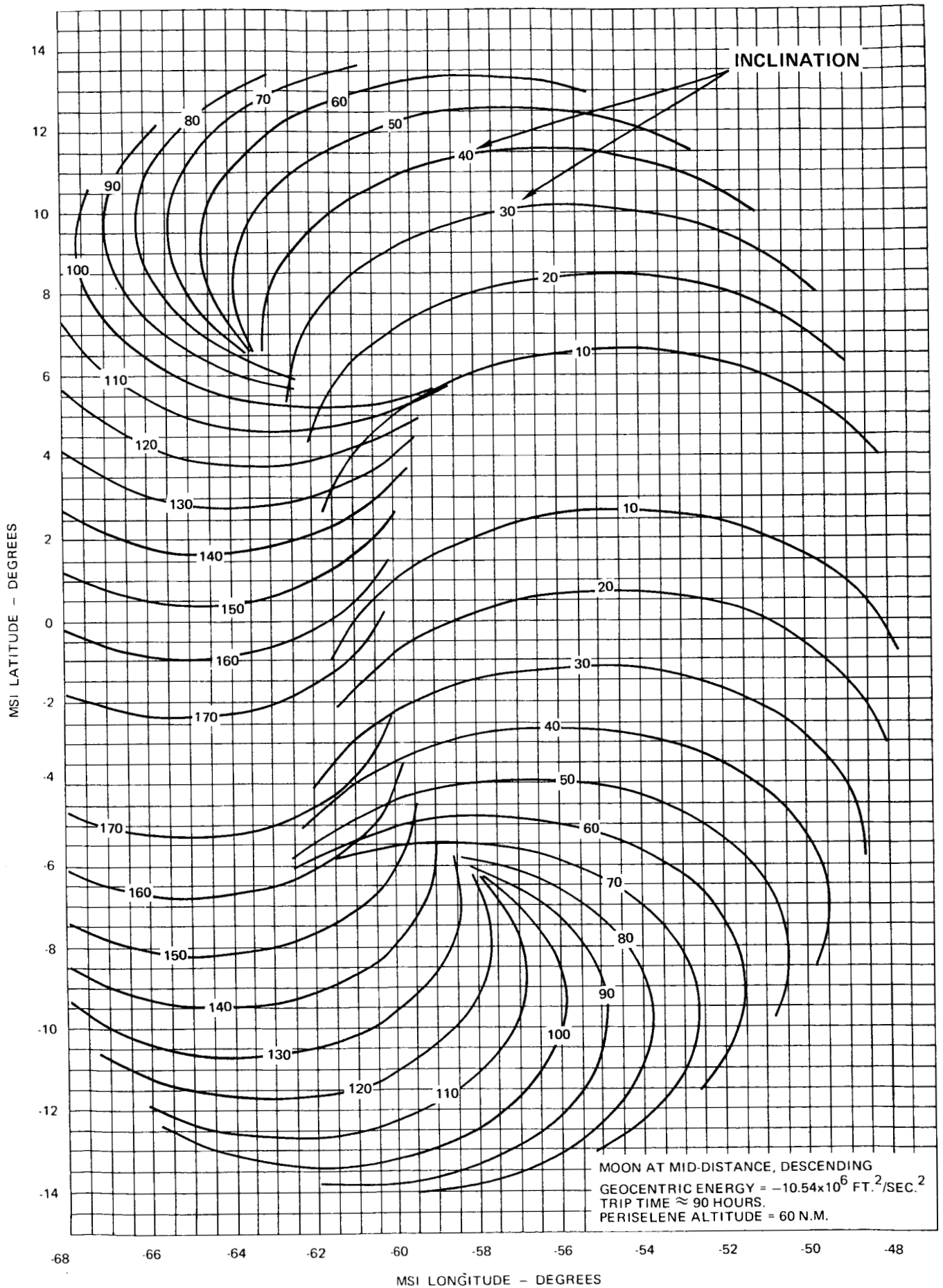


FIGURE 47A - LOCUS OF MSI AIMPOINTS FOR VARIOUS GEOCENTRIC INCLINATIONS

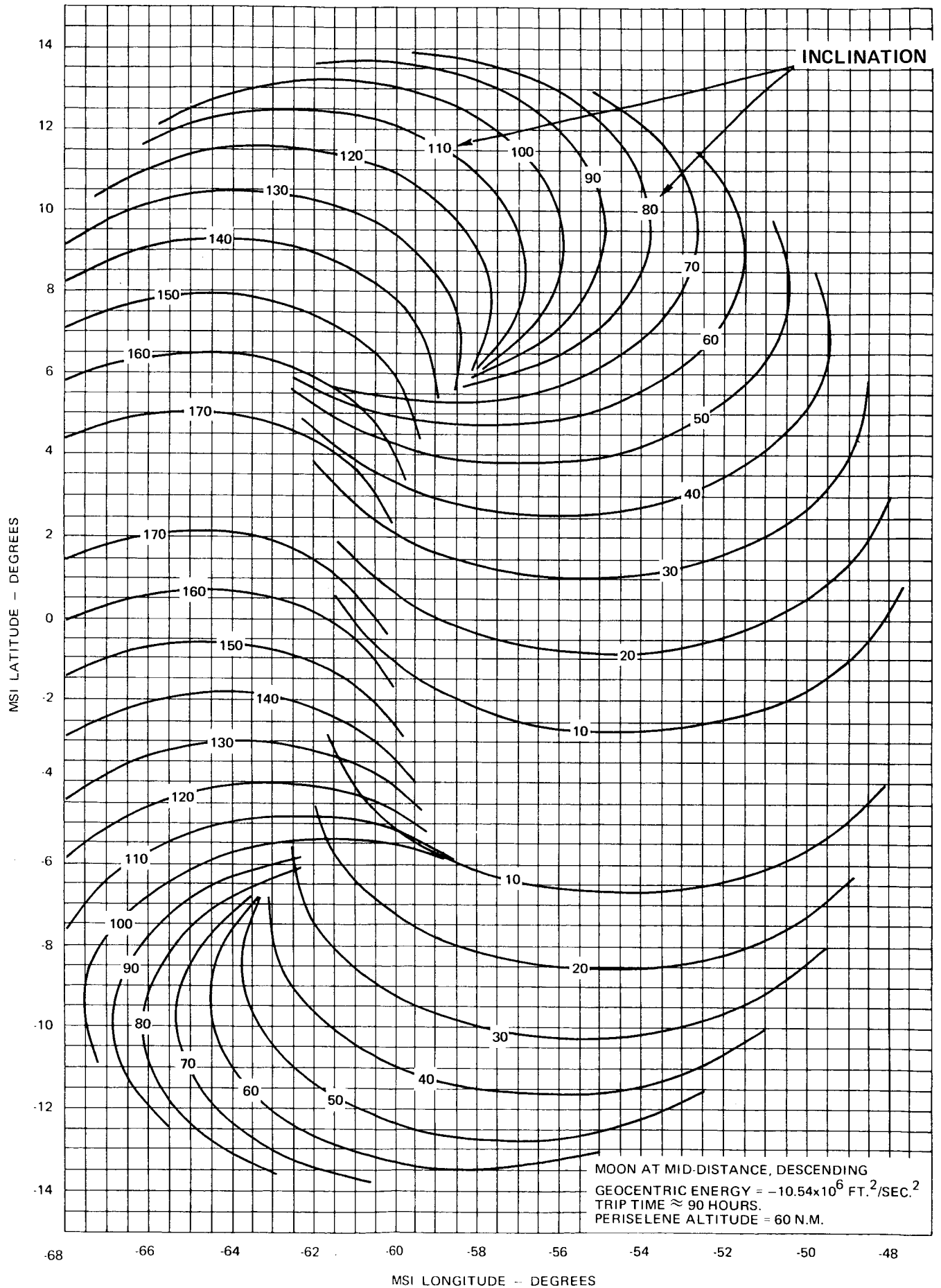


FIGURE 47B - LOCUS OF MSI AIMPOINTS FOR VARIOUS GEOCENTRIC INCLINATIONS

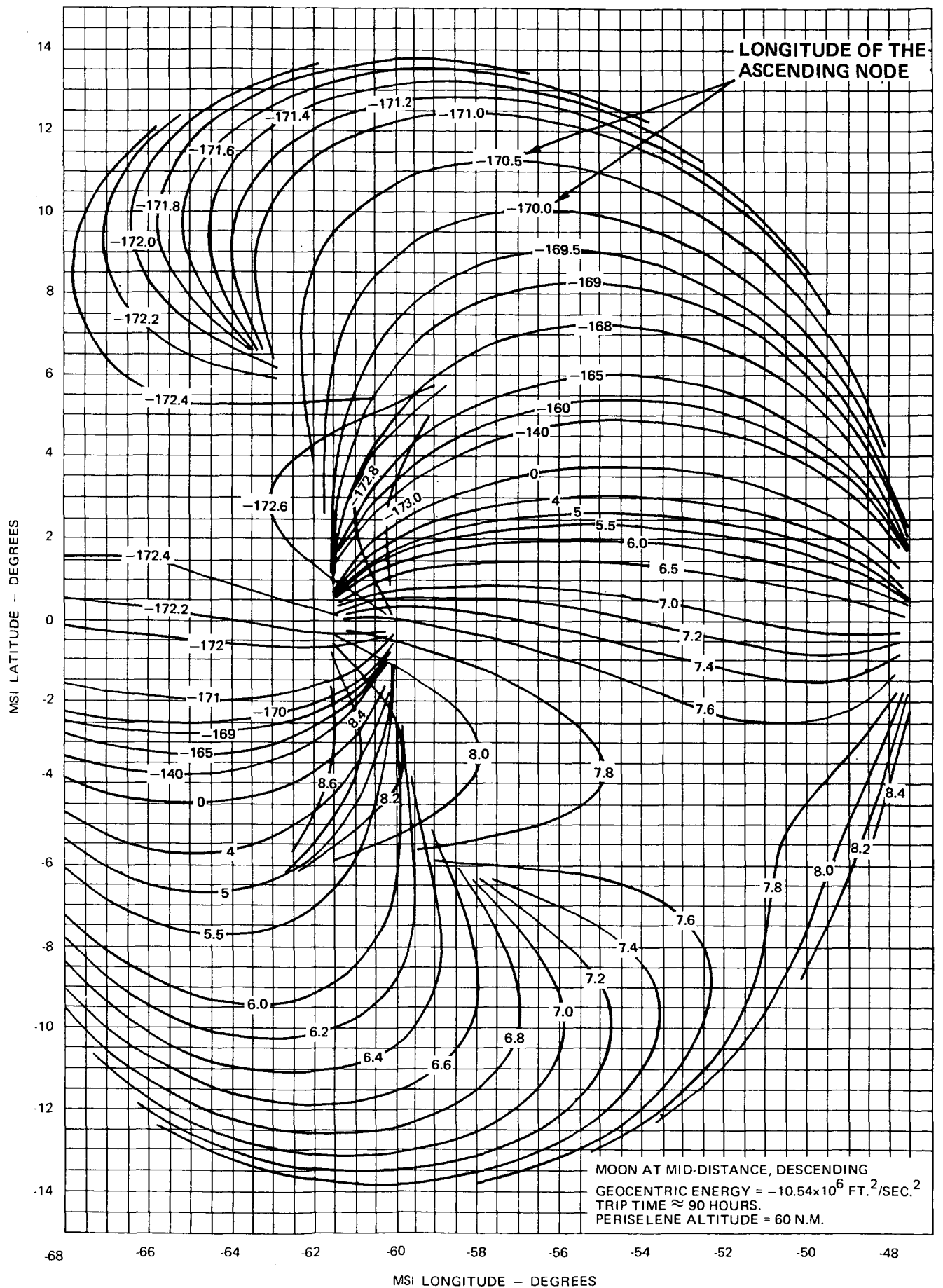


FIGURE 48A - LOCUS OF MSI AIMPOINTS FOR VARIOUS GEOCENTRIC LONGITUDES OF THE ASCENDING NODE

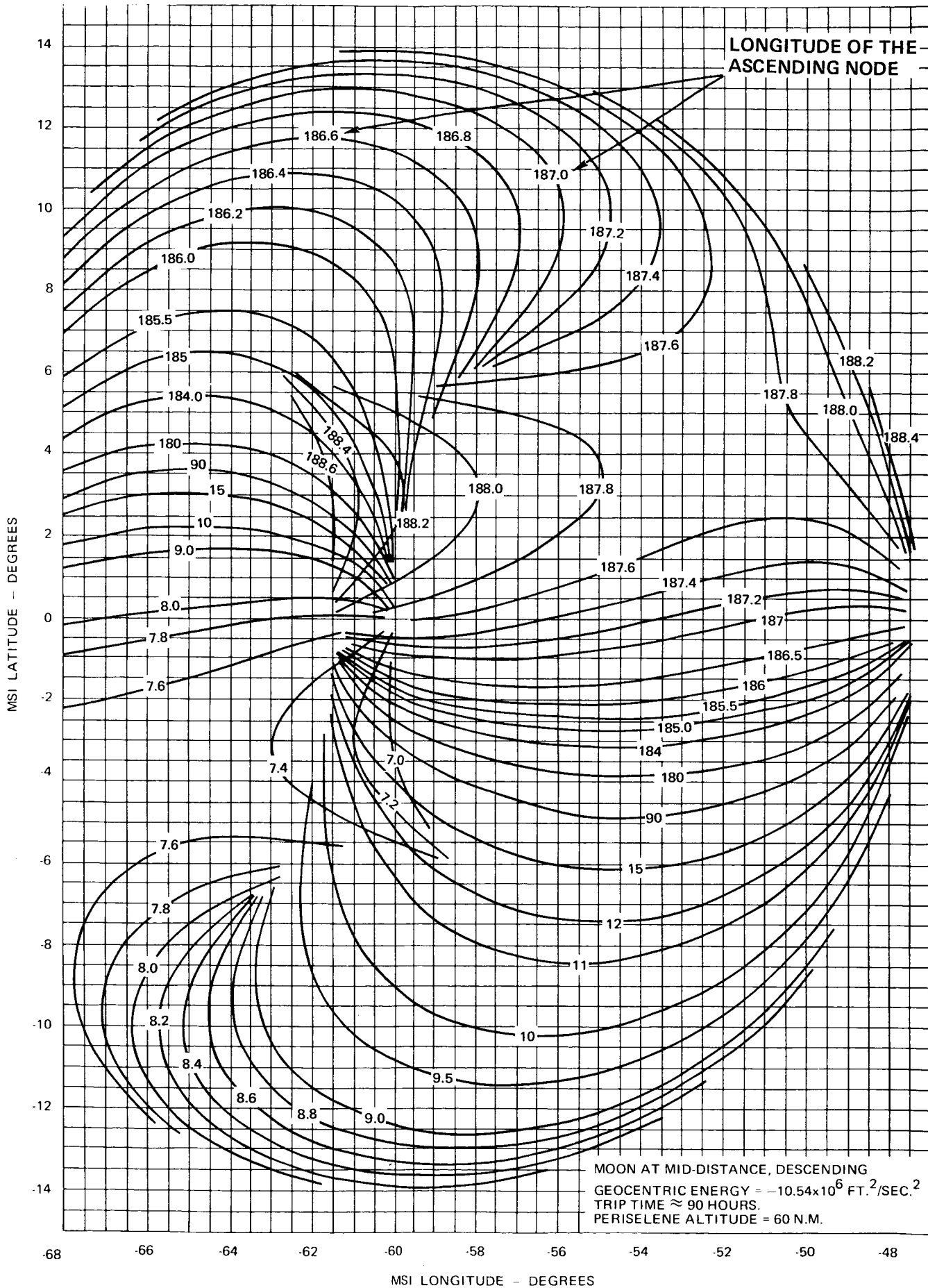


FIGURE 48B - LOCUS OF MSI AIMPOINTS FOR VARIOUS GEOCENTRIC LONGITUDES OF THE ASCENDING NODE

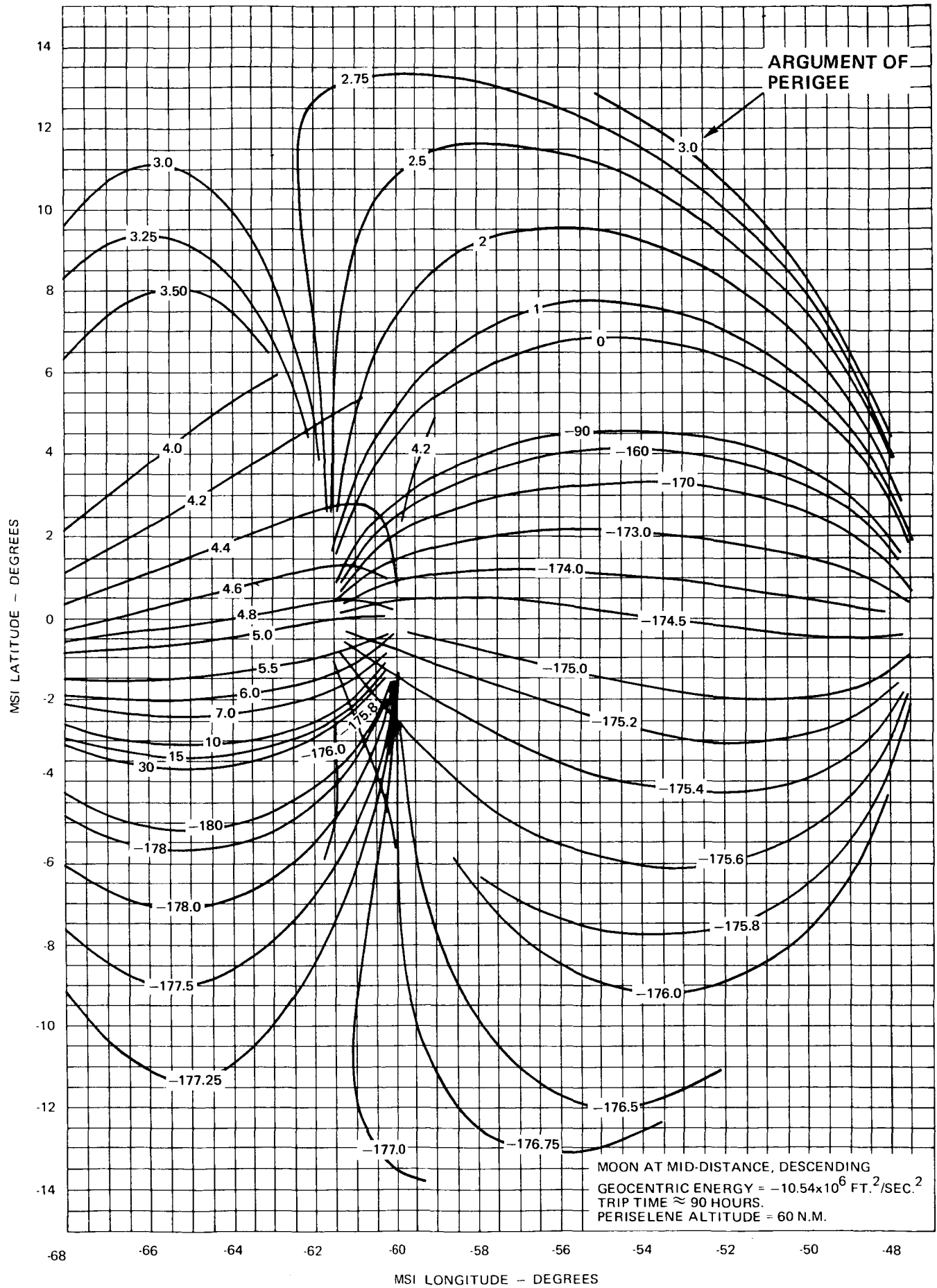


FIGURE 49A - LOCUS OF MSI AIMPOINTS FOR VARIOUS GEOCENTRIC ARGUMENTS OF PERIGEE

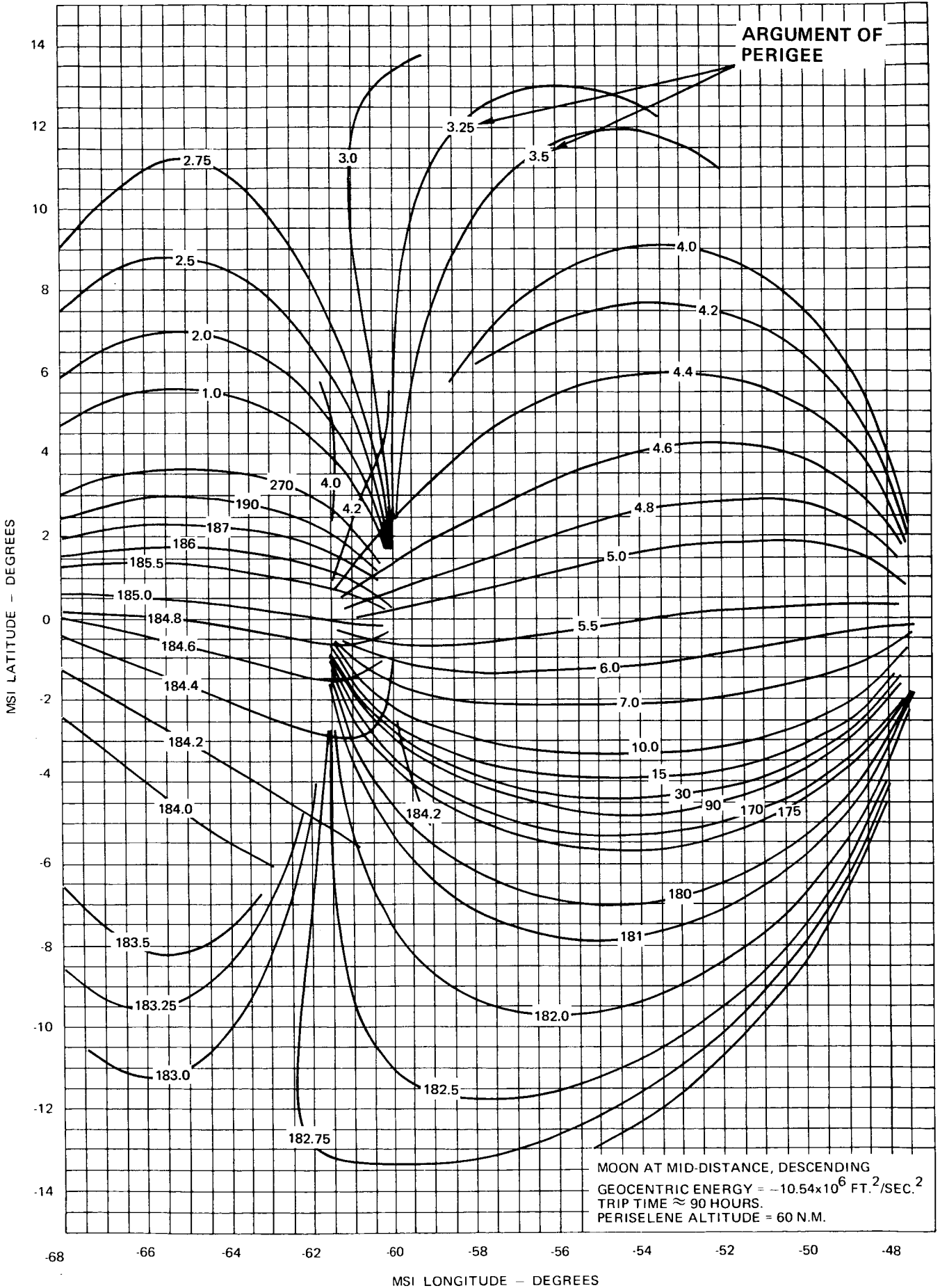


FIGURE 49B - LOCUS OF MSI AIMPOINTS FOR VARIOUS GEOCENTRIC ARGUMENTS OF PERIGEE

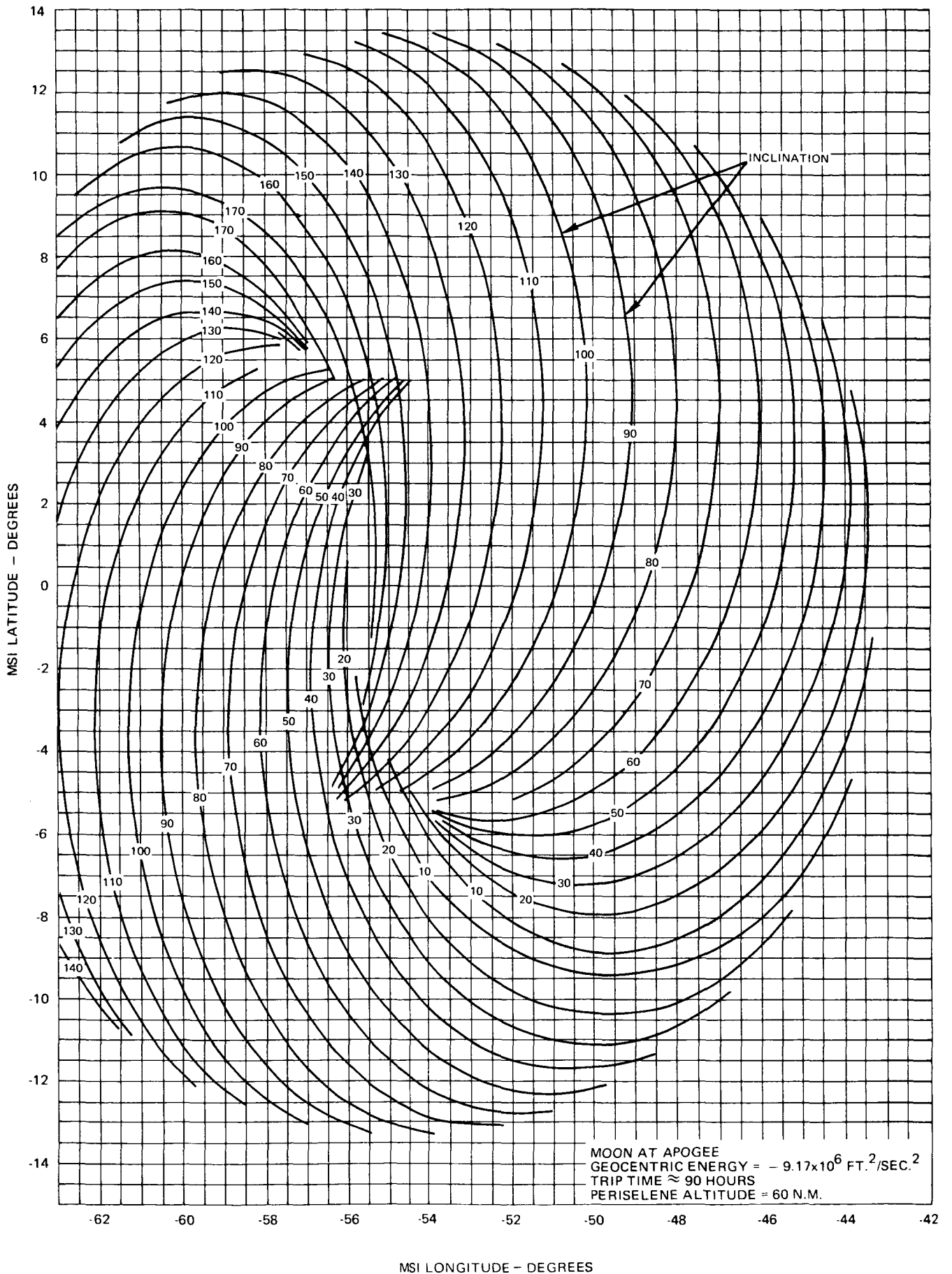
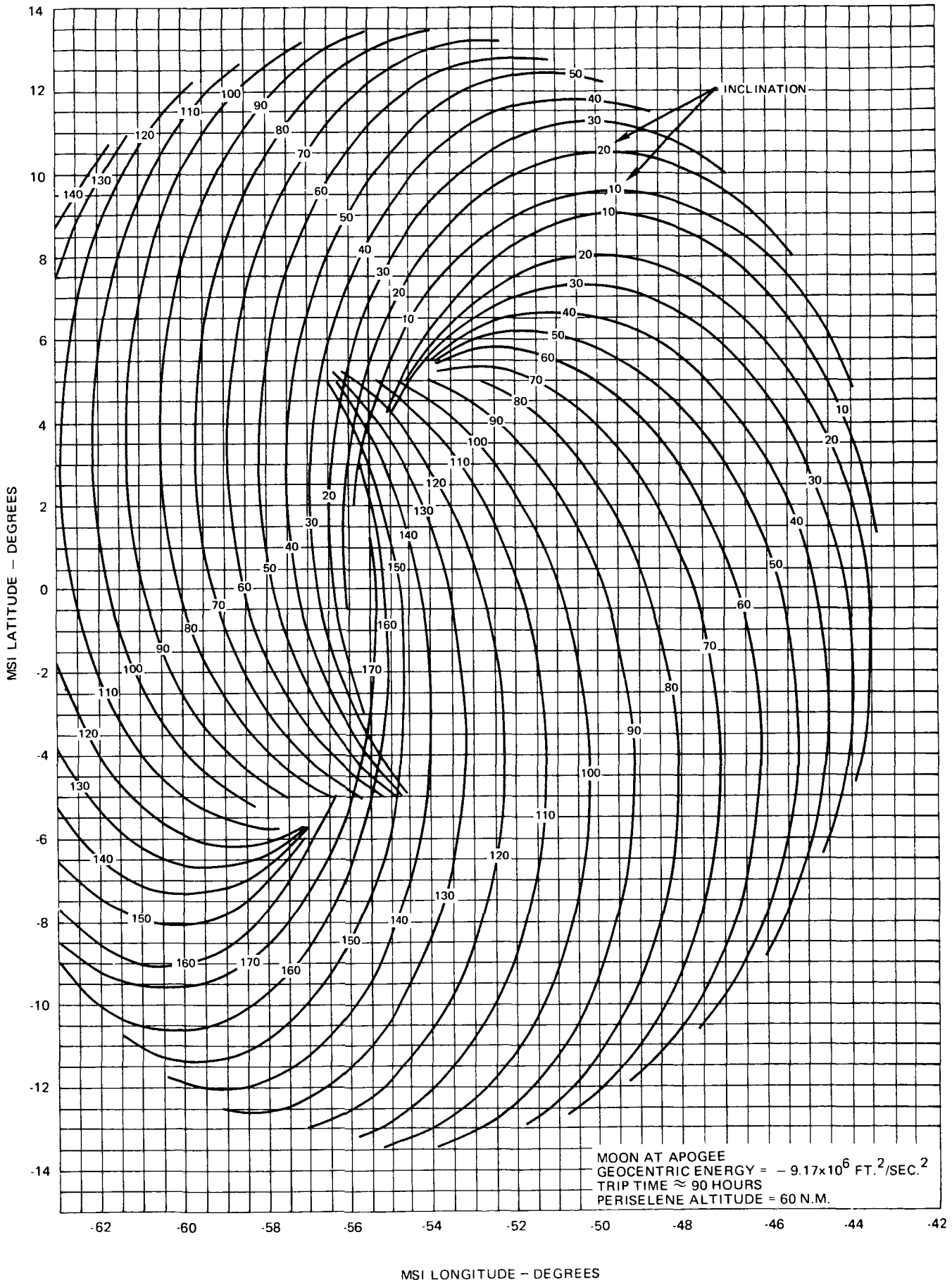
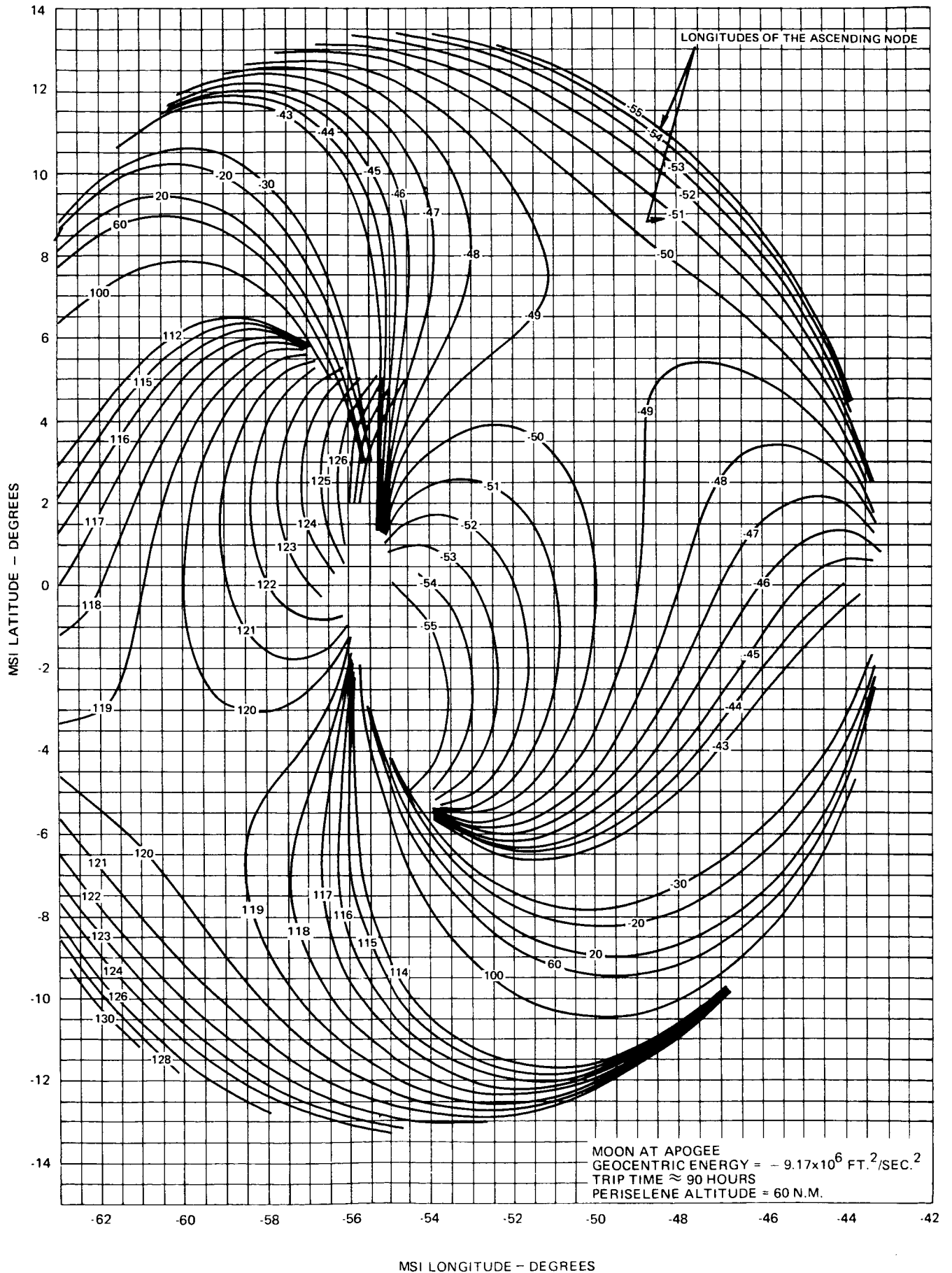


FIGURE 50A - LOCUS OF MSI AIM POINTS FOR VARIOUS SELENOCENTRIC INCLINATIONS



MSI LONGITUDE - DEGREES

FIGURE 50B - LOCUS OF MSI AIM POINTS FOR VARIOUS SELENOCENTRIC INCLINATIONS



MSI LONGITUDE - DEGREES

FIGURE 51A - LOCUS OF MSI AIM POINTS FOR VARIOUS SELENOCENTRIC LONGITUDES OF THE ASCENDING NODE

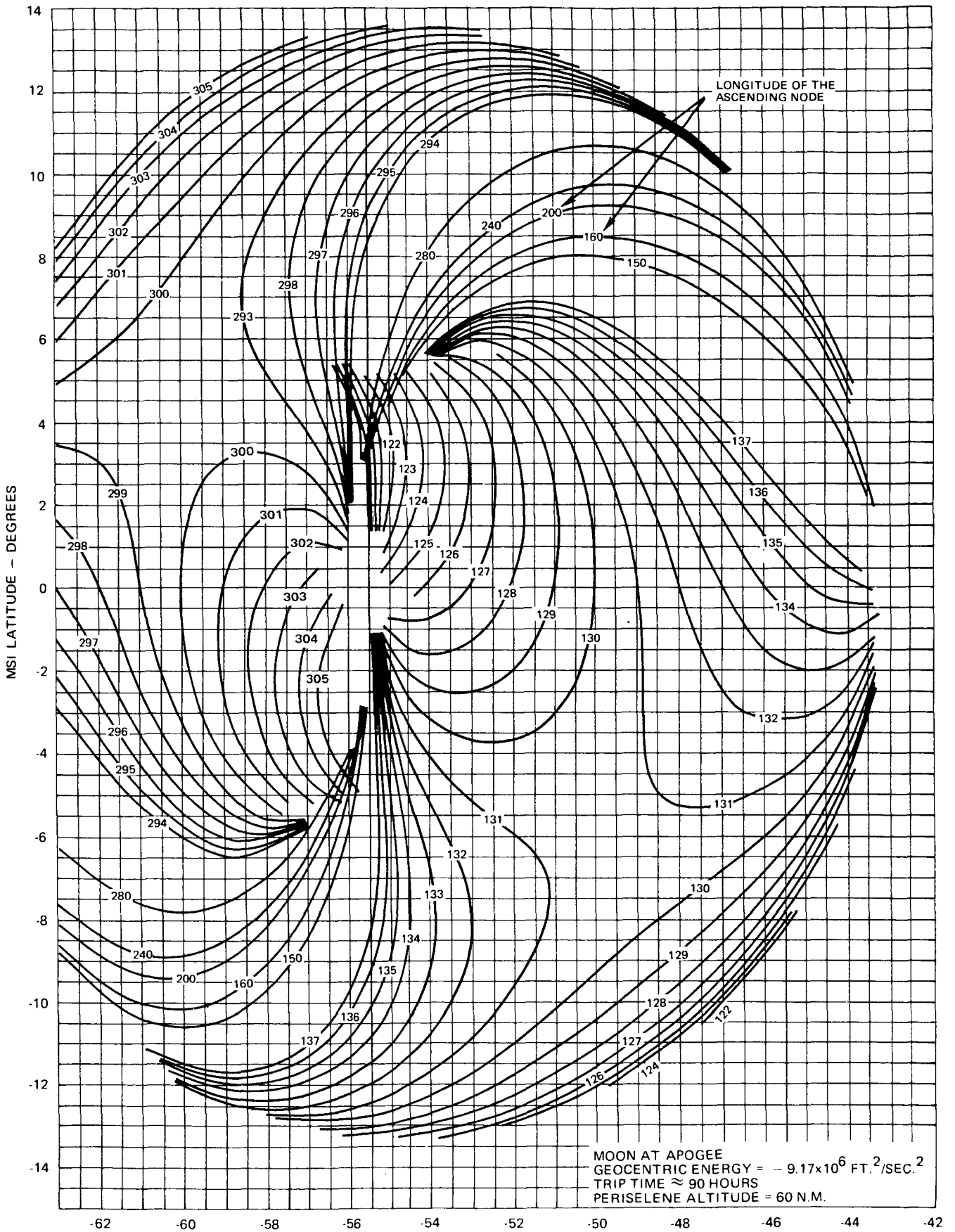


FIGURE 51B - LOCUS OF MSI AIM POINTS FOR VARIOUS SELENOCENTRIC LONGITUDES OF THE ASCENDING NODE

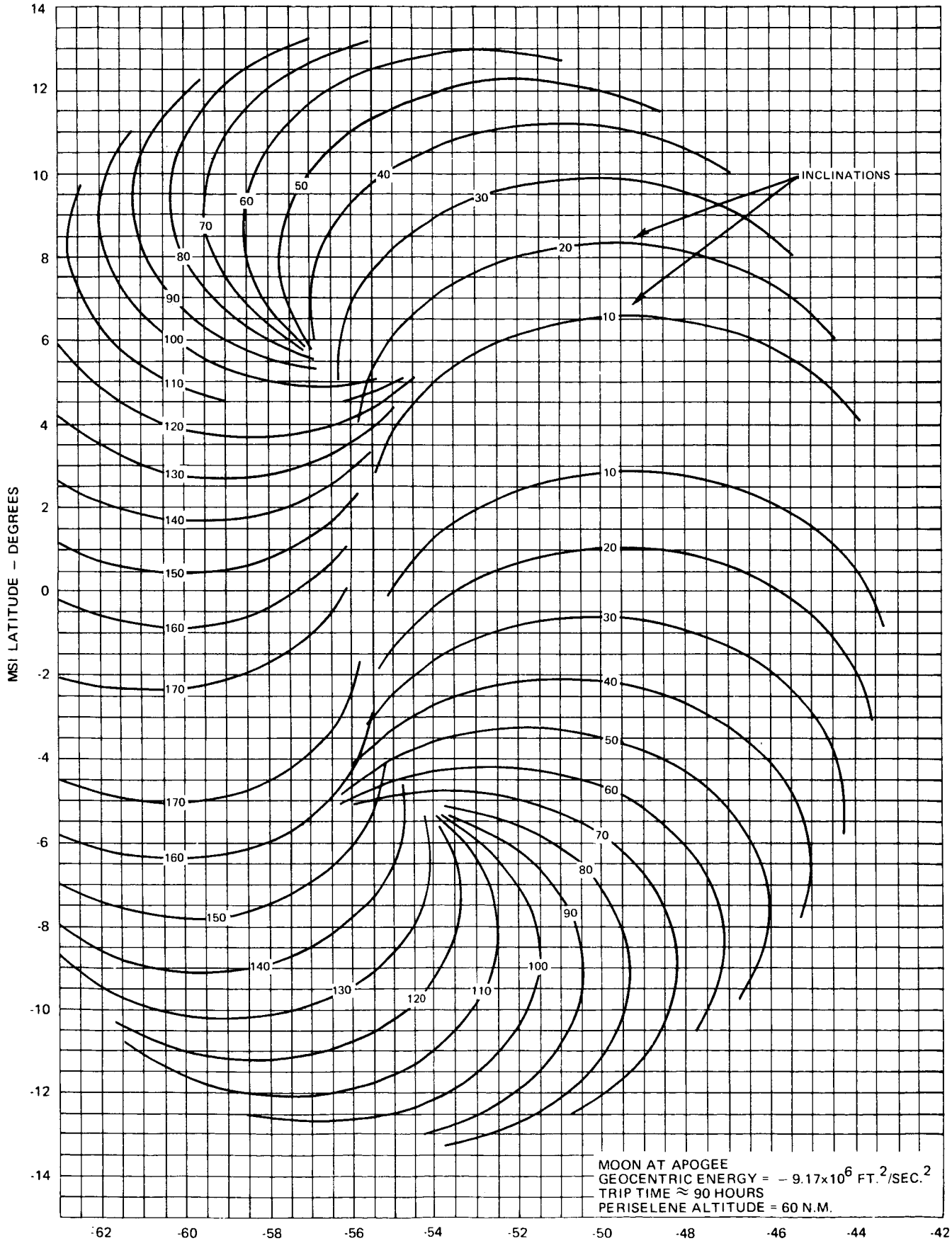


FIGURE 52A - LOCUS OF MSI AIM POINTS FOR VARIOUS GEOCENTRIC INCLINATIONS

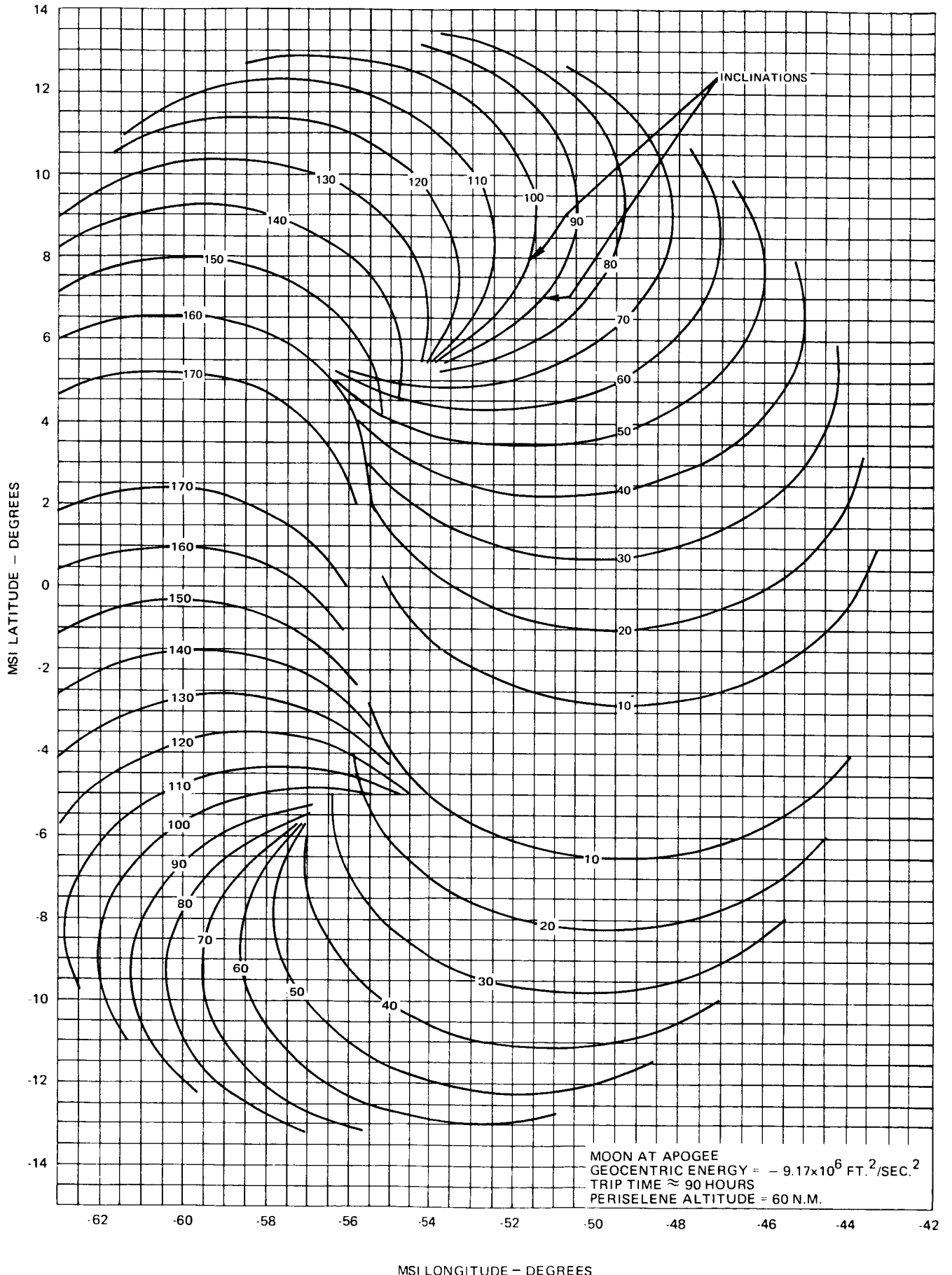


FIGURE 52B - LOCUS OF MSI AIM POINTS FOR VARIOUS GEOCENTRIC INCLINATIONS

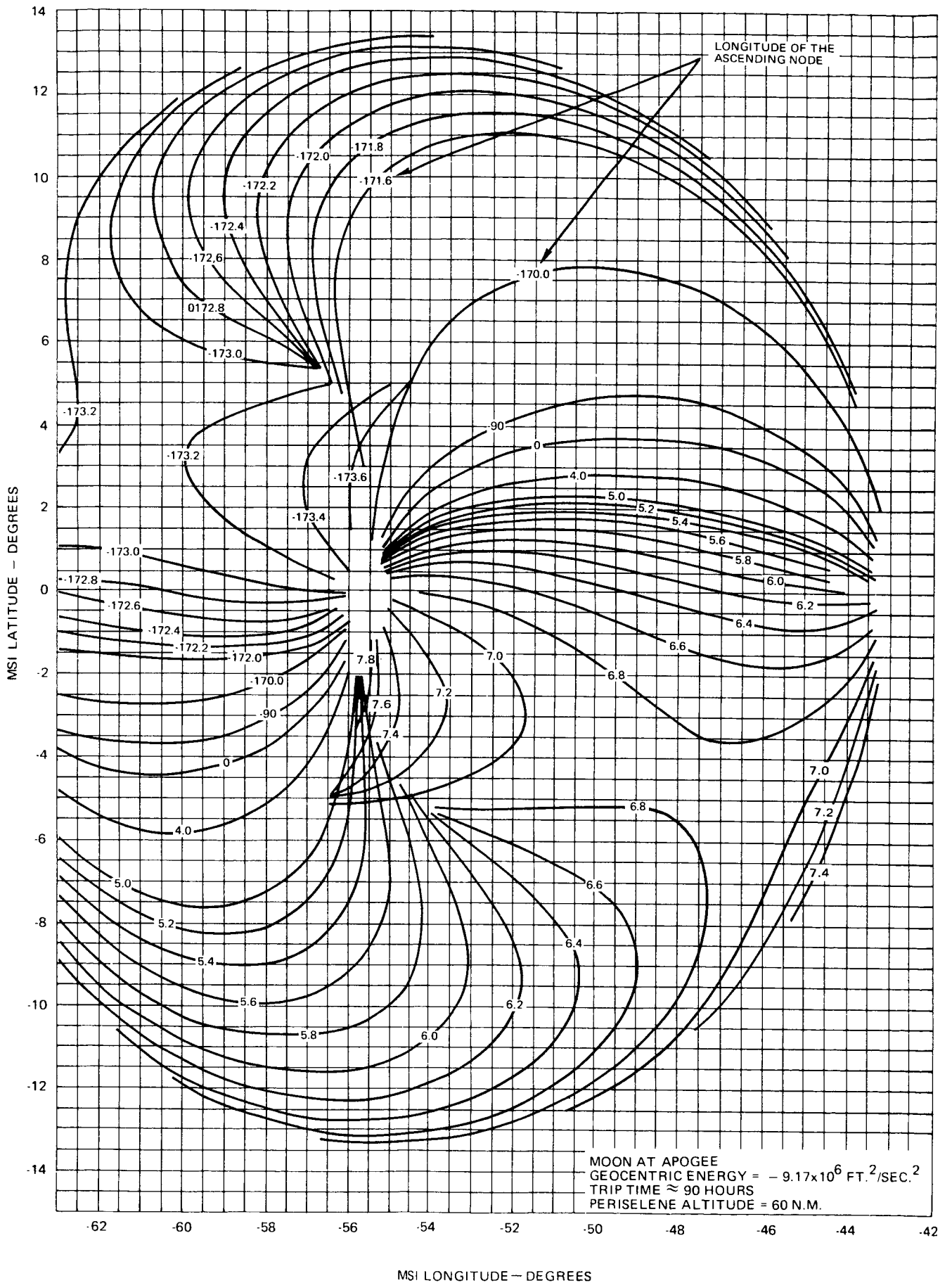


FIGURE 53A - LOCUS OF MSI AIM POINTS FOR VARIOUS GEOCENTRIC LONGITUDES OF THE ASCENDING NODE

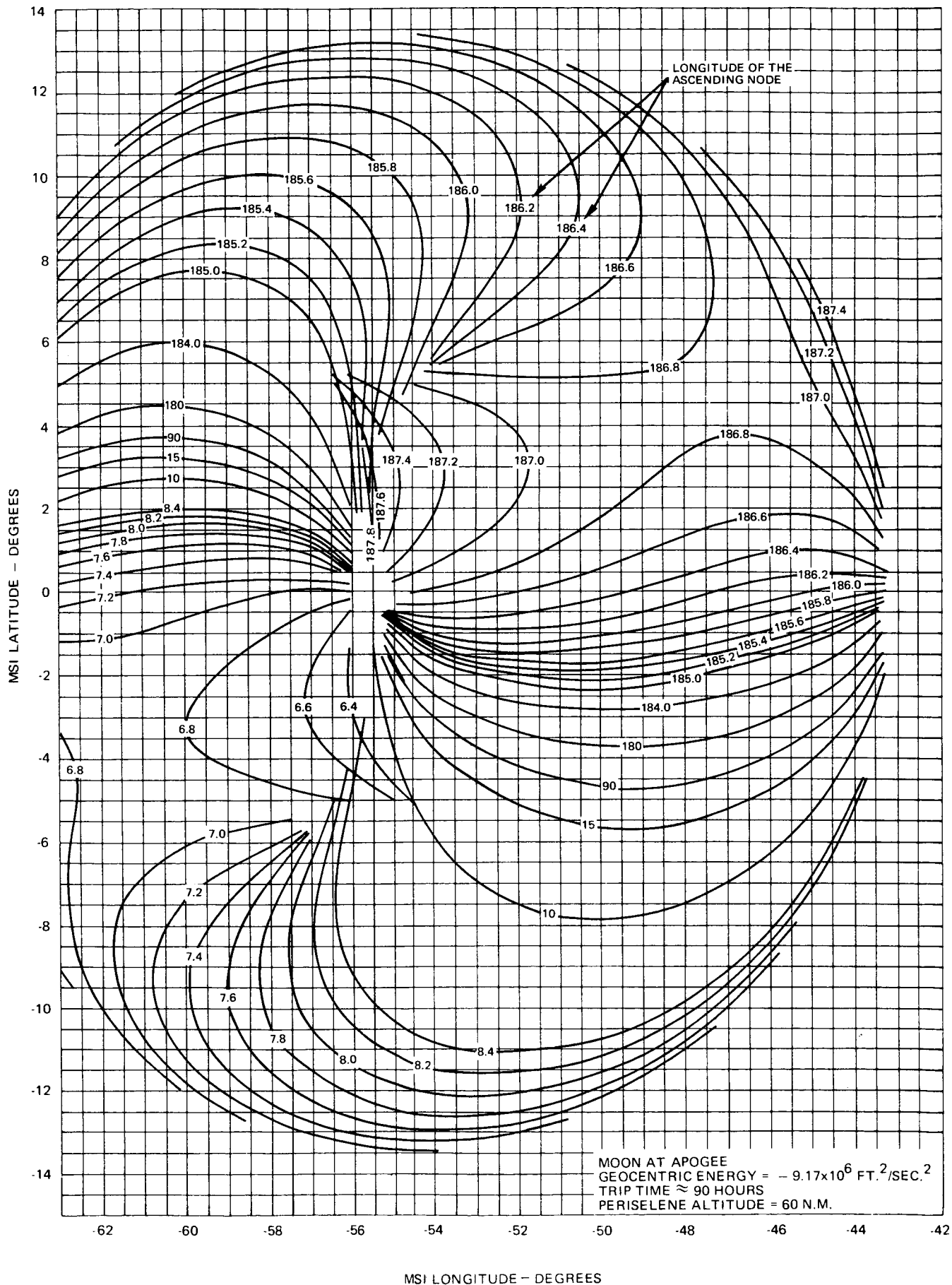


FIGURE 53B - LOCUS OF MSI AIM POINTS FOR VARIOUS GEOCENTRIC LONGITUDES OF THE ASCENDING NODE

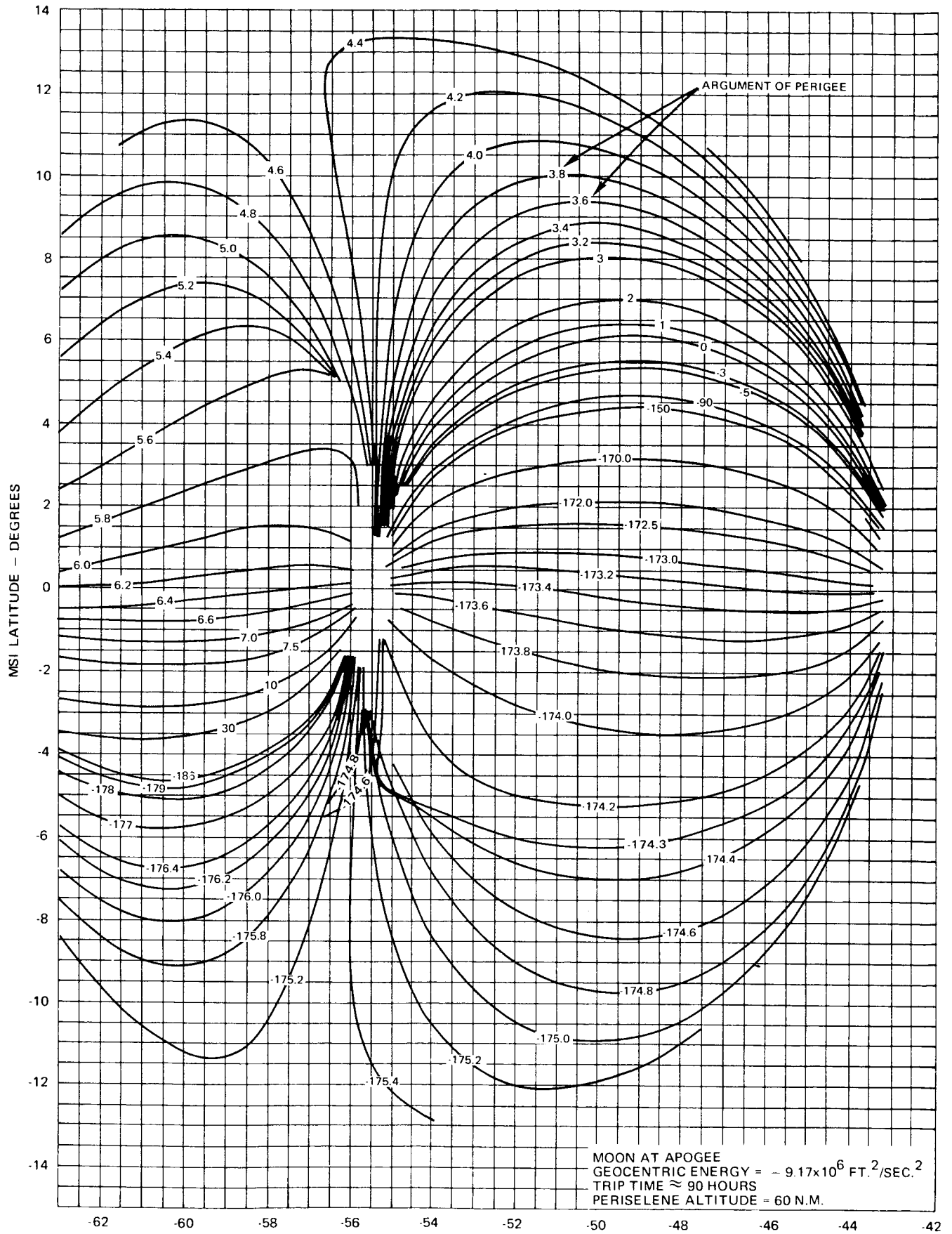


FIGURE 54A - LOCUS OF MSI AIM POINTS FOR VARIOUS ARGUMENTS OF PERIGEE

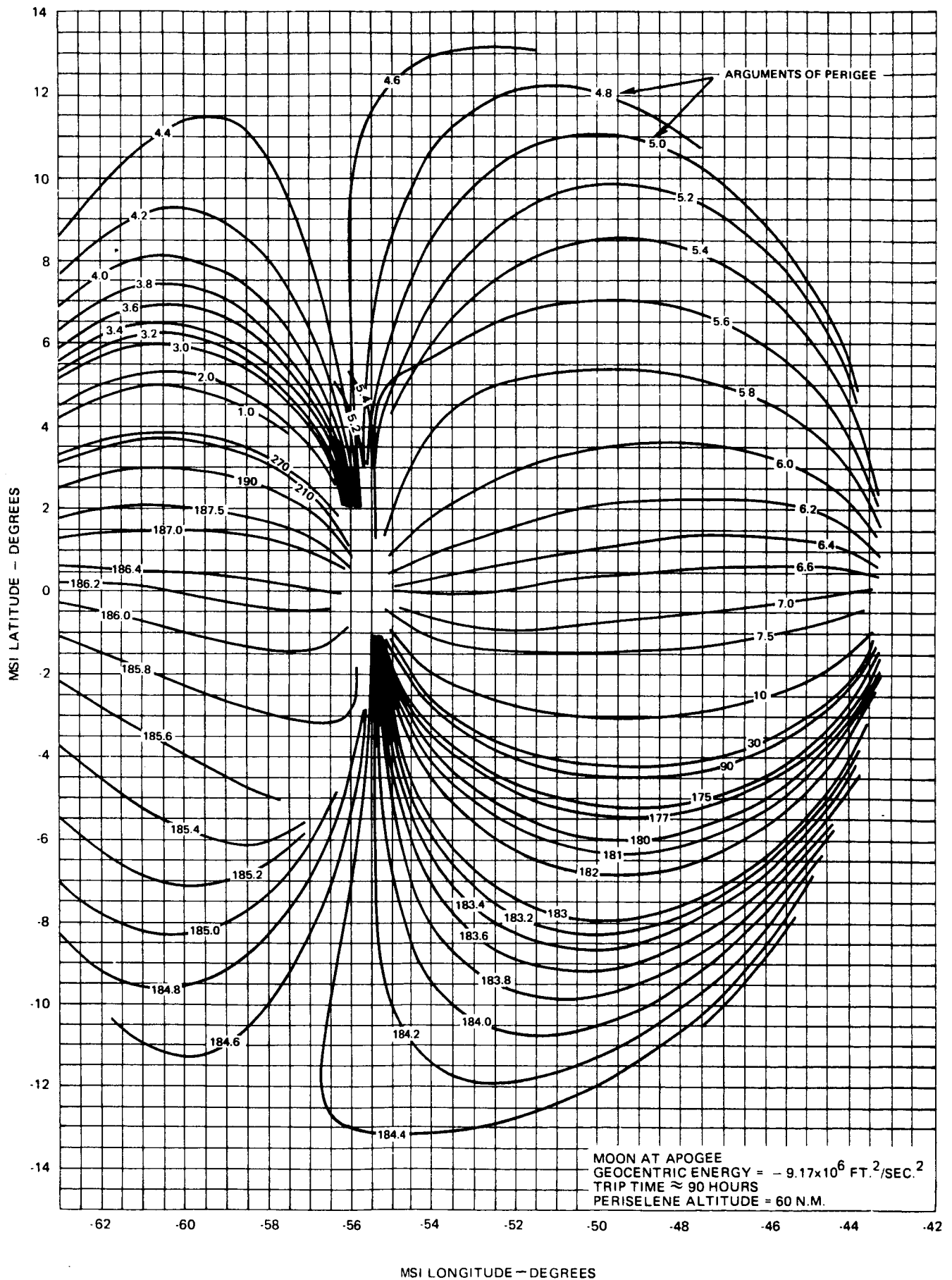


FIGURE 54B - LOCUS OF MSI AIM POINTS FOR VARIOUS ARGUMENTS OF PERIGEE